Hull Monitoring and Assessment of Hatch Corners and Hatch Opening Distortion

Nanna Martine Jacobsen

NORWEGIAN UNIVERSITY OF SCIENCE AND
TECHNOLOGY

MASTER THESIS:

Hull Monitoring and Assessment of Hatch Corners and Hatch Opening Distortion

Nanna Martine Jacobsen

June 9, 2015

NTNU – Trondheim
Norwegian University of
Science and Technology

MASTER THESIS 2015
for
Stud. Techn. Nanna Martine Jacobsen

Hull Monitoring and Assessment of Hatch Corners and Hatch Opening Distortion
Skrogmonitorering og evaluering av lukehjørner og deformasjoner av lukeåpninger

Background and Motivation:
DNV and GL have merged into DNV GL, which is the leading class society within many ship segments, e.g. container vessels. For tankers and bulk carriers, there are common structural rules, while for container vessels it is not. It is therefore up to DNV GL to further develop the industry standard for container vessels, including both rules and standards for design and operation.

While torsion is not important for tankers, and only slightly important for bulk and ore carriers, it is highly important for container vessels. The large deck openings, with slender longitudinal deck strips and slender transverse deck strips, will deform due to torsion in oblique seas. This is an essential strength aspect of container vessels. The torsion will give warping stress, which is axial longitudinal stress in the cross section of the ship, and will hence lead to deformation of the transverse deck strip, referred to as warping deformations or hatch opening distortions. Locally, this will also give axial stresses due to the side shell being exposed to a bending moment when trying to limit the warping deformations. These issues are critical with respect to strength in terms of fatigue, yielding and buckling and needs to be addressed during design and approval, as well as in operation. Besides being a strength issue related to the hull, warping deformation will also affect lashing loads and increase the loading on the hatch coaming stays.

DNV GL have carried out full scale measurements of several container vessels the last decade, with respect to different issues like parametric roll, fuel efficiency, navigation, whipping and springing, and also hatch opening distortions. The latter becomes more important for larger vessels, and the twin island concept is introduced to limit the hatch opening distortion besides other beneficial effects. Twin island concept is therefore used for container vessels of more than 10 000 TEU. The vessels around 10 000 TEU may therefore be expected to have high hatch opening distortions, and an 8600 TEU vessel is equipped with a simplified setup measuring strain at several positions in a transverse deck strip. This can be used to get an understanding of the stress level close to the hatch corners. Preliminary assessment reveals high dynamic stress levels and more detailed assessment should be carried out.

This master thesis deals with the topic of:
- Hull monitoring data from real operation
- Container ship design
- Warping deformations and warping stress
- Fatigue strength
- Ultimate strength
- Hydrodynamic wave induced loads
- Prescriptive rule loads, beam modelling and finite element modelling

It should be emphasised that it is important for the student to understand several of these topics.

This master thesis covers a relatively broad and multidiscipline competence area, which will limit the necessity to go deep into certain aspects, but this can be adjusted based on the results and progress. Reference is given to the rules of DNV GL and associated classification notes, as well as literature and courses at NTNU.

Tools needed are MATLAB, LATEX, Excel, and DNV GL software like SESAM, Waqum Explorer and NAUTICUS 3D-Beam and NAUTICUS Hull. The thesis should be written in English.

Scope of Work for the Master Thesis:

1. A review of literature related to hull monitoring, full scale measurements and design of container vessels, with special focus on torsion and warping, should be performed and summarized.

2. The ship is operating in two different trades. Compare these trades. Standard wave environment can be established based on Waqum Explorer once the route is defined. Results from a hydrodynamic analysis may be used to estimate stresses in deck.

3. Based on the measurement data, evaluate the degree of presence of vibrations due to torsion.

4. With focus on the transverse deck strip, how is the measured stress compared to the rule values with respect to yield criteria for ULS? A global ship model is available and can be used for this purpose. It may be necessary to estimate the rule stress based on DNV GL software.

5. It may be necessary to use a local model to separate nominal stress from hot spot stress, since the measured stress may be affected by the hot spot zone. How much local stress is included in the measurements?

6. How can the measurements be converted to estimate the Hatch opening distortion?

7. With focus on the transverse deck strip, how is the measured stress compared to the design/ rule values with respect to fatigue. What can the magnitude of fatigue at the hatch corners be?

8. Conclusions and recommendation for further work

The candidate will have to sign a confidentiality agreement related to the data and information made available by DNV GL.

The work scope may prove to be larger than initially anticipated. Subject to approval from the supervisors, topics may be deleted from the list above or reduced in extent. In the thesis the candidate shall present her personal contribution to the resolution of problems within the scope of the thesis work.

Theories and conclusions should be based on mathematical derivations and/or logic reasoning identifying the various steps in the deduction.

The candidate should utilize the existing possibilities for obtaining relevant literature.

Thesis Format
The thesis should be organised in a rational manner to give a clear exposition of results, assessments, and conclusions. The text should be brief and to the point, with a clear language. Telegraphic language should be avoided.

The thesis shall contain the following elements: A text defining the scope, preface, list of contents, summary, main body of thesis, conclusions with recommendations for further work, list of symbols and acronyms, references and (optional) appendices. All figures, tables and equations shall be numerated.

The supervisors may require that the candidate, in an early stage of the work, presents a written plan for the completion of the work. The plan should include a budget for the use of computer and laboratory resources which will be charged to the department. Overruns shall be reported to the supervisors.

The original contribution of the candidate and material taken from other sources shall be clearly defined. Work from other sources shall be properly referenced using an acknowledged referencing system.

The report shall be submitted in two copies:
- Signed by the candidate
- The text defining the scope included
- In bound volume(s)
- Drawings and /or computer prints which cannot be bound should be organised in a separate folder.
- The report shall also be submitted in pdf format along with essential input files for computer analysis, spreadsheets, MATLAB files etc. in digital format.

Ownership
NTNU has according to the present rules the ownership of the thesis. Any use of the thesis has to be approved by NTNU (or external partner when this applies). The department has the right to use the thesis as if the work was carried out by a NTNU employee, if nothing else has been agreed in advance.

The knowledge gained through supervising including the results from the thesis can automatically be utilised by DNV GL.

Thesis Supervisor
Prof. Jørgen Amdahl

Thesis Co-Supervisor
Dr. Svein Erling Heggelund/ Gaute Storhaug, Høvik, Oslo.

Deadline: June 10, 2015
Trondheim, January 14, 2015

Jørgen Amdahl

Preface

This report is the result of the master project done by stud.techn. Nanna Martine Jacobsen during the spring semester 2015 at the department of Marine Technology, Norwegian University of Science and Technology. The master thesis work has been done in collaboration with DNV GL. The topic studied is structural strength of large container ships, especially the effect of torsion.

The first part of this work has been a literature study, which is based on a literature study on the same topic, performed during the fall semester 2014. Most of the figures in the thesis are drawn by the author, to illustrate and explain calculations, results and specific subjects described in the text. Both a global and a local Finite Element (FE) model, and measurement data from a 8600 TEU vessel, was provided by DNV GL. The FE-models have been modified, working in GeniE and the measurement data has been post processed in MATLAB

The scope of the master thesis work has been larger than initially anticipated. The work of collecting relevant background theory, modifying the FE-models, performing analyses, assessing results and post processing measurement data, as well as writing the thesis report has been time consuming and challenging, but very educational and interesting.

I would like to thank the problem owner of this thesis, Gaute Storhaug in DNV GL, for providing and explaining the measurement data. I also want to thank Svein Erling Hegglund in DNV GL, for sharing his knowledge. DNV GL employees, Olav Aagaard and Ørjan Fredriksen, and former student at Marine Technology, Christian Andersson, also deserves a thank for valuable discussions during the thesis work. Last, but not least, I would like to thank professor Jørgen Amdahl at NTNU, for the help he has provided during the work with this thesis.

Høvik, June 9, 2015

Nanna Martine Jacobsen

Summary

Torsion is highly important for large container carriers. In order to maximize the container capacity, a large deck area is essential, which often leads to a big bow flare. To simplify loading and offloading, each cargo hold is equipped with huge hatch openings. These large deck openings, with slender longitudinal and transverse deck strips, will deform due to torsion in oblique seas, referred to as hatch opening distortions. This is regarded a vital strength aspect for container carriers. A master project is performed, in order to investigate how torsion contributes to extreme loading. Full scale measurements of a 8600 TEU container vessel, conducted by DNV GL, theoretical methods, and a global and a local Finite Element (FE) model have been used for this purpose. This was done, to get a greater knowledge of torsional behaviour of container carriers, which again can be used to document whether torsion should be included in ship design rules.

The ship has been operating on two different trades. On Route 1, the vessel follows a relatively sheltered passage from Hamburg to Singapore, whereas the vessel crosses the North Pacific Ocean from Singapore to USA on Route 2. Results from a hydrodynamic analysis, and environmental data for each route, was used to calculate the long term distribution of longitudinal stresses in deck. Long term distribution of deck stresses verifies that Route 2, which is known for more rough seas, gives the worst prediction of stresses. However, the measured stresses prove different. In order to find out why measured stresses are higher for Route 1, although Route 2 has more rough seas, the vessel's operating speed was investigated. It was found that the vessel operates at higher speeds on Route 1, than on Route 2. With speed reduction, the ship resistance, and the risk for occurrence of high stresses due to wave induced vibrations, such as whipping, springing and torsional vibrations, is lowered. Additionally, no significant routing has been observed on the first route. On the second route, on the other hand, routing was found, i.e. the roughest seas have been avoided. This will again influence and lower measured stresses. Speed reduction and routing are therefore important reasons why measured stresses are lower on Route 2, than Route 1, despite the fact that the wave environment is more rough on Route 2.

Measurement data have been investigated to evaluate the degree of torsional vibrations present. During the day where most torsion is measured, the ratio of dynamic and wave stresses ≈ 1.10, which indicates that the ship does not experience significant torsional vibrations. Thus, torsional vibrations are found to be of minor concern for the 8600 TEU vessel.

Global FE-analyses of the container vessel have been performed, with respect to

the yielding criteria for Ultimate Limit State, ULS, due to torsion. Additionally, since many modifications were done in order to analyse the model, self-checks of the model with vertical and horizontal bending moments were carried out. A coarse mesh was used to obtain nominal stresses. Rule stresses with respect to ULS were found by applying torsional moments, calculated from ship rules. The results show that maximum measured stresses in the deck strip are approximately 0.69-0.74 of ULS rule stresses for Route 1 and 0.63-0.68 on Route 2, i.e. measured stresses are within the acceptance criteria for ULS, on both routes.

Since local stresses may be included in the measurements, the same analysis of the transverse deck strip was performed with fine mesh. Local stresses, and thus measured stresses, were found to be about 10 - 15 % higher than nominal stresses. The local stresses in the measurements are most likely due to the fact that the sensors are located close to hatch corners and close to a weld between two deck plates, which are source to stress concentrations, i.e. hot spot stresses.

The magnitude of the hatch opening distortion has been calculated from the global FE-model. It was found that hatch opening distortion, due to the maximum measured stress of 131 MPa (measured on Route 1), has a magnitude of 226 mm. In comparison, the expected hatch opening distortion due to estimated ULS stresses is 335 mm at the deck strip where the sensors are located. The largest ULS hatch opening distortion obtained is located further forward, at cargo hold 3, where the deformations reaches 411 mm.

The calculations were also done simplified, with use of hand calculations, 3D-Beam, and a deck strip model. This, to find out if simplified and less time consuming methods can be used in later studies of hatch opening distortions, or if a global model must be used for this purpose. Values for hatch opening distortion for the simplified calculation methods are between 7 - 21 % lower than calculated from the global model. If further studies of other container ships gives the same relation between the simplified methods and the global model, simplified methods might be used, introducing a scaling factor.

Sammendrag

Torsjon er svært viktig for store containerskip. For å maksimalisere containerka-
pasiteten, er et stort dekksareal vesentlig, noe som ofte fører til at containerskip
har svært skrå skipssider i området rundt baugen. For å gjøre lasting og lossing
så enkelt og effektivt som mulig, er det store lukeåpninger over lasterommene.
Lukeåpningene gjør at dekket hovedsakelig består av slanke langsgående og tver-
rgående dekksstriper. Skrogstrukturen til containerskip er derfor svakere enn for
andre skipstyper. Dekkstripene vil deformere seg på grunn av vridning som følge
av torsjon i skrå sjø, også kalt lukeåpningsdeformasjoner. En masteroppgave er
gjennomført for å undersøke hvordan torsjon bidrar til ekstreme belastninger på
skipsstrukturen, som igjen gir høye spenninger. Fullskala målinger for et 8600 TEU
containerskip, teoretiske metoder, samt en global og en lokal element metode mod-
ell (FE-modell), er benyttet til dette formålet. Dette fordi det er viktig å oppnå
en bredere kunnskap om hvordan torsjon påvirker de strukturelle egenskapene til
containerskip, for å kunne vurdere hvorvidt torsjon bør implementeres i skipsreg-
lene for slike skip.

Containerskipet som er undersøkt, har operert på to forskjellige ruter. På Rute
1 følger fartøyet en relativt skjermet passasje fra Hamburg til Singapore, mens
det krysser Nord-Stillehavet fra Singapore til USA på Rute 2. Resultater fra
en hydrodynamisk analyse, samt miljødata for hver av rutene er benyttet til å
beregne langtidsfordelingen av aksiale spenninger i dekket. Langtidsfordelingen
av dekksspenningene verifiserer at Rute 2, som er kjent for mer sjø, gir den ver-
ste estimerte spenningen. Resultater fra måledataene viser derimot at de høyeste
spenningene er målt på Rute 1. Fartøyets hastighet under transitt ble undersøkt
for å finne ut hvorfor målte spenninger er høyere for Rute 1, til tross for at Rute
2 har mer sjø. Det viser seg at skipet opererte med høyere hastigheter på Rute
1, enn på Rute 2. Reduksjon i hastighet, reduserer også skipets motstand, samt
risikoen for forekomsten av bølgeinduserte vibrasjoner, som whipping, springing
og torsjonsvibrasjoner, som igjen forårsaker høye spenninger. I tillegg er det blitt
observert at skipet ikke ruter på den første ruten, i motsetning til på Rute 2,
hvor fartøyet har rutet, og dermed unngått de verste vær og sjøforholdene. Dette
vil igjen påvirke og redusere målte spenninger. Hastighetsreduksjon og ruting er
altså viktige årsaker til at målte spenninger er høyere for Rute 1, til tross for at
sjøforholdene er verre på Rute 2.

Måledata ble også benyttet til å estimere graden av tilstedeværelse av torsjonsvi-
brasjoner. Den dagen det ble målt mest torsjon, er forholdet mellom dynamiske
spenninger og spenninger på grunn av bølgelaster kun $\approx$ 1.10, noe som tyder på
at skipet ikke opplever noen vesentlige torsjonsvibrasjoner. Torsjonsvibrasjoner er

altså ikke bekymringsverdig store for dette spesifikke skipet.

En global FE-modell av containerskipet er blitt modifisert og brukt i FE-analyser med hensyn til flyt kriteriet for Ultimate Limit State, ULS, som følge av torsjon. I tillegg ble det foretatt en kontroll av den globale FE-modellen, med horisontalt og vertikalt bøyemoment, siden det ble gjort mange modifikasjoner for å kunne gjennomføre analyser. Et grovt mesh ble benyttet for å finne nominelle spenninger i skrogbjelken. ULS regelspenninger ble funnet ved å påføre torsjonsmoment, beregnet fra skipsregler for containerskip. Resultatene viser at maksimum målte spenninger i tverrstripen er ca. 0.69 - 0.74 av regelspenninger for ULS, for Rute 1 og 0.63 - 0.68 for Rute 2. Det betyr at målte spenninger er innenfor akseptkriteriet for ULS på begge rutene.

Siden lokale spenninger kan ha påvirket målingene, ble FE-analysen også gjennomført med fint mesh. Det ble funnet at lokale spenninger i tverrstripen, og dermed også målte spenninger, er omlag 10 - 15 % høyere enn de nominelle spenningene som ble funnet i globalmodellen. De lokale spenningene i målingene skyldes antagelig at sensorene er plassert i nærheten av lukehjørnene, samt i nærheten av et skille mellom to plater, som begge er kilder til spenningskonsentrasjoner, også kalt hot spot spenninger.

Den globale FE-modellen ble også benyttet til å beregne størrelsen på deformasjonen av lukeåpningene. Den maksimum målte spenningen i tverrstripen, er på 131 MPa (målt på Rute 1), og tilsier en deformasjon av lukeåpningen på 226 mm. Til sammenligning er maksimum lukeåpningsdeformasjon beregnet fra ULS regelspenninger på 335 mm for den samme dekkstripen. Den største deformasjonen av lukeåpningen beregnet med ULS regelspenning er på 411 mm, og oppstår på en tverrstripe lenger frem på skipet, i lasterom 3.

Beregningene av lukeåpningsdeformasjonene ble også gjort forenklet, ved bruk av håndberegninger, 3D-Beam og en lokalmodell av tverrstripen. Dette ble gjort for å finne ut hvorvidt forenklede og mindre tidkrevende metoder kan benyttes i fremtidige studier av lukeåpningsdeformasjoner, eller om en global FE-modell må benyttes til dette formålet. Verdier for lukeåpningsdeformasjonen for de forenklede beregningsmetodene er mellom 7 - 21 % lavere enn beregnet fra den globale modellen. Dersom lignende studier av andre containerskip gir det samme forholdet mellom de forenklede metodene og den globale modellen, kan det vise seg at forenklede metoder kan anvendes, ved å innføre en skaleringsfaktor.

Contents

List of Figures

List of Tables

List of Abbreviations

$2D$: Two Dimensional

$3D$: Three Dimensional

AP: Aft Perpendicular

BL: Base Line

CL: Center Line

CSA: Computational Ship Analysis

DMP: Sensor - Deck Midship Port side

DMS: Sensor - Deck Midship Starboard

DSS: Decision Support System

$DT1P$: Sensor 1 - Transverse Deck strip Port side

$DT2P$: Sensor 2 - Transverse Deck strip Port side

$DT3S$: Sensor 3 - Transverse Deck strip Starboard

$DT4S$: Sensor 4 - Transverse Deck strip Starboard

DWT: Dead Weight

$FBGA$: Fiber Bragg Grating Analyzer

FE: Finite Element

FLS: Fatigue Limit State

FP: Forward Perpendicular

GM: Metacentric height

GPS: Global Positioning System

GWS: Global Wave Statistics

IMO: International Maritime Organization

LPP: Length between perpendiculars

LOA: Length overall

NPX: New-Panamax

SC: Shear Center

$SOLAS$:   Safety of Life at Sea

ULS: Ultimate Limit State

List of Symbols

A_{WP}:   Water plane area

B: Breadth

C_B: Block coefficient

C_{SWP}:   Water plane area coefficient

D: Accumulated fatigue damage

D: Depth

E: Young's modulus

G: Shear modulus

I: Moment of Inertia

$I_{\Omega\Omega}$:   Sectional Moment of Inertia

I_t: Torsional modulus

L: Rule Length

M_{ST1}:   Rule Torsional Still Water Moment

M_{ST2}:   Rule Torsional Still Water Moment

M_{WH}:   Rule Horizontal Wave Bending Moment

M_{WT1}:   Rule Torsional Wave Moment

M_{WT2}:   Rule Torsional Wave Moment

N_i: Number of cycles before failure

$Q(\Delta\sigma)$:   Probability of exceedance of the stress range $\Delta\sigma$

T: Torque

T: Design draft

T_0:   Torsional moment at the midship section

T_s: Saint Venant Torsional Moment

Ts: Scantling draft

W: Section modulus

f_r: Factor for reducing loads from 10^{-8} to 10^{-4} probability level

h_0:   Long term Weibull shape parameter

q: Weibull scale parameter

s_{aft}:   Backward spacing between web frames

s_{fwd}:   Forward spacing between web frames

t: Thickness

v: Service speed at design draft

z_e: Distance between shear center and 0.7 T

γ_{sz}:   Shear strain in sz-plane

η: Stability factor

$\Delta\sigma$:   Stress range

σ_a: Actual compressive buckling stress

σ_{all}:   Allowable nominal stress

σ_c: Critical Compressive Buckling Stress

σ_{eq}:   Equivalent von Mieses stress

σ_f: Yield stress

σ_x: Stress in x-direction

σ_y: Stress in y-direction

τ: Shear stress

τ_w: Warping shear stress

τ_s: St. Venant shear stress

ϕ: Rotational angle

ϕ':   Angle of twist

1 Introduction

In this master project, the structural strength of large container ships, especially the effect of torsion, has been investigated. The background and motivation for the thesis work is presented in this chapter. Further, the main objective of the thesis is described, before the structure of this report is outlined.

1.1 Background and Motivation

The use of containers in transportation of cargo has been growing over the past decades. This, together with the expansion in the world trade, has resulted in a rapid increase in the demand on containerships (Shama; 2010). The advantage related to use of containers is that the goods can be transported directly from e.g. a factory to its sales outlet. Since import and export becomes more and more common and goods are transported over increasingly longer distances, water transport is used as a link in the transport chain. Therefore, the container ship industry has been growing and the dimensions of the ships are constantly increased, in order to take as many containers as possible.

While torsion is not very important for ship types, such as tankers, bulk and ore carriers, it is highly important for container carriers. Container ships are usually built with double bottom and double, but slender broadsides to minimize the resistance on the hull at high speeds. In order to maximize the container capacity, a large deck area is essential, which often leads to a big bow flare. To simplify loading and offloading, each cargo hold is equipped with huge hatch openings. These large deck openings, with slender longitudinal and transverse deck strips, will deform due to torsion in oblique seas. This is regarded a vital strength aspect for container carriers. To keep the stresses in a container ship at an allowable stress level, it is necessary to stiffen the ship structure against torsional stresses.

Torsion becomes of increased importance as container ships are built constantly larger, especially when transverse structure is considered. Since torsion is not yet well defined in ship rules for container ships, it is important to document the effect of torsion and hatch opening distortions to decide whether or not torsion must be included in ship design rules in the future.

1.2 Objective

The master thesis work has been performed in collaboration with DNV GL. Full scale measurements of a 8600 TEU container vessel have been conducted by DNV GL. The container vessel studied, is a relatively new ship, which was built in 2009. The vessel has a pronounced bow flare angle and operates at high service speeds. The main objective of this thesis was to study full scale measurements, in order to investigate how torsion contributes to extreme loading. In addition to the full scale measurements, theoretical methods, a global Finite Element (FE) model, as well as a local FE-model, have been used for this purpose.

This master project covers a relatively broad and multi-discipline competence area, which limits the need to immerse into certain topics. The following objectives were formulated in collaboration with supervisor:

- A review of literature related to hull monitoring, full scale measurements and design of container vessels, with special focus on torsion and warping, should be performed and summarized.

- The ship is operating in two different trades. Compare these trades. Standard wave environment can be established based on Waqum Explorer once the route is defined. Results from a hydrodynamic analysis may be used to estimate the stress in deck.

- Based on the measurement data, evaluate the degree of presence of vibrations due to torsion.

- With focus on the transverse deck strip, how is the measured stress compared to the rule values with respect to yield criteria for Ultimate Limit State, ULS? A global ship model is available and can be used for this purpose. It may be necessary to estimate the rule stress based on DNV GL software.

- It may be necessary to use a local model to separate nominal stress from hot spot stress, since the measured stress may be affected by the hot spot zone. How much local stress is included in the measurements?

- How can the measurements be converted to estimate the Hatch opening distortion?

- With focus on the transverse deck strip, how is the measured stress compared to the design/ rule values with respect to fatigue. What can the magnitude of fatigue at the hatch corners be?

2

As the scope of work proved to be more extensive than initially anticipated, it should be noted that the last point in the above mentioned objectives, has been omitted in agreement with the supervisor. However, literature related to this topic, is included in the report.

1.3 Structure of the Thesis

The first three chapters in this thesis contain theory found relevant for the work carried out during the project. In the remaining chapters, methods used during the work, results obtained, conclusions, and proposals for recommendations of further work, are presented. The thesis is organised as follows:

Chapter 2:   In Chapter 2, background theory found relevant for the execution of the thesis work is presented. First, theory concerning container ships in general, and different container ship configurations is presented. Further, phenomena that occurs due to container carriers structural design, i.e. torsion and warping, and load conditions creating torsional moments, global wave loads and wave induced vibrations, are described.

Chapter 3:   Different class societies have developed rule requirements for Ultimate Limit State and fatigue control of ship structures. This, to ensure that all parts of a hull structure have sufficient strength and fatigue life. In Chapter 3, rule requirements found relevant for the thesis work, developed by DNV GL are summarized.

Chapter 4:   Measurement data of a 8600 TEU Container vessel are conducted by DNV GL. In this chapter, the vessels main particulars and operating routes, as well as the hull monitoring system, used to collect measurement data, is presented and described.

Chapter 5:   Several computer programs were used during this thesis work, in order to investigate the full scale measurement data and modify Finite Element models, provided by DNV GL, as well as for performing FE-analyses and assessing the results. All computer programs used, are briefly described, followed by a more detailed description of computing and analyses.

Chapter 6:   The full scale measurements of the 8600 TEU container ves-
              sel, together with theoretical methods, a global Finite Ele-
              ment (FE) model, as well as a local model have been used
              to investigate how torsion contributes to extreme loading and
              hatch opening distortions. In this chapter, results from the
              measurement investigations and FE-analyses carried out in
              the thesis work, are presented and discussed.

Chapter 7:   Conclusions from the work carried out, and the results ob-
              tained are summarized and presented in this chapter.

Chapter 8:   Based on experiences and knowledge gained during the the-
              sis work, recommendations for further work are proposed in
              Chapter 8.

2 Theory Related to Container Ships

In this chapter, background theory relevant for this thesis work is presented. First, container ships and different container ship configurations will be presented in Section 2.1. Further, torsion is described in general, before introducing the effect of torsion in container ships. As warping is directly associated with torsion, the warping phenomena is also described. Furthermore, load conditions creating torsional moments, global wave loads and wave induced vibrations, including whipping and springing, are described.

2.1 Container Ship Design

Container ships are usually build with double bottom and double, but slender broadsides. In order to maximize the container capacity, and simplify loading and offloading, the hatch openings over each cargo hold stretches over the whole breadth of the ship, such that horizontal movement of containers can be avoided. Thus, the on/off-loading process becomes more efficient and the number of hours in port, reduced. This is economical and operative as well as competitive beneficial. Although there are many advantages having huge hatch openings, they also cause structural limitations. A consequence is that container ships have open cross sections, and hence a weaker hull structure compared to e.g. tankers, especially in terms of torsion. This is regarded an vital strength aspect for container carriers.

To obtain an additional competitive benefit, container ships are operating at high speeds, usually up to 25 knot. To minimize the resistance on the hull at high speeds, a slender ship structure is necessary. This, in combination with maximizing the container capacity leads to structural challenges in container ship design (Amdahl; 2010). A big deck area is essential to take as many containers as possible, thus container ships often have a definite bow flare. The bow flare is a result of the demand of a huge deck space for containers. Because of the bow flare, the hull is exposed to high wave loads at high speeds (Storhaug; 2013a).

Today, container ships are divided into two main categories, namely intercontinental container ships and container feeders. Intercontinental container ships can only dock in the largest ports, due to its dimensions and the ports' transfer capacity. Hence, the smaller container feeders are used to transport containers from big to smaller ports, and vice versa (Van Dokkum; 2008).

Intercontinental container ships are again divided into different sub groups, among others Panamax and post Panamax. Panamax ships have a maximum width less

than 32.3 meter, which is the maximum breadth for ships that can pass the locks in the Panama Canal. Post Panamax ships on the other hand, are too wide to pass through the Panama Canal (Van Dokkum; 2008). However, the ongoing Panama Canal expansion project, called "The Third set of Locks Project" will allow even larger ships, with a width up to 49 meter, to pass through the Panama Canal in the future. Due to the Panama Expansion project, a new type of Panamax ships may be introduced. These New-Panamax (NPX) ships will be designed relatively shorter, wider and deeper, due to the limitation of the lock dimensions (Tozer and Penfold; 2007).

2.2 Single vs. Twin Island Configuration

The conventional container ship configuration has developed during the last decades, due to the increasing size of container ships and the need for extra stiffening of the hull structure. This development has resulted in the single island concept, which is already proven technically feasible by the ultra large container ship, Emma Maersk (Tang-Jensen and Shi; 2007). The single island concept has, in conformity with the conventional configuration, only one superstructure. However, unlike conventional container ships, the superstructure on container ships using the single island concept is placed approximately up to 0.5 L forward of Aft Perpendicular (AP), see Figure 2.1. It turns out that the relocation of the superstructure from the conventional to the single island concept has been beneficial, especially with respect to container capacity on deck.
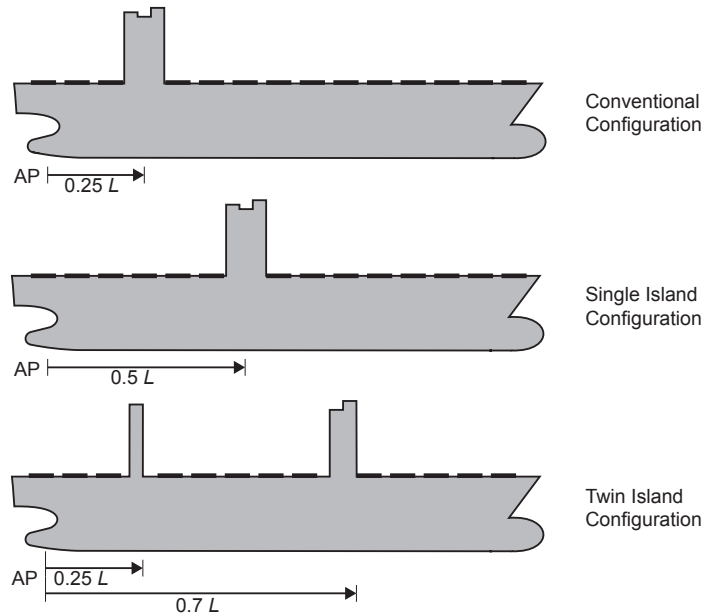
Figure 2.1: Conventional, Single Island and Twin Island Configurations

The need for a New-Panamax container ship design, optimized to the lock dimensions of the new locks in the Panama Canal, has led to discussion and speculations. The main topic is centred on a new configuration for deck house and engine room, called the "Twin Island configuration". In contrast to conventional container ships which are built with only one superstructure placed about $0.25\ L$ forward of AP, the Twin Island concept is characterized by two superstructures. The first superstructure is placed on the same position as for a conventional container ship, namely 0.25 L forward of AP. The second superstructure is placed approximately 0.7 L forward of the AP (see Figure 2.1).

The International Maritime Organization (IMO) limits the container capacity on deck with the International Convention for Safety of Life at Sea ($SOLAS$). According to SOLAS's Regulation 22, the requirement for Navigation Bridge Visibility only concerns forward visibility and there are no regulations for visibility aft (IMO; 2014). Hence, the area behind the bridge, where the containers may be stored in higher stacks, increases when the deck house moves forward, which again increases the container capacity. Further advantages and disadvantages with the different configurations, found in Tozer and Penfold (2001) and (2007), and Tang-Jensen and Shi (2007), are presented in Table 2.1.

Table 2.1: Container ship configurations - Advantages and Disadvantages

	Advantages	Disadvantages
Conventional Configuration	• Conventional configuration of container vessels is the originally used configuration in the container ship industry. The configuration is well developed and widely used.	• Decreased container capacity compared to Single- and Twin- Island configurations. • Lower torsional strength than ships of similar size, with Single or Twin-Island configurations.
Single Island Configuration	• Increased container capacity compared to conventional container ships, as a result of IMO's visibility requirements. • Two large regions for container handling, makes on-/off-loading more efficient than for Twin Island configuration.	• Requires a long shaft line, because of the forward placement of superstructure, and hence also machinery. Causes hull structural deflections.
Twin Island Configuration	• Shorter shaft line due to the placement of machinery beneath the rare deck house. • Easier access to engine room due to the location in the rare deck house. • Spare space under accommodation, which is located in the deck house midships. • The noise level is kept satisfactory low, due to the accommodations location away from vibratory sources, such as the main engine and propeller. • Increased ship and crew safety, since accommodation and auxiliary machinery room is separated from the engine room. • Enhanced torsional strength of the ship hull, due to reduced warping and increased torsional stiffness	• The superstructures obstructs movement of cranes from one region to another, slowing down the on-/off- loading process.

The most significant advantage is the increased torsional stiffness for the Twin Island configuration. The increased torsional stiffness is achieved due to the fact that the two superstructures represents torsional restraints (which is further described in Section 2.5). In addition, the container capacity is increased, due to the forward location of the bridge as a result of IMO's visibility requirements, which only concerns forward visibility. However, a disadvantage is that the loading and offloading process is delayed, as a result of the two superstructures, which tend to obstruct the movements of cranes for cargo handling. This will increase the time in port, which again may become expensive due to port fees. A study of operation expenses is therefore necessary to decide which configuration is the most economical beneficial.

The 8600 TEU container vessel investigated in the thesis work, has the conventional container ship configuration. Since the torsional strength is lowered for conventional configuration compared to ships of similar sizes with Single- or Twin-Island configurations, torsion becomes an important aspect. Therefore, torsion and theory related to torsion, will be further described in the following sections.

2.3 Theory of Torsion

Torsion is defined as the twisting moment about the longitudinal axis of an object. A prismatic beam can be used to describe the torsional behaviour of ship structures. Such beams can counteract a twisting moment in two ways. In a closed cross section, shear stresses tends to go in circle. Hence, the prismatic beam resists the twisting moment by producing a circular shear flow in the cross section, as illustrated in Figure 2.2. This phenomenon is called Saint Venant torsion and is in general only valid for closed cross sections. It can therefore be neglected in thin-walled and open cross sections (Shama; 2010). The second way a prismatic member can resist a twisting moment, is to use the change in axial stresses to induce shear stresses. The phenomenon is called warping torsion and is the case for an open cross section, where stresses tend to move back and forth. The difference in the stress distribution over the thickness in a cross section exposed to Saint Venaint torsion and warping torsion respectively, is illustrated in Figure 2.2. For an open cross section, stresses are linearly distributed with respect to thickness, which gives zero stresses in the centerline of the plate thickness.
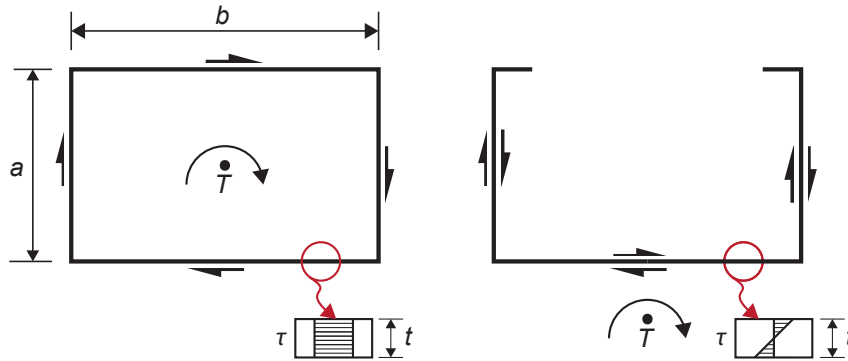
Figure 2.2: Distribution of shear forces - closed and open cross section

An estimate of the shear stress, τ, in a closed and an open cross section respectively, can simplified be calculated using the following formulas (Amdahl (2010)):

$$\tau_{closed} = \frac{T}{2abt} \tag{2.1}$$

$$\tau_{open} = \frac{T}{\frac{1}{3}(2a+b)t^2} \tag{2.2}$$

Where T is the torque, a is the height, b is the breath and t is the thickness of the cross section, see Figure 2.2.

The relation between shear stresses in an open and a closed cross section can then be found to be:

$$\frac{\tau_{open}}{\tau_{closed}} = \frac{\dfrac{3T}{(2a+b)t^2}}{\dfrac{T}{2abt}} = \frac{6ab}{t(2a+b)} \tag{2.3}$$

From the formulas above, it can clearly be seen that with the same thickness and torque acting on the cross sections, shear stresses in an open cross section will be of greater magnitude than the shear stresses in a closed cross section.

Asymmetric vertical and horizontal forces acting an offset distance from the shear center of the cross section causes torque. This because the torque acting on a cross section is calculated about the shear center. The shear center is the point that a cross section rotates about when it is exposed to torsion. For open cross sections,

the shear center is placed outside the cross section, whereas it is inside the cross section for closed cross sections. The location of the shear center outside the cross section of an open cross section, results in greater torque from lateral loads than for a closed cross section. This can be found directly from Figure 2.3, showing that the distance from the point where the force is acting, to the shear center is greater for an open cross section than for a closed cross section.
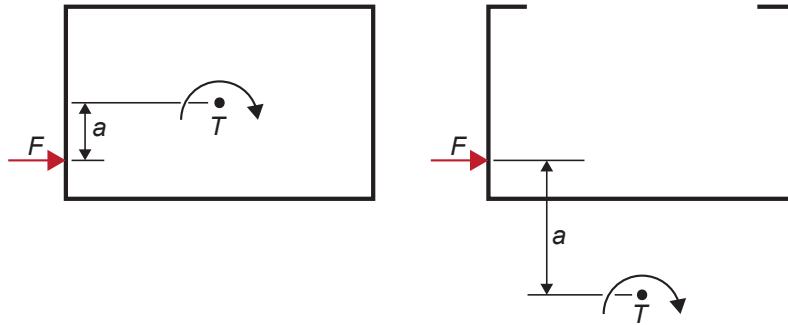
Figure 2.3: Shear center location - closed and open cross section

The torque is calculated as the force acting on the cross section times the distance between the force and the shear center. This implies that the magnitude of the torque is greater for an open cross section than for a closed cross section. Open ship structures will therefore have higher shear stresses at the same torque, as well as a larger torque than a closed ship structure, which is exposed to the same wave loads.

2.4 Theory of Warping

Although ship structures are stiffened, transverse sections tend to deform, which again will give great bending deformations of transverse girders between cargo holds. This torsion deformation results in a phenomenon called warping which gives axial deformations of the cross section (Amdahl; 2010). An ice cube tray made of silicon was used to visualize the bending deformation between cargo holds in particular, and to get a better understanding of the torsional behaviour of open cross sections in general. In Figure 2.4, which shows the silicon form, it can be seen how the transverse strips obtains a "S-form" after deformation, which is typical for transverse deck strips in container ships. Navier's hypothesis, which assumes that plane cross sections remain plane after deformation, is no longer valid. Hence, linear beam theory cannot be used to calculate the stresses acting on the cross section.

11

Figure 2.4: Torsion of an ice cube tray - an auxiliary model

The type of end constrains decides the degree of warping of a cross section. In general, two different conditions are used to calculate the magnitude of the warping deformation due to torsional deformations, depending on the type of end constrains. These two conditions are namely free and constrained warping.

2.4.1 Free Warping

Free warping appears when a thin-walled open cross section, which is free at both ends, is subjected to a torsional moment. The result is rotational torsion deformation, also called twist, as well as an axial, linear warping deformation. Since the section is free at both ends, and thus free to warp, no in-plane stresses are induced. Hence, the cross section will deform as shown in Figure 2.5. How the cross section deforms in terms of magnitude of the axial warping deformation and the angle of twist, is dependent on the greatness of the torsional moment, as well as the cross sections geometrical configuration, dimensions and scantlings.

Figure 2.5: Free Warping

2.4.2 Constrained Warping

When a cross section is fixed at one or both ends, constrained warping occurs. Since rotational deformations are prevented at the fixed ends, normal stresses

arises. Figure 2.6 illustrates an open thin-walled cross section, which is fixed at one end and exposed to a torsional moment at the free end. As it can be seen from the figure, the cross section remains un-deformed at the fixed end, but distorts at the free end. The magnitude of the deformation at the free end, depends on the magnitude of the applied torsional moment, the degree of constraint and the geometry of the cross section.
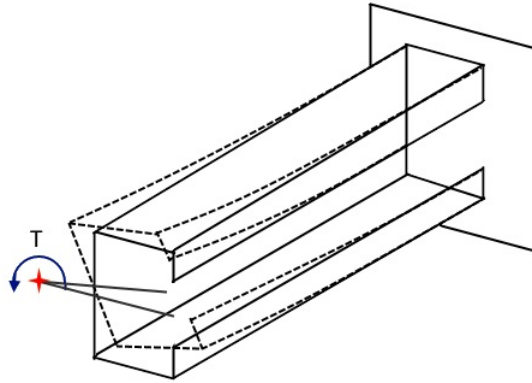
Figure 2.6: Constrained Warping

A container ship will experience constrained warping, since superstructure, such as the deck house and forecastle, represents torsional constraints. However, these constraints will not fix the structure completely against warping, and the magnitude of the warping deformations depends on these constraints. Torsion and warping in container ships will be further described in Section 2.5. First some examples are presented, to get a better understanding of the difference between, and the consequence of free and constrained warping, respectively.

2.4.3 Free vs. Constrained Warping

In the following, an I-beam is used as example to illustrate and explain the difference between free and constrained warping. The examples (Case 1 and Case 2) are taken from Haslum and Tonnessen (1973). In the first case, the I-beam is free to warp at both ends. In other words, the beam is free to deform longitudinally at both ends. In the second case, the beam is completely restrained against warping at the left end and hence, the beam can only deform longitudinally at the free right end.

The Torsional modulus, I_t, of a plate is defined as:

$$I_t = \frac{1}{3}bt^3 \tag{2.4}$$

An I-beam can be considered as an open cross section, consisting of three plates. These three plates will twist the same amount when the beam is subjected to a constant torque, T. The torsional modulus for an I-beam can hence be computed as the sum of the torsional modulus for each plate:

$$I_t = \frac{1}{3}\sum bt^3 \tag{2.5}$$

Further, the Angle of twist, ϕ', also called the "twist" is defined as follows:

$$\phi' = \frac{T}{GI_t} \tag{2.6}$$

where G is the Shear modulus. The product GI_t is commonly referred to as the torsional constant of the cross section.

When the beam is exposed to a torque, T, shear stresses arises. These shear stresses are varying linearly over the thickness of the cross section, as illustrated in Figure 2.7b. The maximum value is found at the outermost edges of the cross section and is calculated as shown in equation 2.7.

$$\tau_s = \frac{T}{I_t}t \tag{2.7}$$

The notation s in τ_s, indicates that the shear stresses are St. Venant shear stresses. These shear stresses results in a torsional moment, called the St. Venant torque, T_s.

$$T_s = GI_t\phi' \tag{2.8}$$

The Saint Venant Torsional Moment counteracts the torque T, which is applied to the beam.

2.4.3.1 Case 1: I-beam, Free to Warp

As already mentioned, an I-beam which is free at both ends, is also free to warp at both ends. When a constant torque, T, is applied to the beam (see Figure 2.7), the resultant of the shear stress τ_s is the St. Vernant torque, T_s. This is also the only resultant, which means that for an free I-beam, the St. Venant Torque, T_s,

is equal to the total torque acting on the beam:

$$T_s = T$$
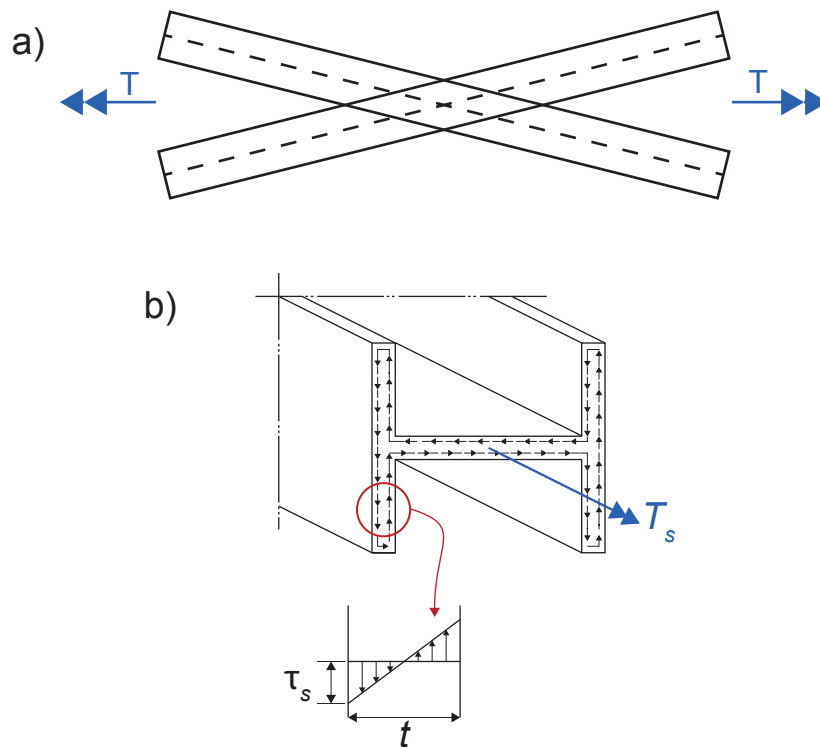
Figure 2.7: I-beam - free to warp

Since the beam is free to warp, all cross sections will have the same magnitude of warping. The magnitude of the warping can be found, since the St. Venant shear stresses τ_s are varying linearly over the plate. Hence, the warping deformation is zero in the middle plane of the plate (see Figure 2.7b).

15
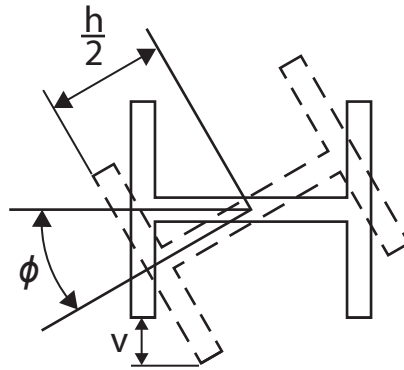
Figure 2.8: Torsional deformation of an I-beam cross section

From Figure 2.8, the deformation of the plane of the flanges, sz-plane, is found to be:

$$v = \frac{h}{2}\phi \tag{2.9}$$

Since there are no shear deformations in the middle plane of the plate, this implies that the shear strain, γ_{sz}, is zero in the sz-plane.

$$\gamma_{sz} = \frac{\delta v}{\delta z} + \frac{\delta w}{\delta s} = 0 \tag{2.10}$$

Hence, the slope of the flanges can be found by combining Equation 2.9 and 2.10:

$$\frac{\delta w}{\delta s} = -\frac{\delta v}{\delta z} = -\frac{h}{2}\phi' \tag{2.11}$$

The consequence of free warping is a warping deformation given by:

$$w = -\frac{h}{2}\phi' s \tag{2.12}$$

where s is measured from the midpoint of the flange.

2.4.3.2   Case 2: I-beam, Warping Restrained

The same I-beam is restrained against warping at one end of the beam, but free to warp at the other side of the beam.
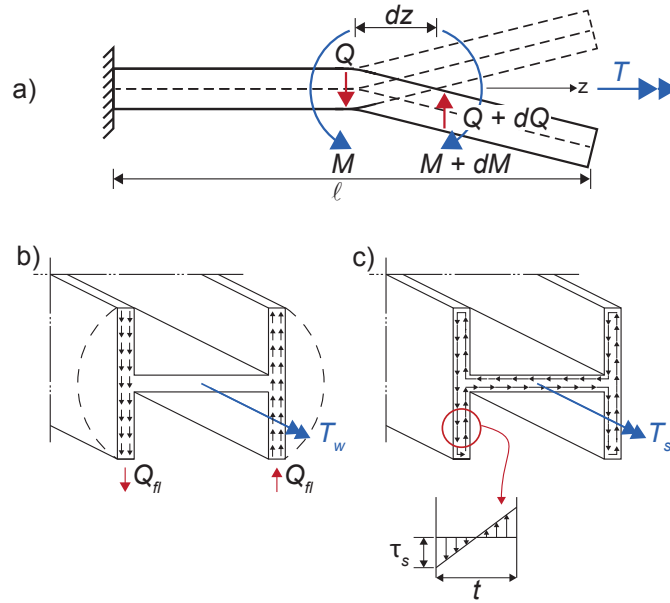
Figure 2.9: Warping restrained I-beam

In addition to the resulting St. Venant Torque, the total Torque, will now consist of an extra component, namely the warping torque, T_w, hence:

$$T = T_s + T_w$$

How this warping torque, T_w arises is described in the following.

As for the free beam the deformation of the flanges is found from Figure 2.8.

$$v = \frac{h}{2}\phi$$

However, in this case the flanges tend to bend. Their curvature is found to be:

$$\frac{\delta^2 v}{\delta z^2} = \frac{h}{2}\phi'' \tag{2.13}$$

which results in the bending moment:

$$M_{fl} = EI_{fl}\frac{h}{2}\phi'' \tag{2.14}$$

Where I_{fl} is the moment of inertia of the flanges.

The applied torque also gives raise to shear forces in the flanges. These are given by:

$$Q_{fl} = \frac{\delta M_{fl}}{\delta z} = -EI_{fl}\frac{h}{2}\phi'' \tag{2.15}$$

The shear forces is a result of parabolic distributed shear stresses over the width of the flanges, (see Figure 2.9b). These shear stresses, which are constant over the thickness of the flanges are called warping shear stresses, τ_w, and are caused by the constraints. The warping torque, T_w, is the resultant of the shear stresses acting on both flanges.

$$T_w = Qh = -E(I_{fl}\frac{h^2}{2})\phi''' \tag{2.16}$$

where $I_{fl}\dfrac{h^2}{2}$ is the sectional moment of inertia, $I_{\Omega\Omega}$

The resulting torque, T, for the beam in this case, therefore becomes an differential equation of equilibrium and can generally be written as:

$$T = T_s + T_w = -EI_{\Omega\Omega}\phi''' + GI_t\phi' \tag{2.17}$$

which results in the following expressions for the St. Venant torque:

$$T_s = T - T_w = T[1 - \frac{cosh(k(l-z))}{cosh(kl)}] \tag{2.18}$$

Where:
$$k^2 = \frac{GI_t}{EI_{\Omega\Omega}} \tag{2.19}$$

From Equation 2.18, it comes clear that a consequence of the constraints at the left end of the beam, is that the magnitude of the warping is not the same for all sections, but varies from maximum at the free end to zero at the constrained end. The warping shear stresses τ_w also give rise to shear deformations which will affect the magnitude of warping. However in classical, approximate theory of torsion these shear stresses are neglected. Hence, the warping in the flanges is assumed to be proportional with the twist, as in the case of a free I-beam.

$$w = -\phi'\frac{h}{2}s \tag{2.20}$$

Another consequence is that the constraints at the left end of the beam, give rise to normal strains in the longitudinal direction of the flanges, and hence, also corresponding normal stresses. The resultant of these normal stresses due to warping is called the bimoment and has the dimension $(force)(length)^2$.

2.4.4 Warping Bimoment

If a cross section is warping restrained, warping shear stresses arises. These warping shear stresses will cause shear deformations, which again affects the magnitude of warping deformations. However, this is hard to account for. Thus, shear stresses are neglected in classical, approximate theory of torsion (Haslum and Tonnessen; 1973). This can be compared with neglection of shear lag in bending of beams. Warping restraints causes warping normal stresses in addition to the shear stresses. The resultant of these normal stresses is called bimoment, since it is a pair of equal and opposite bending moments acting on parallel planes (Shama; 2010). Figure 2.10 illustrates a warping bimoment acting on the flanges of an I-beam. The value of the bimoment is proportional to the second derivative of the rotational angle, ϕ'', and is at it's largest at the supports. If the bimoment is zero, St. Venant's principle can be used when considering an equilibrium group of normal stresses (Haslum and Tonnessen; 1973).

To get a better understanding and explanation of the effect of a moment and an axial force acting on an open cross section, and hence the bimoment, the analogy between torsion and the more well known bending theory has been consulted. The analogy between torsion and bending is included in Appendix A.
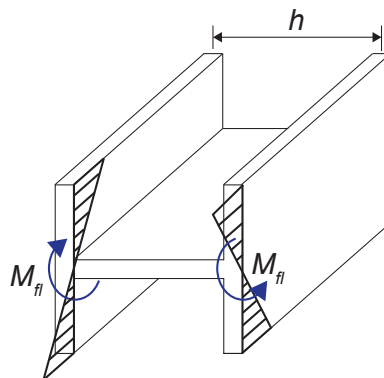
Figure 2.10: Bimoment acting on the flanges of an I-beam

2.5 Torsion in Container Ships

For closed ship structures, classical theory for torsion of thin-walled beams may be applied to analyse the ship structure with respect to torsion. This method is simpler to use, and less time-consuming than a finite element analysis of the same ship structure. The finite element analysis gives greater accuracy. However, analysis done with classical theory for torsion gives a relatively accurate result. It also gives the possibility of analysing several alternatives in early design stages. (Haslum and Tonnessen; 1973). However, ship types consisting of open cross sections such as container ships are more complicated. It is therefore important to notice that the formulas from Section 2.3, only gives a rough estimate.

In reality, container ships have closed cells between the cargo holds, which will stiffen the hull structure and give lower shear stresses than estimated. However, for a container ship, shear stresses will still be considerably higher and the hull structure weaker with respect to torsion, than for a ship with closed cross-section.

To keep the stresses in a container ship at an allowable stress level, it is necessary to stiffen the ship structure against torsional stresses. This is done by building powerful transverse or vertical girders, often called "torsion boxes" and transverse deck strips between the hatch openings. In addition, hatch covers or hatch coamings can contribute to transverse stiffening of a container ship, see Figure 2.11. Transverse girders, hatch covers and hatch coamings, together with double bottom and double sides will give an increased torsional stiffness relative to the calculations carried out in Section 2.3.
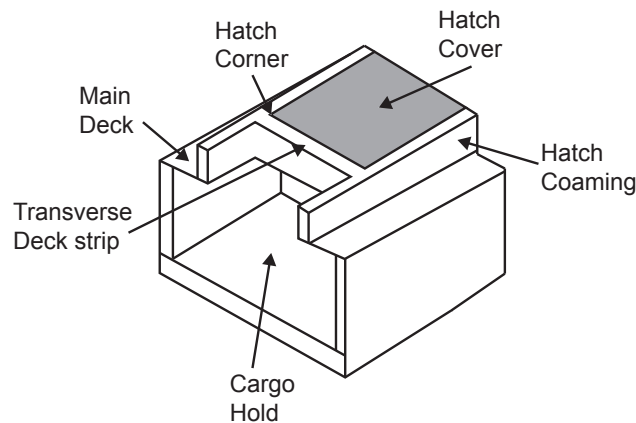
Figure 2.11: Container ship - Definitions

Several forces are acting on a ship hull girder, among others; shear loading, torsional moments, bending moments and transverse, and local loading. The magnitude and distribution of torsional moments along the ship length is mainly dependent on how the cargo is distributed over the breath and the length of the ship. In addition, the direction of the ships forward thrust relative to the incoming waves, will influence the magnitude and distribution of torsional moments. The magnitude of torsional moment's increases noticeably when the ship structure is exposed to oblique sea, and becomes important for ships with open structures, such as container ships. Figure 2.12 illustrates a ship sailing in oblique sea.
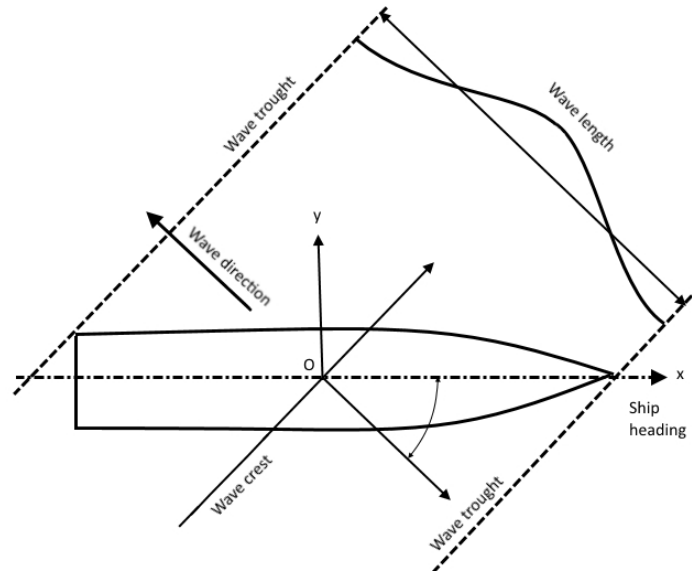
Figure 2.12: Ship sailing in oblique waves

Torsional moments are, as mentioned in Section 2.4, divided in Saint Venant torsional moments, T_s, and warping moment, T_w. The torsional loading on a ship hull girder can therefore be found by composing the two moments (Shama; 2010):

$$T = T_s + T_w \tag{2.21}$$

However, in most practical cases, one of the components may be neglected since the other component is of greater significance. Since Saint Venant torsion is only valid for closed cross sections, this term can be neglected in analysis of the ship hull girder of container ships.

All external forces acting on a ship hull will produce torsion, unless the force is acting through the axis of the shear center of the ship. This implies that all ships are

exposed to torsional moments along the ship length. However, open ships are exposed to an additional torsion loading induced by the horizontal component of the shear force. This because the shear center is located beneath the ship hull. These torsional moments tend to twist the hull girder, which induces warping stresses. These stresses may lead to increased stress concentrations, i.e. hot-spot stresses, close to hatch corners. Torsional stiffness of the hull structure is normally with regard to prevent excessive deformations of the structure. However, as container ships are built larger and larger, torsional stiffness of the ship hull decreases and hence torsional deformations becomes of greater importance.

A ship can be exposed to still-water torsion moments due to the load distribution of cargo and fuel. Therefore, it is of great importance that cargo and fuel is properly loaded. In addition, as already mentioned, torsional moments increases noticeably when the ship is exposed to oblique sea. Torsional moments from oblique sea is a result of wave-induced torsion. When a ship is exposed to wave-induced torsion, vertical bending moments lowers, whereas horizontal bending moments and torsional moments increases, compared to when the ship is sailing in head sea. A seagoing vessel is subjected to torsional moments due to both hydrostatic and hydrodynamic forces, including slamming. Furthermore, mass-acceleration forces due to the ship motions also influence the torsional moments on a seagoing vessel. According to Shama (2010) a large dynamic influence of rolling has been shown on the induced torsional loading in model experiments.

In Figure 2.13 the most important stress components acting on the hull girder of a container ship are shown. These stresses are (DNV; 2013b):

- Design still water bending moment and vertical wave bending moment due to hogging

- Horizontal bending moment

- Warping, induced by wave and still water torsional moments

- Bending of deck strips, as a result of wave and still water torsional moments

The first three bullet points, have components in the longitudinal direction, and are effects that are taken into account when estimating the combined longitudinal stress in oblique sea. Container ships are hogging vessels and design still water vertical hogging bending moments are therefore of greater importance than sagging bending moments. Since the sagging moments are of minor significance compared to hogging moments, it is adequate to calculate combined stresses applying only vertical hogging bending moments (DNV; 2013b).
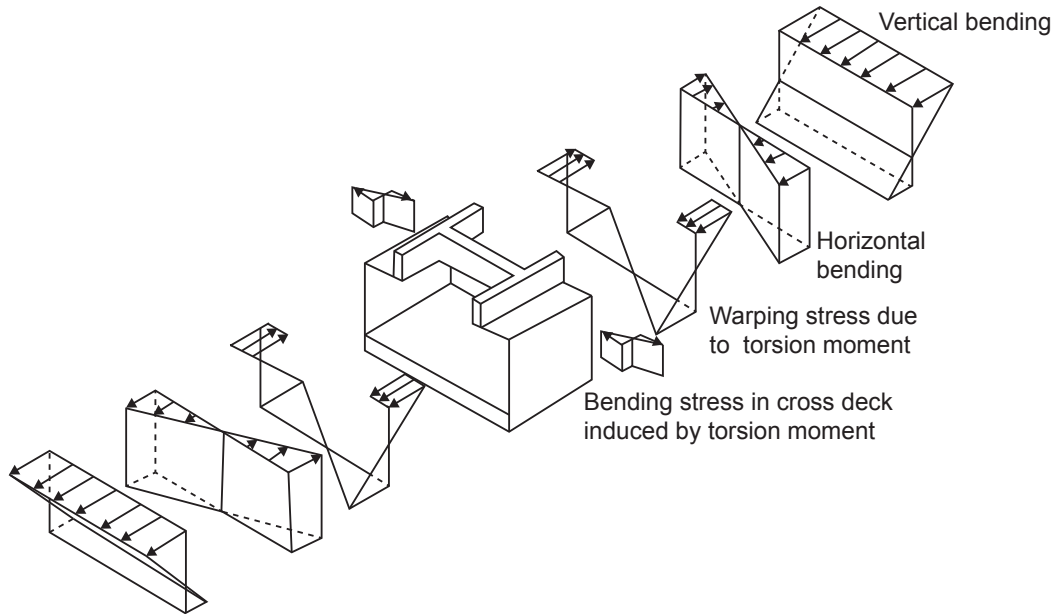
Figure 2.13: Stresses acting on a container ship in torsion (DNV; 2013b)

In container ships, the torsional strength and rigidity depends primarily on the structural arrangement in the parallel middle body of the cargo space. Torsional strength and rigidity also depends on the structural arrangements of both ship ends, which induces constraints, e.g. the deck house and forecastle. Furthermore, the distribution of torsional loading over the length of the ship, which is illustrated in Figure 2.14, is given by Equation 2.22. The equation does not provide the exact torsional distribution, but can be used as a simplified approach during early design stages (Amdahl; 2010).

$$T = \frac{T_0}{2}(1 - cos(2\pi\frac{x}{L})) \tag{2.22}$$

Where T_0 is the Torsional moment at the midship section and L is the rule length.

The torsional distribution along the length of the ship, is important with respect to torsional strength and rigidity of container ships. The figure also illustrates the extent of the ship sections, which can be assumed to have closed and open cross sections. The torsional response of a ship structure, in terms of twist of the ship and the warping deformation, is found to be a function of the extent of open sections over the length of the ship, the degree of torsional rigidity of the ship structure at both ends and the geometry of transverse section (Shama; 2010).
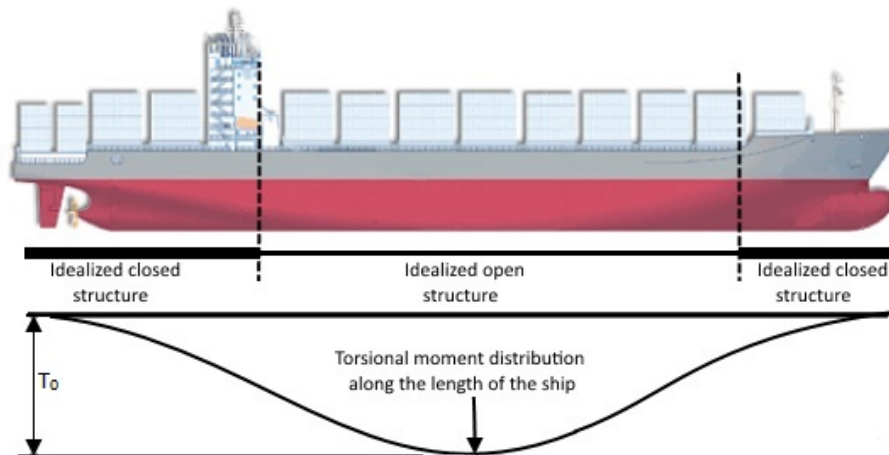
Figure 2.14: Distribution of torsional moment along the length of a container ship

2.5.1 Warping Deformation in Deck and Deck Strips

At both ends of the ship, the cross section is closed to make space for necessary equipment, such as machinery etc. The result is an increased stiffness and rigidity at both ends of the ship. In addition, the superstructure will contribute to stiffen the after ship, whereas e.g. the collision bulkhead gives extra stiffening in the fore ship. This increased stiffness and rigidity will form virtual constraints at both ends of the ship. The warping deformation of the deck structure in a container ship depends on these virtual constraints. Further, the rigidity of deck strips between holds will influence the magnitude of the warping deformations in the deck structure, including the deck strips. In addition, both horizontal and vertical torsion boxes in the cross section will affect the greatness of the warping deformation of deck and deck strips. However, torsion boxes are three times less effective in reducing warping than the transverse deck strips (Haslum et al.; 1973).

The magnitude and distribution of the torsional loading a ship is exposed to will naturally decide the greatness of the induced stresses acting in the deck structure. This again, causes warping deformations. In other words, the magnitude of warping deformations in the deck structure and in the ship hull girder in general is also dependent on the distribution and greatness of the torsional moment acting on the ship. Warping in a container ship will lead to a typical "S-formed" deformation of the deck stips, as illustrated in Figure 2.15. Due to the virtual constraints at the boundary between the deck house and the first cargo hold, which fixes the structure against rotation and deformation at this point, the warping deformation is zero. This is indicated in Figure 2.15c.

24
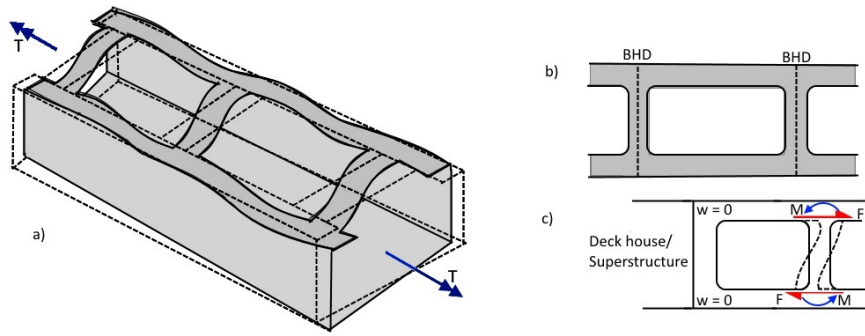
Figure 2.15: Warping deformation in deck and deck strips of container ships

2.5.2 Warping Deformation of Ship Sides

The warping of the ship sides, which are subjected to torsion, are mainly restrained by cross sectional variations and the distribution and magnitude of the torsional loading along the length of the ship. In addition, an extra significant warping resistance may be present due to internal transverse structures. External bimoments (see Subsection 2.4.4 and Appendix A) acting at discrete points along the ship hull can be used to account for the effect of such structures (Haslum and Tonnessen; 1973).
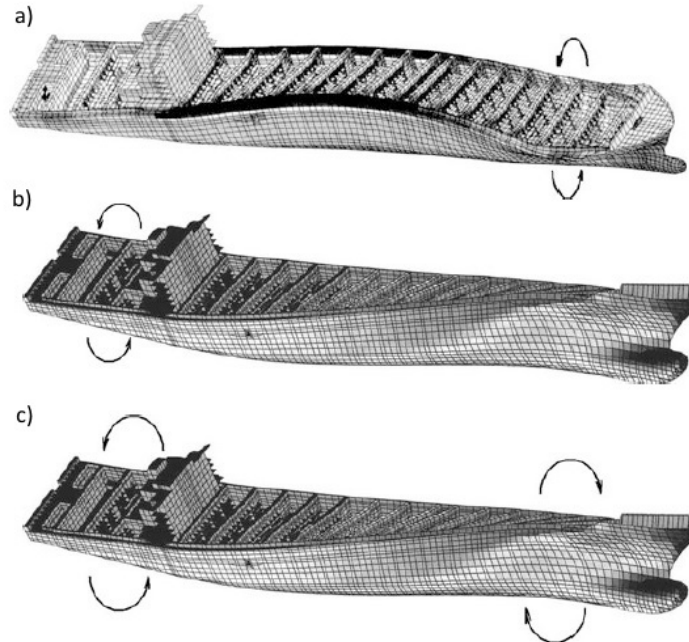
Figure 2.16: Deformation of a container vessel exposed to torsion (Shama; 2010)

Figure 2.16, shows a deformed container ship due to a torsional moment acting in the fore ship (a), in the aft ship (b) and at both ends (c), respectively.

2.6 Load Conditions Creating Torsional Moments

Different load conditions can create torsional moments with different magnitudes. As mentioned in Section 2.3, forces that do not pass through the shear center axis of the cross section of the ship hull, causes torsion. Torsional moments acting on a ship structure can mainly be divided in static (still water) torsion and dynamic (wave induced) torsion. Non-symmetrical cargo loading over the breadth of the vessel causes still water torsional moments. Since transport of containers is mostly well planned, and hence container ships are usually fully and evenly loaded over the ship breadth, still water torsional moments are most important in port during loading and offloading. (Paik et al.; 2001)

Wave induced torsion acts on the ship during transit, and is caused by non-symmetrical distribution of hydrodynamic and hydrostatic forces over the breadth of the ship. Additionally, mass acceleration forces will arise due to the motion of the ship and will contribute to dynamic torsional moments. Since container ships are normally evenly loaded over the breadth of the ship, the dynamic torsion due to the ship's motions becomes dominant. The magnitude of wave induced torsional moments depends on among others, the shape of the hull structure, the heading profile of the vessel relative to the waves, wave height and the location of the shear center. In seaway, wave induced torsional moments are of greatest magnitude if the vessel sails into oblique waves (Shama; 2010). When a container vessel encounters oblique waves with wave lengths roughly between 60 % and 80 % of the ship length, the torsional moments are of its greatest. However, the maximum vertical wave bending moment is improbable to occur synchronously with the maximum wave torsional moment and maximum horizontal wave bending moment (DNV; 2013b). In other words, vertical wave bending moments are reduced, whereas torsional moments and horizontal bending moments are increased.

Theoretical and numerical analysis, together with full scale measurements, indicates that torsion induced shear stresses will reduce the ultimate bending moment of the ship hull (Paik et al.; 2001). From the same analysis, it was found that for ductile hull materials there is only a minor influence of torsion induced warping stresses on the ultimate hull girder bending strength. Warping stresses have minor effect on ultimate torsion strength as long as elastic buckling is prevented and warping restraints are ensured (Paik et al.; 2001). However, it should be noted

that warping may affect the torsional stiffness of the hull structure significantly. Furthermore, it is seen from analyses that as long as the magnitude of torsion is not major, torsion is not a sensitive load component when it comes to affecting ultimate vertical bending moments of ship hulls. Nevertheless, if the torsional rigidity of the ship hull is small, the ultimate bending stress of the ship hull can decrease significantly if the torsional moments are large.

2.7   Investigation of Torsion at Design Stage

There are different methods for studying torsional behaviour of container ships, depending on how far the ship is in its design process. Both using finite element formulations and experimental methods, such as model testing, can be used to estimate the magnitude of torsional stresses and deformations of a ship structure. However, these methods are time consuming and expensive, and are therefore mostly used for analysis of critical areas of the ship structure during late design stages, to ensure that the structural integrity is maintained (Shama; 2010).

At early design stages it is sufficient to use a simplified approach to estimate torsional behaviour of the ship structure. This simplified approach is based on torsional behaviour of thin walled cross sections. However, the results from a simplified approach may become inaccurate, and correlation with full-scale measurements from similar ships is necessary to verify the validity of the results (Shama; 2010).

2.8   Wave Loads and Wave Induced Vibrations

Global wave loads acting on the hull structure are important for larger ships. These wave loads causes among others wave-induced bending moments, shear forces and torsional moments (Faltinsen; 1993). However, global wave loads are also sources to more specific problems. For example when a ship sails in head sea, vibrations in the hull girder are induced. These vibrations are induced due to interaction between the hull structural response and the wave loads. A ship structure is elastic, which implies that the structure can and will distort if it is exposed to loads, such as wave loads. Since the ship structure is not rigid, this affects the hydrodynamic loading and the structure will respond to these loads by deforming or vibrating, which are hydro elastic effects. The vibration stresses are caused by resonance vibrations and transient elastic vibrations, which respectively are called springing and whipping (Storhaug; 2013a). For large container ships, vibrations owing to

torsion may also occur (Storhaug; 2012). Whipping and springing is not yet implemented in ship design rules. One reason might be that hydro elastic effects are problematic to handle and even the best tools are neither very reliable nor efficient in use (Storhaug; 2013a).

The relative importance of whipping and springing for a specific ship varies, and is dependent on the wave condition, load condition and the choice of ship design. Due to low damping it may be difficult to distinguish whipping and springing (DNV; 2014a). Both whipping and springing mainly occurs when a vessel sails in bow quartering to head sea (see Figure 2.17) and the vibration increases in rough seas (Storhaug; 2013a). In addition, the two phenomena appear more or less simultaneously and continuously. Hence, from a fatigue consequence point of view they are commonly refereed to as wave induced vibrations (DNV; 2014a).
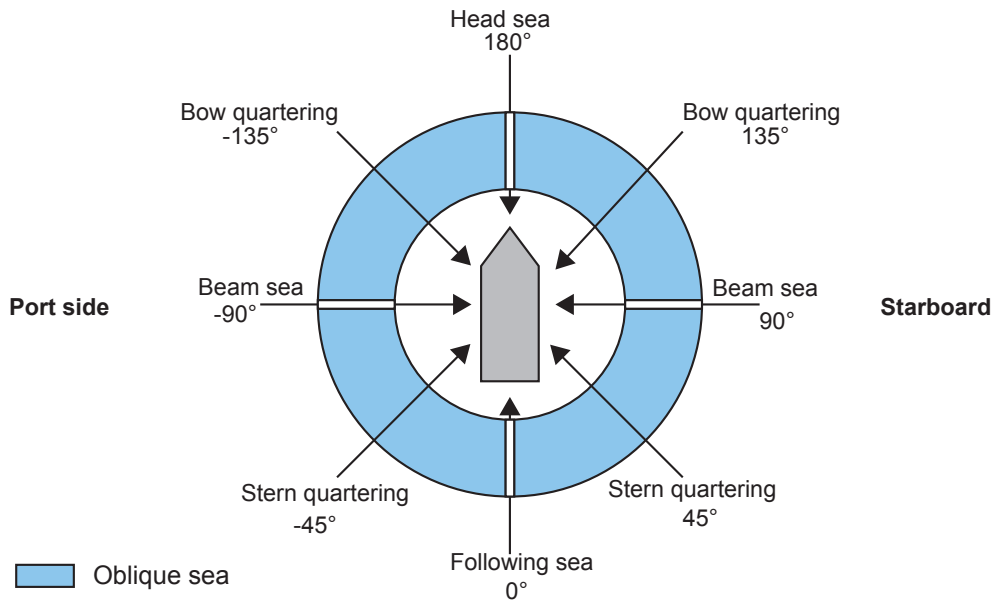
Figure 2.17: Definition of heading angles

2.8.1 Springing Induced Stresses

Springing is a phenomenon which is caused by linear and non-linear excitation mechanisms and results in steady-state elastic vibrations. Oscillating loads along the hull causes linear springing and gives resonance when the meeting frequency of the hull corresponds to the lowest natural frequency of the hull girder, also called the springing frequency (Storhaug; 2013a). Springing is triggered during wave

conditions with small wave lengths compared to the ship length, and arises due to resonance vibrations in heave, pitch and roll (Faltinsen; 1993). Non-linear springing occurs due to 2nd order sum-frequency effects, for example when the springing frequency is two times the encounter frequency of the waves. Structural designs which can trigger non-linear springing are non-vertical ship sides, bow reflection and the bulb (Storhaug; 2013a).

Figure 2.18 shows measured springing vibrations for the 8600 TEU vessel investigated in the thesis work, December 2, 2010. High frequency signals are plotted against low frequency signals. The stress level is low for both stress signals. From the figure it can be seen that for each cycle of low frequency (wave response) signals, there are approximately 5 cycles of high frequency (vibration response) signals, which indicates that linear springing is present.
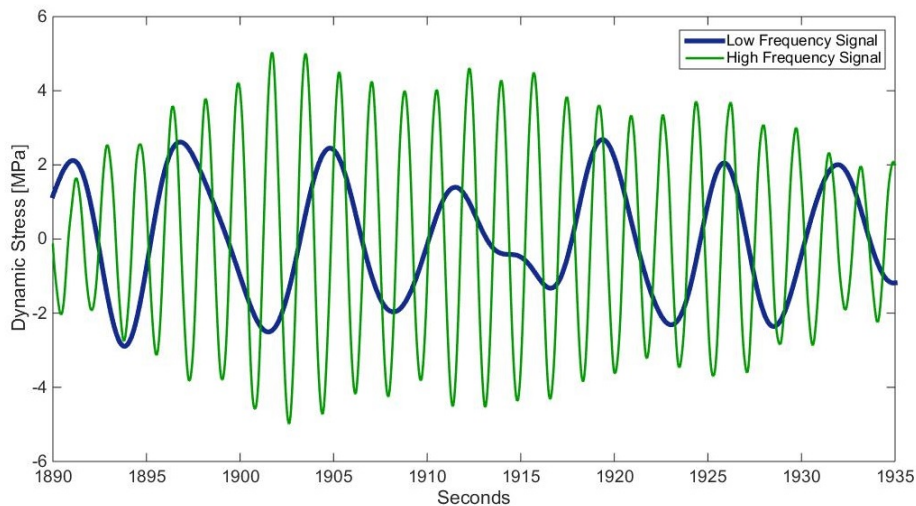
Figure 2.18: Measured linear springing vibrations

Resonance vibrations due to springing are limited by damping. For large container ships the damping is high since the damping is affected by the number of containers on board. This implies that springing vibrations lower, the larger the ship is. For large container ships, resonance vibrations due to springing are therefore relatively low and hence not of particular concern. For this reason, vibrations owing to whipping are of greater importance than vibration due to springing when it comes to large container vessels (Storhaug; 2013a).

2.8.2   Whipping Induced Stresses

Whipping describes the phenomenon where transient elastic vibrations occurs due to non-linear excitation such as wave impacts. In addition, for large container ships whipping can be induced as a result of slamming. This because of the pronounced bow and stern flare on large container ships, which especially at design draft, causes slamming impacts more frequently (Kahl et al.; 2014). Slamming refers to impacts between the liquid and the structure and has consequences for both local structural integrity and global elastic behaviour (Faltinsen; 1993). Slamming can be physically observed even with an untrained eye since it generates water spray, particularly during sea states with head sea and steep waves (Storhaug; 2013a). Whipping contributes to fatigue and gives high maximum stresses, and is also of concern when it comes to operation and comfort. Figure 2.19 shows measured whipping vibrations for the 8600 TEU container vessel. From the figure it can be seen that whipping occurs in sagging (negative values) at about 3390 seconds.

The whipping response tend to increase with the square of the ship speed. Hence, lowering the speed in sea states where whipping occurs is of significant importance when it comes to fatigue damage and risk of collapse. Whipping is commonly assumed to contribute to collapse, although this is not yet confirmed (Storhaug; 2013a).
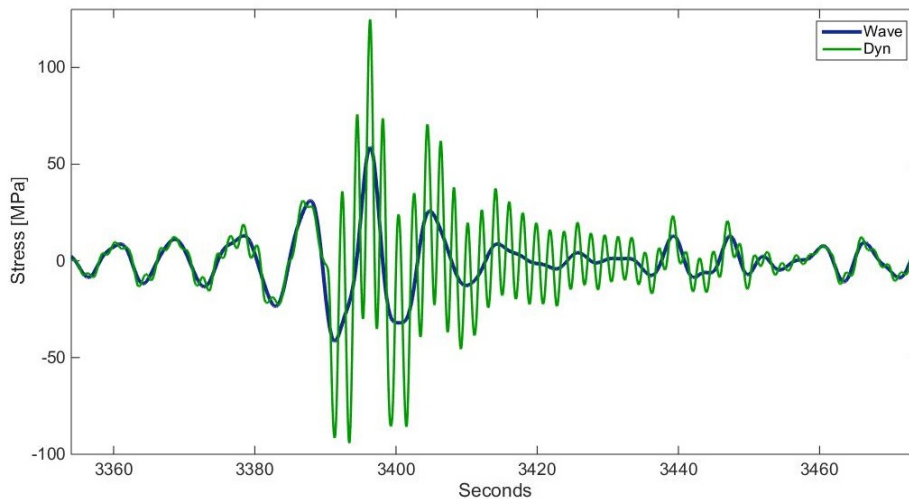
Figure 2.19: Whipping vibrations measured on the 8600 TEU container vessel

3   Ship Rule Requirements

Over the last century, multiple class societies have been established. The classification societies have developed rules for structural design of ships and offshore structures, with the aim of preventing accidents at seas. All recent accidents, such as the MSC Napoli accident in 2007, are investigated and reported, and then used as basis for developing new rules to avoid similar accidents in the future.

Different class societies have developed rule requirements for Ultimate Limit State and fatigue control of ship structures. This, to safeguard a ship against structural collapse and to ensure that all parts of a hull structure that is exposed to dynamic loading, and hence fatigue, have sufficient strength and fatigue life. DNV GL is the world's leading ship and offshore classification society, which is continuously working on further development of existing ship rules, as well as formulating new guidelines for implantation of e.g. wave induced vibrations and torsion in future ship rules.

DNV GL have split their service documents into several categories. The main category includes the ship rules for classification. These rules must be followed in the approval process. Several subcategories, such as Classification Notes, Recommended Practices and Standards, can be refereed to in the ship rules. If a subcategory is refereed to in the ship rules, these categories are governing rules and must be fulfilled. Otherwise they are only considered as recommendations. In this chapter, rule requirements with respect to fatigue and ultimate strength, developed by DNV GL, are introduced.

In the following, a review of the relevant rule requirements found in among others, *DNV Rules for Classification of Ships - Hull Structural Design 100 meters and Above* (DNV; 2004) and in accompanying Classification Notes; *Strength Analysis of Hull Structures in Container Carriers* (DNV; 2013b), *CSA - Direct Analysis of Ship Structures* (DNV; 2013c) and *Fatigue Assessment of Ship Structures* (DNV; 2014a), are presented.

3.1   Ultimate Limit State - *ULS*

The Ultimate Limit State is defined as the limit where the structure or a part of the structure exceeds the design requirement for ultimate resistance for carrying loads (DNV; 2014b).

The Ultimate Limit State can be exceeded due to several failure modes, among others:

- Excessive yielding or buckling, causing loss of structural resistance.

- Component failure due to brittle fracture.

- Excessive deformation or collapse causing transformation of the structure into a mechanism.

- Ultimate deformation of components or exceeding the ultimate resistance, causing failure of critical components.

- Capsizing or similar, due to loss of static equilibrium of the structure.

Ultimate capacity limits of hull structural elements in the cargo region, such as plating, stiffeners, brackets, stringers and girders shall be assessed in ULS analysis. In addition, the analysis shall cover assessment of dimensioning against material yield and buckling and ensure sufficient global strength. The latter, to prevent compartment flooding, ductile hull skin fracture and hull girder collapse (DNV; 2013c).

There are three different analysis levels for assessing torsional ULS on container vessels, depending on the ships dimensions, see Table 3.1.

Table 3.1: Analysis levels - Torsional ULS

	Level 1	Level 2	Level 3
Type	Rule calculation	Extended Rule calculation	Comprehensive analysis
Mandatory torsional ULS calculations	Rule torsional calculation for longitudinal members and hatchway corners	Global FE analysis for Rule torsional load cases	Global FE analysis with direct calculated wave loads.
Remarks	Intended for container ships with $B \leq 40m$	Mandatory for container ships with $40m < B \leq 52m$	Mandatory for container ships with $B > 52m$

Since Level 1 analysis is intended for container ships with breath less than 40 meters, ans only covers ULS in longitudinal members, this analysis will not be further described in this thesis.

3.1.1   Level 2 Analysis - Rule Torsional Moments

In a Level 2 analysis, rule torsional moments are used in ULS calculations. The rule torsional wave moment acting on the length of the ship, M_{WT1} and M_{WT2}, are calculated as follows:

$$M_{WT1} = M_1 + M_2 \qquad (3.1)$$

$$M_{WT2} = M_1 - M_2 \qquad (3.2)$$

Where M_1 and M_2 are given as:

$$M_1 = K_{T1}L^{5/4}(T + 0.3B)C_B z_e \qquad (3.3)$$

$$M_2 = K_{T2}L^{4/3}B^2 C_{SWP} \qquad (3.4)$$

z_e is measured at the midship section and is the distance in meter between the shear center and to a distance $0.7T$ above baseline. The water plane area coefficient, C_{SWP}, is defined as:

$$C_{SWP} = \frac{A_{WP}}{LB} \qquad (3.5)$$

where A_{WP} is the water plane area, given in square meters, at draft T.

K_{T1} and K_{T2} is given as follows:

$$K_{T1} = 1.40 sin(2\pi \frac{x}{L}) \qquad (3.6)$$

$$K_{T2} = 0.13(1 - cos(2\pi \frac{x}{L}) \qquad (3.7)$$

The resulting torsional moment distribution along the length of the ship is illustrated in Figure 3.1.

33
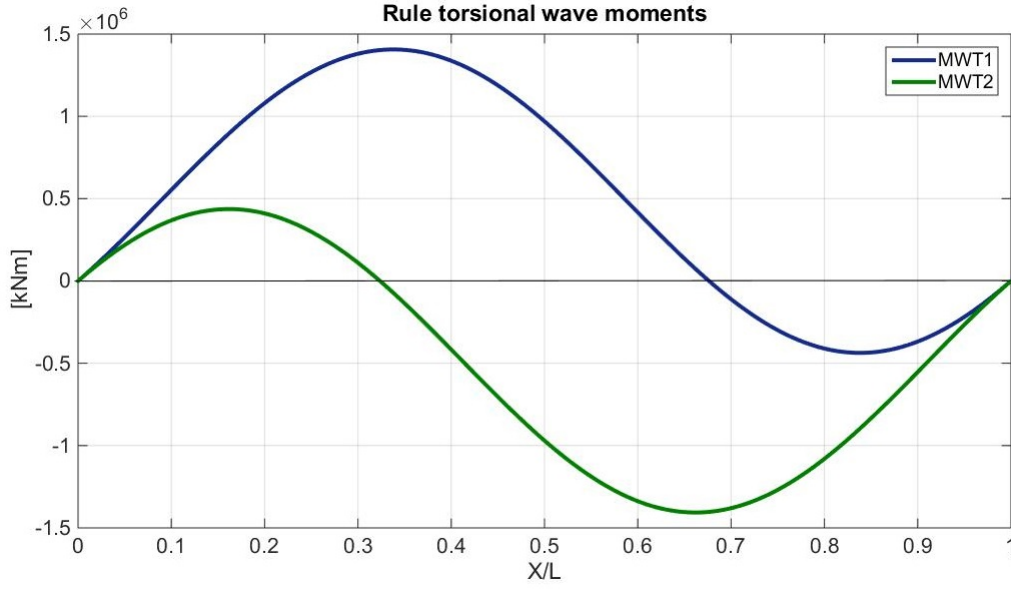
Figure 3.1: Distribution of rule wave torsional moments along a container carrier

The rule still water torsional moment distribution along the length of the ship is assumed to be the same as for the wave torsional moment. The maximum value of the torsional moment can be taken as:

$$M_{ST(max)} = 0.3LB^2 \tag{3.8}$$

As for the wave torsional moments, two different moment distributions shall be applied for the torsional still water moments, namely M_{ST1} and M_{ST2}:

$$M_{ST1} = \frac{M_{ST(max)}M_{WT1}}{M_{WT1(max)}} \tag{3.9}$$

$$M_{ST2} = \frac{M_{ST(max)}M_{WT2}}{M_{WT2(min)}} \tag{3.10}$$

There are two load cases covering ULS due to torsion. They are as follows:

$$LC_{H\&T1} = M_{WH} + M_{WT1} + M_{ST1} \tag{3.11}$$

$$LC_{H\&T2} = M_{WH} + M_{WT2} + M_{ST2} \tag{3.12}$$

Where M_{WH} is the horizontal wave bending moment. However, the horizontal wave bending moment does not induce any stresses in cross decks (see Figure

34

2.13), and can be neglected when checking transverse deck strips with respect to ULS. Hence, the load cases can be simplified to:

$$LC_{T1} = M_{WT1} + M_{ST1} \tag{3.13}$$

$$LC_{T2} = M_{WT2} + M_{ST2} \tag{3.14}$$

A global coarse Finite Element model is used in the Level 2 analysis. The torsional moment distribution for each load case is applied to the FE model by using coupled vertical forces acting in opposite directions, along the length of the ship. These force couples are applied as point loads at the second deck in the FE model, as shown in Figure 3.2. The forces are defined positive pointing upwards at port side and downwards at star board side, and can be calculated from Equations 3.15 - 3.17.
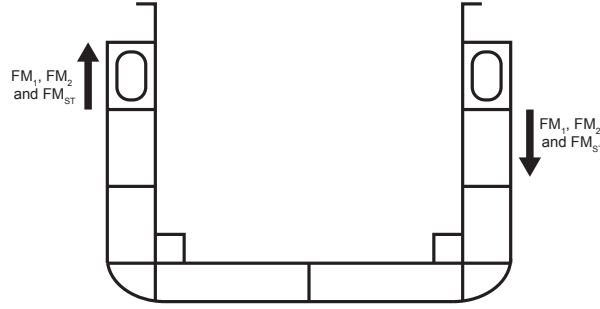
Figure 3.2: Application of torsional moment by coupled vertical forces

$$F_{M1} = -\frac{M_1(x_2) - M_1(x_1)}{b} \tag{3.15}$$

$$F_{M2} = -\frac{M_2(x_2) - M_2(x_1)}{b} \tag{3.16}$$

$$F_{MST} = -\frac{M_{ST}(x_2) - M_{ST}(x_1)}{b} \tag{3.17}$$

b is the breadth of the ship at the position where the force is applied and x_1 and x_2 are given as follows:

$$x_1 = x - \frac{s_{aft}}{2} \tag{3.18}$$

$$x_2 = x - \frac{s_{fwd}}{2} \tag{3.19}$$

Where s_{aft} and s_{fwd} is the spacing in meter between the web frame considered and the adjacent web frame aft or forward, respectively. x is the distance in meter from AP to the considered web frame.

3.1.2 Level 3 Analysis - Design Torsional Moments

A linear global Finite Element model is used in the design assessment of local *ULS*. A loading condition and a governing wave condition/ sea state, defines a specific design condition.

The vessels loading manual is used as basis when the design loading conditions are determined. For a container ship, following loading conditions should be analysed (DNV; 2013b):

- Minimum or maximum still water sagging moment midships. Generally in ballast condition.

- Maximum still water hogging moment midships. Generally with a container loading condition, which is light homogeneous and on scantling draft, with maximum TEU.

- Container loading condition. Generally heavy homogeneous, with scantling draft, and maximum Metacentric height, *GM*. The latter because high *GM* values gives larger roll angles and accordingly higher torsional moments.

The governing wave condition/ sea state, i.e. the dynamic loads, are established based on a long term distribution of motions. The motions a ship will experience during its operating life, normally assumed to be 20 years, forms the basis of this long term distribution. In the North Atlantic, this corresponds to a maximum wave response with an probability of exceedance of 10^{-8}. Any significant effects due to yaw, sway, surge, heave, roll and pitch in irregular waves are included. The the occurrence of different heading angles are usually assumed to be uniformly distributed (DNV; 2004).

Dynamic loads and loading conditions are to be chosen in such way that they together represent the most critical structural response. For various failure modes or parts of the structure being analysed, different combinations of dynamic loads and loading conditions may result in the "worst case". Therefore, it is important to first choose what to be analysed, then choose dynamic loads and loading conditions accordingly, such that maximum response is ensured (DNV; 2013c).

The chosen loading condition and dynamic loads are used as inputs in a hydrodynamic analysis. This, to obtain the design waves and design stresses associated with the respective loading condition and dynamic loads. The dynamic loads and loading conditions estimated through the hydrodynamic analysis, are then transferred into a structural FE model.

3.1.3 Finite Element Analysis

After the loads are calculated, using either Level 2 or Level 3 analysis, and applied to the FE model, a linear nominal stress assessment is performed. The nominal stresses are to be compared with the values for material yielding and buckling (see Subsections 3.1.4 and 3.1.5) (DNV; 2013c). For areas with high peak stresses, such as hot spot stresses, local models with fine meshes must be applied. The nominal stresses obtained from the FE analysis can be divided into different stress components, as listed below (DNV; 2013c):

- Hull girder bending moment

- Hull girder axial loads

- Hull girder shear force

- Hull girder effects due to warping and torsion

- Bottom/ double side bending

- Local bending of plates

- Local bending of stiffeners

- Transverse stresses due to sea pressure and cargo

- Transverse and shear stresses due to double hull bending

- Other stress effects due to local design such as cut outs, misalignments etc.

3.1.4 Acceptance Criteria - Yield Check

The yield check is based on the flow of nominal stresses in the structure and the acceptance criteria for allowable equivalent von Mises membran stress is given in formulas 3.21 - 3.22 (DNV; 2013b).

Formula 3.21 and 3.20 gives the acceptance criteria for longitudinal members when interaction between hatchway cover and main hull structure is, and is not, included in the stress calculation, respectively.

$$\sigma_{all} = 0.9\sigma_f \tag{3.20}$$

$$\sigma_{all} = 0.95\sigma_f \tag{3.21}$$

For transverse members, such as a deck strip between two cargo holds, the acceptance criteria for allowable nominal stress is given as:

$$\sigma_{all} = 0.85\sigma_f \tag{3.22}$$

where σ_f is the minimum upper yield stress for the material and σ_{all} is the equivalent von Mieses stress, σ_{eq}, which is given as (DNV; 2014c):

$$\sigma_{eq} = \sqrt{\sigma_x^2 + \sigma_y^2 - \sigma_x\sigma_y + 3\tau_{xy}^2} \tag{3.23}$$

where σ_x and σ_y are stresses in x- and y-direction respectively, whereas τ_{xy} is the shear stress in the xy-plane. Out of plane bending is neglected.

3.1.5 Acceptance Criteria - Buckling Check

The buckling check is based on compressive nominal membrane stresses in the bilge area and the stool bench area. The compressive nominal stresses are found from an *ULS* analysis with a coarse global FE model. An uni-axial assessment of buckling, σ_c, is performed in accordance with the following requirements (DNV; 2013b):

$$\sigma_c \geq \frac{\sigma_a}{\eta} \tag{3.24}$$

where σ_a is to be taken as the compressive stress in plate panels. In the case of linearly varying stresses across the plate panel, the largest stress in the plate panel shall be considered (DNV; 2004). σ_a has to fulfil the acceptance criteria for material yielding, $(\sigma_a = \sigma_{all})$ given in formulas 3.21 - 3.22 in Section 3.1.4. η is to be taken as described below (DNV; 2013b):

$$
\begin{aligned}
\eta \quad &= \quad 0.85 \quad &&\text{for longitudinals} \\
&= \quad 0.9 \quad &&\text{for transversely stiffened side plating, bottom and inner bottom} \\
&= \quad 1.0 \quad &&\text{for longitudinally stiffened side plating, deck and single bottom}
\end{aligned}
$$

3.2 Fatigue Limit State - *FLS*

Fatigue Limit State is defined as the limit when the structure, or part of the structure, experiences failure due to the effect of cyclic loading. An example of a fatigue limit state for a ship structure is cumulative damage due to repeated loads (DNV; 2014b).

The fatigue life of a structural detail can be estimated based on relevant fatigue damage data and can be used as basis when choosing the structural design, such as selection of steel, scantlings and local details. Estimated fatigue life can also be used when planning inspections of the ship during fabrication and operation.

According to DNV (2004), a fatigue assessment should be performed and supplemented by detailed fatigue analysis if necessary. This, to ensure that the structure will fulfil its intended function. Welded joints, attachments and other places where stress concentrations may arise, and be a potential source of fatigue cracking, should be considered individually.

3.2.1 Simplified Fatigue Calculations

Fatigue design can be carried out by methods based on estimation of cumulative damage. One method uses the approach of Miner Palmgren's rule, which assumes linear cumulative damage. Thus, the total damage is expressed as the accumulated damage from all load cycles at different stress levels, see Equation 3.25 (DNV; 2014a).

$$D = \sum_{i=1}^{k} \frac{n_i}{N_i} \leq 1 \tag{3.25}$$

Where
n_i = number of cycles at stress level i
N_i = number of cycles before failure
D = Accumulated fatigue damage

Fatigue life of a container ship is normally not to be less than 20 years when a fatigue assessment is performed. Accumulated fatigue damage during the life time of the vessel is not to exceed a usage factor of $D = 1$.

Fatigue damage can also be estimated based on fatigue tests such as SN data. A fundamental requirement for fatigue analysis is long term distribution of stress range. There are various ways to determine the long term stress range distribution.

However, in this review the focus is on a method assuming Weibull distribution for the long term stress ranges, see Equation 3.26. This assumption leads to a simple formula for fatigue damage calculation (DNV; 2014a):

$$Q(\Delta\sigma) = exp[-(\frac{\Delta\sigma}{q})^h] \qquad (3.26)$$

Load effects are found directly based on ship rules. Before entering the SN-curve, nominal stresses must be multiplied with appropriate stress concentration factors to calculate local hot spot stresses.

where:
$Q(\Delta\sigma)$ = Probability of exceedance of the stress range, $\Delta\sigma$
h = Weibull shape parameter
q = Weibull scale parameter

The different stress components can be calculated based on beam theory combined with respective stress concentration factors. Beam theory can be used since the stress response in plating and stiffeners is mainly subjected to axial loading due to hull girder loading, and local bending due to lateral pressure. Internal and external pressure loads cause local stresses and these should be combined with global stress components which are induced by hull girder wave bending. This stress combination must be applied for each loading condition. For container vessels, torsional stresses may have to be included. However, assessment of torsional strength at design stage is not properly clarified in today's classification rules.

After the long term stress distribution is found, using Weibull distribution for different load conditions, based on the calculated stress components, the cumulative damage of the ship structure can be estimated using an one-slope SN-curve, as illustrated in Figure 3.3.
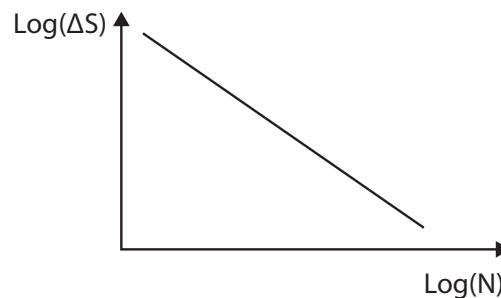
Figure 3.3: One-slope SN-curve

3.2.2 Level 2 Analysis - Rule Torsional Moments

Fatigue damage accumulation due to wave induced torsional moments are complex and therefore often neglected in analysis. However, the MSC Napoli incident proves that detailed investigation of structural response in container ships is necessary to ensure safety for these vessels. The concern with respect to fatigue resistance for container ships increases as the vessels are built larger and larger. This because of their huge hatch openings and their heigh service speeds. According to Li and Ringsberg (2012), the greatest fatigue damage usually occurs in head seas for the deck structure of container ships, whereas the greatest fatigue damage is in bow seas for the bilge area. In addition, analysis have shown that the ship speed has a significant impact on fatigue damage accumulation. From these analysis the torsional effect on fatigue damage accumulation seems to be of minor significance since torsional moments are of greater magnitude in oblique seas. However, this assumption needs to be further examined before drawing any conclusions.

Fatigue life assessment with respect to torsion, is performed with the same rule-defined torsional moments as calculated for ULS (described in Section 3.1.1). However, ULS calculations estimates the torsional moments on a 10^{-8} probability of exceedance, whereas fatigue assessment of container vessels uses a 10^{-4} probability of exceedance. Hence, a factor reducing the load from 10^{-8} to 10^{-4} probability level is introduced (DNV; 2013b).

$$M_{wt1} = f_r M_{WT1} \tag{3.27}$$

$$M_{wt2} = f_r M_{WT2} \tag{3.28}$$

Where the factor, f_r, to reduce the load from 10^{-8} to 10^{-4} probability level is defined as:

$$f_r = 0.5^{1/h_0} \tag{3.29}$$

h_0 is the long-term Weibull shape parameter, given as:

$$h_0 = 2.21 - 0.54 log_{10}(L) \tag{3.30}$$

It is also important to notice that today's rules do not take fatigue damage due to wave induced vibrations into consideration, but this may be estimated based on full scale measurements and weather data.

3.2.3 Uncertainties in Fatigue Life Predictions

There are several uncertainties related to predictions of fatigue life. It is difficult to calculate the loads acting on the ship due to uncertainties in distribution of waves, wave height and periods. This leads to uncertainties in calculated stresses. Since small changes in stresses results in a significant change in fatigue life, it is important to ensure that stresses are realistic.

Another uncertainty is related to determination of SN-curves. There is a scatter in the test results that are used as basis for estimation of SN-curves. This scatter are generally accepted and assumed to be caused by variations in weld imperfections within normal workmanship.

4 Full Scale Measurements

Full scale measurements are obtained by installing a system on board for instance ships or offshore platforms. The monitoring system is used to collect continuous time series and half hour statistics. By combining different strain sensors, global load components can be separated to find the relative importance of for example warping, axial stresses, vertical bending, horizontal bending and hatch opening distortion (DNV GL; 2013). Sensors may be applied to the hull structure, engines, shafts etc. and can provide essential information about structural strength, fatigue life time, vibrations, motions, comfort or environmental data.

The main objective with full scale measurements obtained from container ships, is to investigate how whipping, springing and warping stresses contribute to extreme loading and fatigue. This to document whether or not these effects must be included in ship design rules. The effects of wave induced vibrations on extreme loading and fatigue life may be increased due to several factors, among others; larger container ships, high tensile steel, climate changes and future trades due to widening of the Panama Channel (DNV GL; 2013). In addition, the hull monitoring system can be used to compare strains and stresses acting on the ship with allowable limits. Additionally, stresses can be controlled from the bridge, which may improve the quality of seamanship. (Storhaug; 2013b).

4.1 The 8600 TEU Container Vessel

The container vessel studied in this thesis (see Figure 4.1) is a relatively new Post Panamax ship, built in 2009. See Table 4.1 for main dimensions. The container ship has a pronounced bow flare angle and a high service speed.

Figure 4.1: The 8600 TEU Container ship analysed in this thesis

Table 4.1: Main particulars for the container vessel

Length overall	LOA	339.6 m
Length between perpendiculars	LPP	324.82 m
Rule Length	L	318.41 m
Breadth	B	45.6 m
Depth	D	24.6 m
Scantling draft	Ts	14.5 m
Design draft	T	13.0 m
Shear Center	SC	- 13.635 m
Service speed at design draft	v	26.8 knots
Bow flare angle	-	63°
Dead Weight	DWT	95 810 tonnes
Container Capacity	-	8 562 TEU
Block coefficient	C_B	0.621 [-]
Water plane area coefficient	C_{SWP}	0.825 [-]

Measurement data is collected during a time period from April 2009 to July 2014. During this period the vessel has been operating on two different trades. The vessel was first operating on a trade between Singapore and Hamburg, seen in Figure 4.2. The vessel was operating on this trade between April 2009 and October 2013.

Figure 4.2: The Vessels Trading route between April 2009 and March 2013

After October 2013 the vessel began operating on a new trade, from Singapore to USA, see Figure 4.3. This is the vessels current trade. The weather and wave environment on this route is more harsh than for the route between Hamburg to Singapore.

44
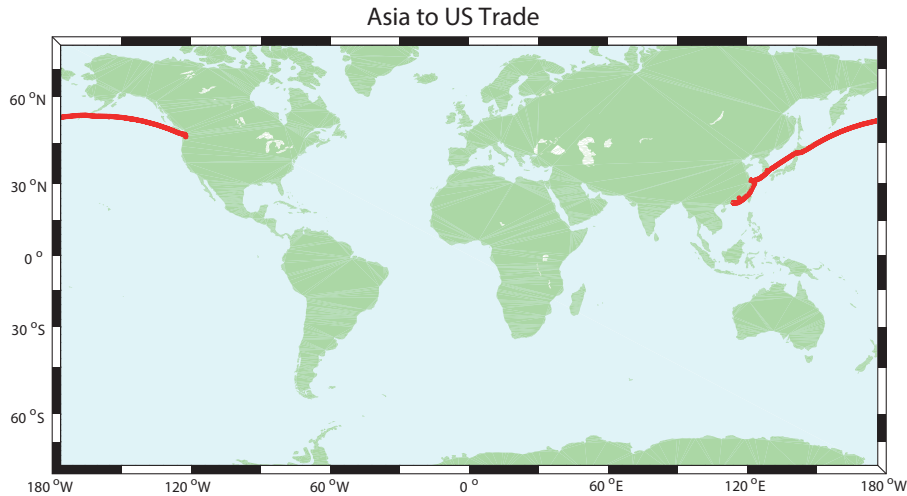
Figure 4.3: The Vessels current Trading route

The vessel is classified by DNV, with the class notation *"1A1 Container Carrier E0 CSA-2 NAUTICUS(Newbuilding)"*. The NAUTICUS(Newbuilding) notation implies that a comprehensive calculation procedure is performed during the design phase of the vessel, as a part of the verification of the hull structure. These calculations includes both structural and hydrodynamic analysis using the finite element method to determine scantlings in the midship area. The CSA-2 notation implies that an additional analysis, with respect to ultimate strength, is performed for all structural members in the cargo hold area (DNV; 2004).

4.2 SENSFIB Hull Monitoring System

The hull monitoring system on board is a SENSFIB system issued by Light Structures AS and installed by both the ship yard and the maker. Figure 4.4, shows the components in a typical SENSFIB system used for hull monitoring (Light Structures; 2009). Light Structures has the maintenance responsibility, i.e. they perform updates and provides new hard disks when the old ones exceed their storage capacity. They also bring used hard disks onshore, passing on the measurement data to DNV GL. In addition, it becomes more frequent that a decision support system (DSS) is installed on the bridge, such that the Captain can monitor measured data, to ensure that stresses are kept on an allowable level.
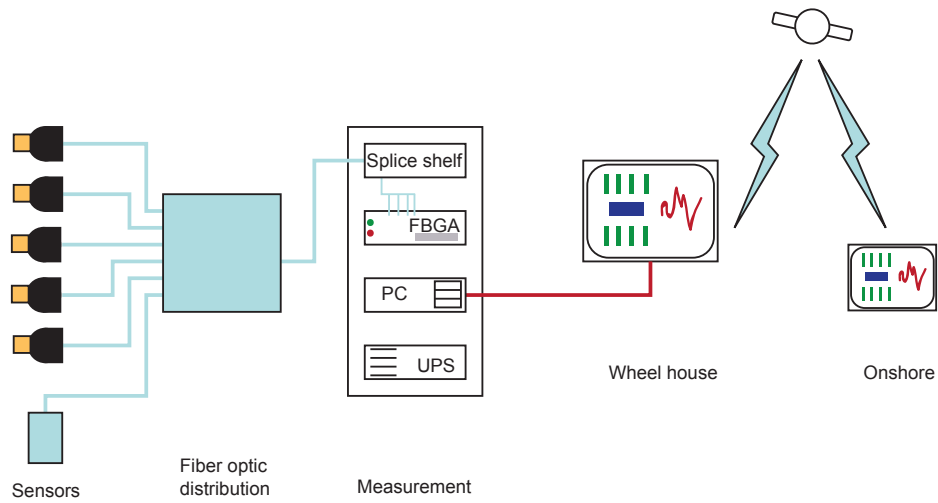
Figure 4.4: Components in a typical Hull monitoring system

The system consists of 20 fiber optic sensors which measure strains and local temperatures. The measured strains are dependent on loading condition, vibrations, wave loads and temperature gradients. Normally, the sensors are located on longitudinal stiffeners to obtain the best possible representation of the hull girder stress. The sensors are glued to the stiffener before they are covered with protective composite material and painted. Figure 4.5 shows a sensor package glued to a stiffener before coating.

Figure 4.5: Sensor glued on stiffener before coating (Light Structures; 2009)

In addition to the sensors, an accelerometer is connected to the SENSFIB system. The accelerometer measures the vertical acceleration of the ship at the center line in the fore peak. Thus, both ship motions due to sea conditions and wave impacts, e.g. slamming can be identified.

46

The signals from the sensors are transferred to the measurement unit through a fiber optic cable, called *Fiber Bragg Grating Analyzer, FBGA*. The FBGA converts the optical signal measured by the sensors to a digital signal. Further, the converted signals are sent to a measurement computer. The computer also receives signals form other systems, for instance the navigation system. An *Uniterruptible power supply* provides stable backup power to the system components. If a power failure occurs the backup power is automatically switched on (Light Structures; 2009).

4.3 Placing of Sensors

Sensors are placed at several positions along the length of the ship, both on starboard and port side of the ship. Figure 4.6 shows the location of the different sensors including sensors for local and global hull response, slamming sensors and accelerometer.
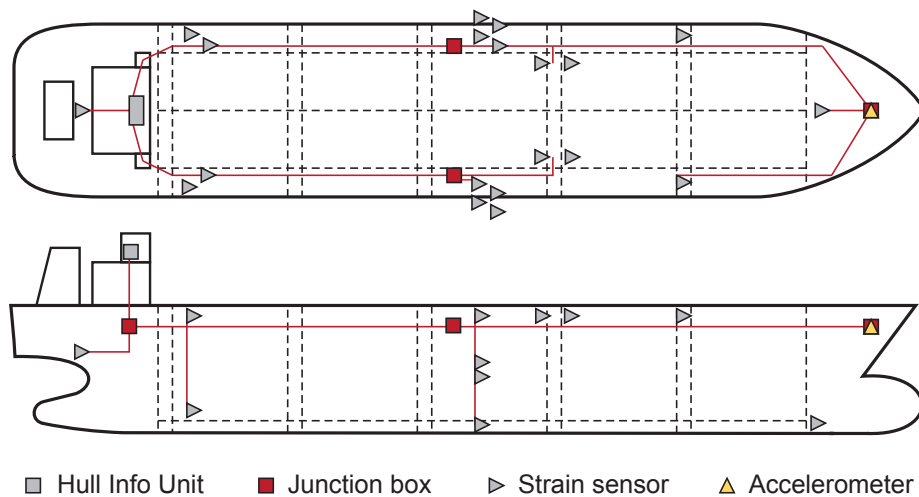
Figure 4.6: Arrangement of the SENSFIB system

From Figure 4.6 the location of sensors along the length of the ship can be summarized as follows:

- 4 sensors at engine room bulkhead, *2 port side and 2 starboard*

- 8 sensors midships, *4 port side and 4 starboard*

- 4 sensors at the transverse deck strip forward of the mid ship cargo hold, *2 port side and 2 starboard*

- 2 sensors at forward quarter length, *1 port side and 1 starboard*

- 2 slamming sensors, *1 in after ship and 1 forward*

- 1 accelerometer at the center line in the fore peak

In this work mainly two sensors on deck midships, and the four sensors at the transverse deck strip, forward of the mid ship cargo hold, will be considered. Their exact position is listed in Table 4.2. Figure 4.7 accompanies the table and illustrates the definition of axis in the global coordinate system.

Table 4.2: Location of sensors in deck midships

Sensor	Location	Distance from AP, (x)	Distance from CL, (y)	Distance from BL, (z)	Definition
$DT1P$	Frame 105 - 127 mm	165.083 m	19.55 m	24.52 m	Port side
$DT2P$	Frame 104 + 100 mm	163.51 m	19.55 m	24.52 m	Port side
$DT3S$	Frame 105 - 100 mm	165.110 m	-19.55 m	24.52 m	Starboard
$DT4S$	Frame 104 + 129 mm	163.537 m	-19.55 m	24.52 m	Starboard
DMP	Frame 104 (L/2)	163.41 m	22.29 m	24.34 m	Port side
DMS	Frame 104 (L/2)	163.41 m	- 22.29 m	24.34 m	Starboard
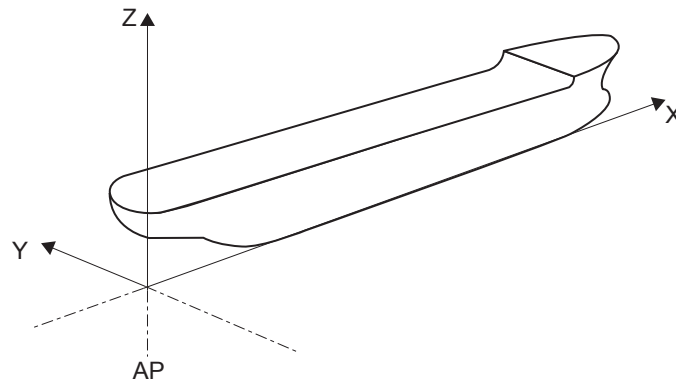
Figure 4.7: Definition of axis, global coordinate system

When it comes to the placement of sensors at the transverse deck strip, some considerations must be addressed. To obtain a reliable recreation of stresses from measurements, with respect to Ultimate (yielding) and Fatigue Limit States, it is desired that the measurements include local stresses, i.e. stress concentrations close to hatch corners. Stress concentrations must be included to obtain the maximum stresses in the deck strip, which are governing for the limit states. On the other hand, when calculating hatch opening distortions, only nominal stresses are wanted in the measurements, as the distortion arises due to nominal stresses in the deck strip.

5 Computing and Analyses

Several computer programs were used during this project, in order to investigate the full scale measurement data and modify a Finite Element model, provided by DNV GL, as well as for performing FE-analyses and assessing the results. All programs used are briefly described in Table 5.1, below:

Table 5.1: Computer programs used in the thesis work

MATLAB	Description	MATLAB is a mathematics program, which is used for numerical computations, visualizations and analysing data.
	Usage	MATLAB has been used to analyse the measured data obtained from the 8600 TEU Vessel. This was one of the main tasks, and is further described in Section 5.1.
NAUTICUS Hull	Description	NAUTICUS Hull is a DNV GL software, used to generate reports containing hull cross sectional properties for specific ships. NAUTICUS Hull can for some ship types, also be used to perform rule checks of the hull structure.
	Usage	NAUTICUS Hull was used to generate a report containing information about the cross sectional properties of the midship area of the 8600 TEU vessel, such as location of shear center, section modulus in deck, bottom and sides, etc.
NAUTICUS 3D-Beam	Description	DNV GL Software, NAUTICUS 3D-Beam is a simple program for conducting linear static analysis of $2D$ and $3D$ frame structures.
	Usage	NAUTICUS 3D-Beam was used as a simplified approach, in order to calculate hatch opening distortions of a transverse deck strip midships.

Waqum Explorer	Description	Waqum Explorer is a software developed by DNV GL, used to calculate long term statistics for specific vessels, based on results from hydrodynamic analyses and measurement data.
	Usage	Results from a hydrodynamic analyses and measurement data, were used in Waqum Explorer, to establish wave climate for the two routes, and to calculate hull girder moments of the 8600 TEU vessel.
Microsoft Excel	Description	Microsoft Excel is a spreadsheet software, which can be used for calculations, making graphs, etc.
	Usage	Microsoft Excel was among others used for plotting route specific scatter diagrams (see Chapter 6.1), and to calculate hatch opening distortions along the length of the 8600 TEU vessel (see Chapter 6.5.4).
Adobe Illustrator	Description	Adobe Illustrator is an advanced graphics editing program, using vector graphics.
	Usage	Adobe Illustrator was used to make the figures that illustrates relevant theory etc. presented in this report.
LaTeX	Description	LaTeX is a text editor.
	Usage	LaTeX is used in the writing process and the formatting of this report.

SESAM Package

SESAM (Super Element Structural Analysis Modules) contains several computer programs, developed by DNV GL and is used for structural engineering analysis, based on the Finite Element Method. The following programs are part of the SESAM Package.

		Description	GeniE is a program used for modelling of structures. Complex structures, such as ships, can be modelled using beam and plate elements.
GeniE		Usage	GeniE was used to work on the model of the 8600 TEU vessel, provided by DNV GL. Since a lot of time was spent working on the model in GeniE, a more detailed description of the program and modifications done, are further described in Section 5.2.
Patran Pre		Description	Patran Pre is a program similar to GeniE, used for modelling of structures.
		Usage	Patran Pre was first used editing the model of the 8600 TEU vessel. However, since GeniE is more commonly used by DNV GL employees, GeniE was used instead. Anyhow, much time was spent on learning basic modelling in Patran Pre.
Sestra		Description	Sestra is a program used for running linear structural analysis of FE-models.
		Usage	Sestra was used for running linear structural analysis of the FE-model.
Xtract		Description	Program to visualize and assess the results obtained from FE-analysis.
		Usage	Results from the FE-analyses in Sestra were opened in Xtract to visualize and assess the results from the analyses.

As stated in Table 5.1, MATLAB and GeniE have been extensively used throughout the project. A further description of the usage of these programs is presented in the forthcoming Sections, 5.1 and 5.2.

5.1 Dataprocessing in MATLAB

MATLAB has been used to analyse the measured data obtained from the 8600 TEU Vessel. During the time period investigated, from 5th June 2009 to 12th July 2014, 5.0 years of effective measurements were stored. This implies that the hull monitoring system has been running 98 % of the time the vessel has been in operation. For some periods during the time interval there were lack of measurements. The Hull Monitoring system has been turned off for short periods, for example from 14th of August 2010 to 28th of August 2010.

5.1.1 Description of Input Files

Measurement data are stored in binary files. In the MATLAB programs two different inputs are used to post process the measurement data. The first type of input is 30-minute statistics. 30-minute statistics are binary files where measurements are stored every 30 minute. These files are used to get an overview over the vessels measured stresses over the whole operation period, or parts of the period. Other interesting statistics, such as GPS coordinates and vessel speed are also obtained from the 30 minute statistics.

The second type of input for measurement data in the MATLAB programs, are raw data. The raw data is data, which is continuously measured and stored. Unfortunately, the backup device where the raw data is stored only has a storage capacity of 100 hours. Therefore, this backup device is continuously overwritten and measurements which are not manually saved are lost. However, data representing extreme values are not deleted, but saved to a "worst case" register.

The different measurement types, such as measured stresses, fatigue rates, GPS coordinates etc. are stored in different channels. 298 channels are used in the binary files to store information from the different sensors. An overview over information stored in the different channels, is found in the Sensor List, enclosed in Appendix B. Data from different channels, found relevant for calculations and analysis, are read into MATLAB and combined in order to investigate the desired measurement input. This has been an important and time consuming part of the thesis work.

5.1.2 Description of MATLAB Programs

In order to read out the desired information from the binary files, several functions are used in the MATLAB programs. To separate MATLAB programs and functions, all programs have a name starting with *"HG_"*, whereas function names

starts with *"IMO_"*. All functions are provided by DNV GL, and are used without any modifications. They will therefore not be further described in this chapter.

HG_mapplot: MATLAB was used to make a program, reading in the ships GPS coordinates during its time in operation, and to make a map plot of all voyages for both routes. The program can also read in data for shorter periods such as one voyage if desired (See Appendix C.1).

HG_speed: This program reads in the ship speed over ground, and generates graphs with ship speed as percent of time in operation (See Appendix C.2).

HG_GPScoord_WaqumExplorer: This MATLAB program was provided by DNV GL and modified to run for the 8600 TEU vessel. GPS coordinates for latitudes and longitudes are found from the 30-minute statistics. An output file which can be used in Waqum Explorer to make scatters, is written (See Appendix C.3).

HG_cleanplot_extreme: A MATLAB program was made to read in 30-minute statistics, plotting time series, finding maximum and minimum measured stresses, and identifying days were torsional vibrations may be present. For the time periods of interest, the MATLAB program inquires whether raw data is available. Bar diagrams, showing the ratio between measured dynamic stresses and measured wave stresses are plotted, which give an indication of the magnitude of torsional vibrations. In order to plot time series, non-trustworthy results had to be identified and filtered away. Filtered and unfiltered time series are plotted to find out whether non-trustworthy results are filtered away properly (See Appendix C.4).

HG_Raw_spectrum: A function to transform time series to frequencies was provided by DNV GL. A MATLAB program was made, which reads in raw-data containing continuous time series of measurements. Further, the program uses the function in order to plot the frequency spectrum's for measured vibrations (see Appendix C.5).

HG_ULS: A MATLAB program was made in order to calculate ULS load cases according to the rules described in Chapter 3.1.1. The program reads in an input file containing information about the frame spacing along the length of the ship, in order to calculate where forces should be applied to the global model. The program generates an output file, containing information about the magnitude and positions for application of the calculated forces. This output file is written as a Java script, and can be used in GeniE to apply forces to the global model (See Appendix C.6).

5.1.3 Sensor Reliability

In order to evaluate the degree of the reliability of the results, the measured stresses for all 4 sensors located on the deck strip, were investigated in detail. Figure 5.1, shows measured stresses for the 4 sensors, for a short period of time. From the plot, it is seen that Sensors DT1P and DT2P are in phase with DT4S and DT3S, respectively. Sensors DT1P and DT4S fluctuates about zero, with a phase difference of 180 degrees compared to sensor DT2P and DT3S.
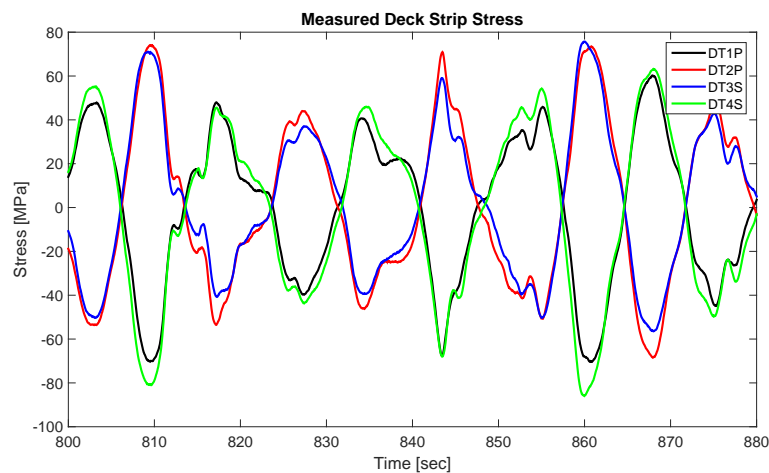
Figure 5.1: Raw stress, measured in deck strip sensors

In Figure 5.2 the mean raw stress measured in the four sensors on the deck strip midships, is plotted. From the Figure 5.2, it can be seen that sensor DT2P and DT3S are nearly overlapping, which is reasonable since they have the same phase. Sensor DT4S experiences a shift in mean measured stress. The shift in mean stress in Sensor DT4S starts in February 2010, and happens gradually. Therefore, the stresses measured with this sensor are considered less reliable than the other sensors. From the same figure it is seen that measured mean stresses for Sensor DTP1 are somewhat lower than for Sensor DT2P and DT3S. This is most likely true. However, it is difficult to verify the reliability of sensor DT1P, since it cannot be compared with sensor DT4S, due its shift.
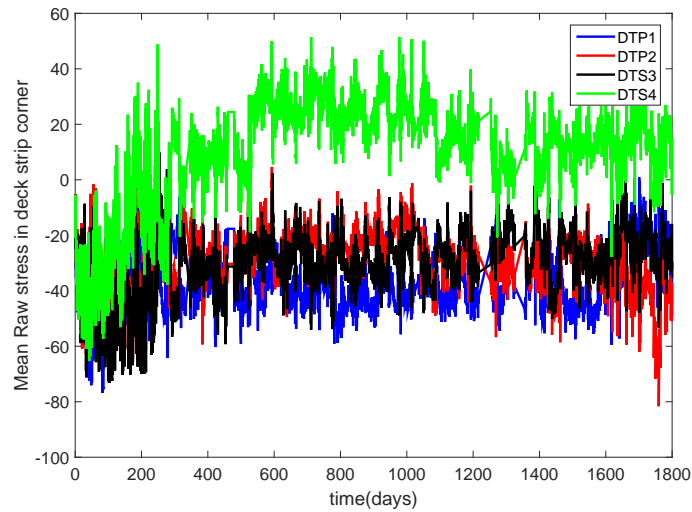
Figure 5.2: Mean raw stress, 30 minutes statistics

Time series for all sensors were plotted and investigated to evaluate whether measured stresses are reasonable. In Sensor DT2P an artificially high value was measured for dynamic stresses the 30th of August 2011. This can be seen from Figure 5.3, around day 800. It was found that the filter, filtering out spurious stresses did not work properly for sensor DT2P that day.
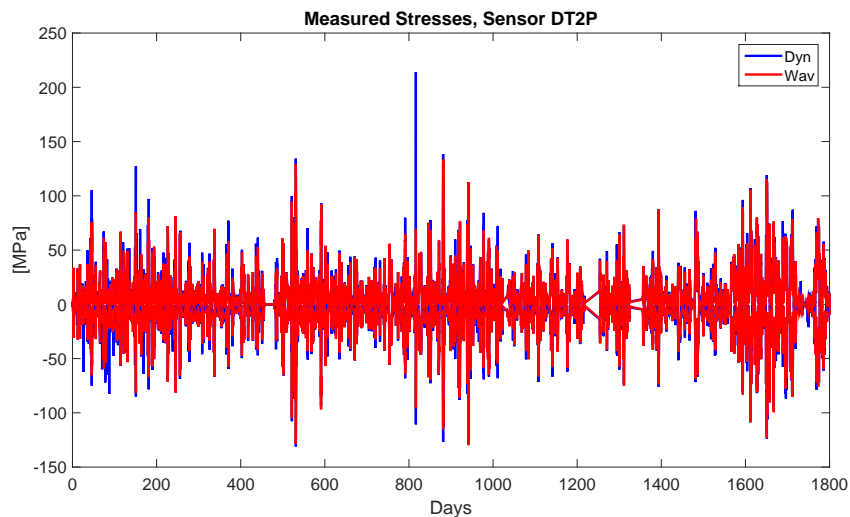
Figure 5.3: Measured dynamic and wave stresses, Sensor DT2P

Since stresses measured in sensor DT2P are badly filtered, and the reliability of sensor DT1P is difficult to verify because of the shift in mean stress for Sensor

DT4S, Sensor DT3S is considered the most reliable sensor. Although, Sensor DT3S seems to be the most reliable sensor, most calculations are done and presented for all 4 sensors. Figure 5.4 shows the time history for measured stresses in Sensor DT3S.
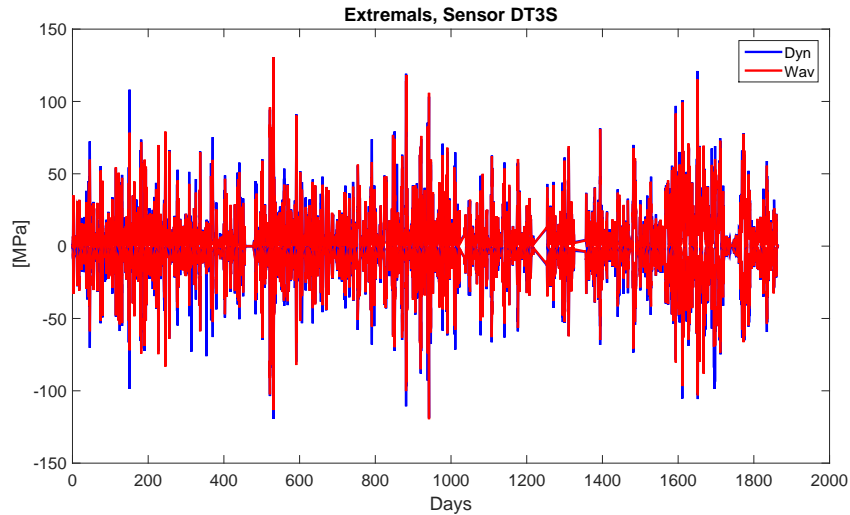
Figure 5.4: Measured dynamic and wave stresses, Sensor DT3S

Both sensors measuring longitudinal stresses in deck midships, DMP and DMS, are considered reliable. Since Sensor DT3S is located at starboard side, Sensor DMS, which is also located at starboard side, was used for investigating longitudinal stresses in deck midships.

5.2 Finite Element Modelling and Analysis

For complex ship structures it is necessary to perform a Finite Element analysis of the ship hull. This gives a more accurate estimation of the stress response in the hull structure. Different finite element models are used depending on the detail being investigated. The most commonly used models are:

- **Global stiffness model;** Represents the overall stiffness and global stress distribution of primary members of the structure.

- **Cargo hold model;** Model of a cargo hold in the midship area, used to analyse nominal stresses and deformation response of primary members.

- **Frame and girder models;** Are used to analyse stresses in main girders and frames.

- **Local structure models;** Used to investigate stresses in stiffeners in among others, side, bottom and inner bottom. Here, the stiffeners are exposed to large relative deformations.

- **Stress concentration models;** Considers details like panel knuckles, brackets and flanges to analyse fatigue life for details where geometrical stress concentrations are unknown.

For analysis, a global stiffness model, and a local structure model is used. The global model is used to obtain a reliable reconstruction of the ships behaviour for comparison with measurements data. The local structural model was used to obtain a more detailed reconstruction of stresses in transverse structure, than obtained from the global model. These models are further described in Sections 5.2.1 and 5.2.3.

5.2.1 Global Finite Element Model

A Global Finite Element analysis is performed with a relatively coarse FE model of the ship hull. The purpose is to determine the global stress distribution in primary members, and to obtain a reliable reproduction of the overall hull girder stiffness. All primary longitudinal and transverse members, such as watertight and non watertight bulkheads, cross decks and transverse webs must be included in the model. In addition, all structural members that have influence on the hull girder stiffness due to bending, shear and torsion, should be represented in the model. This implies that deck house and forecastle should be modelled, since they represent torsional restraints (DNV; 2013b).

Assumptions introduced in the modelling process will influence the degree of accuracy of the models behaviour compared to the real structure. To ensure that the model represents the reality as good as possible, the sources of uncertainties must be kept in mind when making the model, conducting the analyses and assessing the results. There are several errors which can reduce the reliability of the approximation of the real situation. These may among others be (Moan; 2003):

- Insufficient input data, such as lack of information about geometry, material etc. to describe the mathematical model

- Simplified assumption in the mathematical model

- Discretization error

- Numerical round-off error in the computer when solving the simultaneous equations

- Error in interpreting the results

When results from FE-analyses are obtained, it is therefore important to evaluate whether the results seem reasonable based on experience, or conductions of simplified calculations. In case of suspecting questionable results, the model must be thoroughly examined with respect to the above mentioned bullet points. This was the case for the global FE-model examined in this thesis work, which resulted in time consuming and challenging work troubleshooting the model.

5.2.2 Global Model of the 8600 TEU Vessel

A Global FE-model of the vessel was made by the contractor and later handed over to DNV GL for a hydrodynamic analysis. This model has been modified and is used in FE-analyses in this project. The model was original a Patran Nastran model, and therefore not compatible with DNV GL software, which uses the SESAM package (Patran Pre and GeniE). With help from software support, which had a Patran Nastran license, the model was converted to SESAM.

A SESAM compatible model can be opened in both Patran Pre and GeniE. Since the model originally was a Patran model, Patran Pre was first used to apply loads and perform a FE-analysis. However, the analysis failed Sestra. Sestra is a program used by SESAM, to actually run the FE-analysis. Because of that, and the fact that most employees in DNV GL are more skilled in GeniE than Patran Pre, GeniE was chosen to work with the model.

In Figure 5.5, the global model is shown, after being converted to SESAM and opened in GeniE. However, also in GeniE, the model failed. After a while, a document was found enclosed to the results from the hydrodynamic analysis, indicating that the model never had passed a linear structural analysis in Sestra.
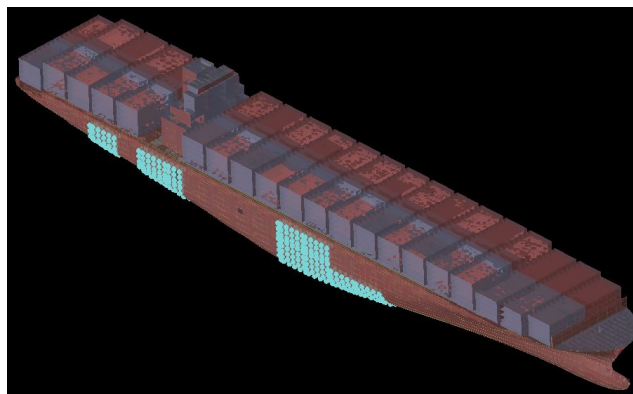
Figure 5.5: Global model - GeniE

The work to get the model to pass Sestra began, and turned out to be a time consuming process. Multiple double beams, mass points and plates were found in the model, which gave "severe errors" no one had seen before. A reason why several beams, plates, etc., in the model were double may be the conversion from Patran Nastran to SESAM. Originally, L-stiffeners were most likely modelled consisting of two parts, one representing the web and the other the flange (see Figure 5.6). Information regarding stiffener geometry has then been lost in the conversion process, resulting in two overlapping circular cross sections, i.e. one of the overlapping beams represents the flange and the other one the web.
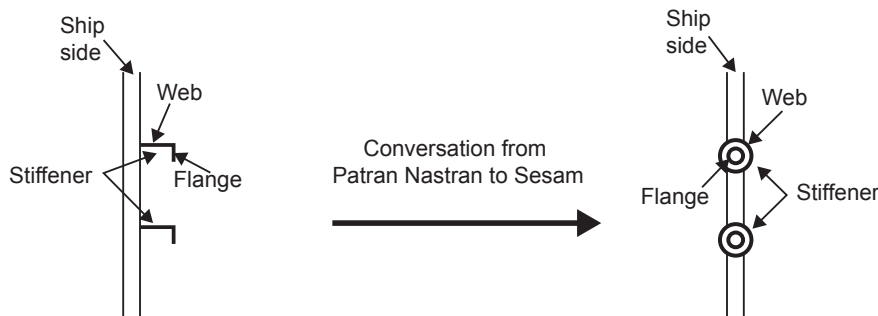
Figure 5.6: Modelled Stiffeners

A Java script was made to merge all double beams and mass points into one, which solved many of the errors. Figure 5.7 shows all overlapping beams in the model. From the figure it is seen that almost all longitudinal beams were overlapping.
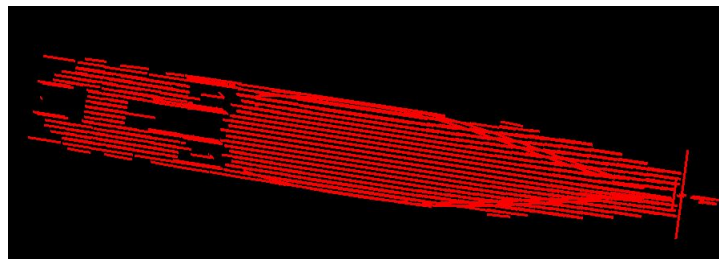
Figure 5.7: Overlapping beams - GeniE

For the double plates, however, it was not that easy. Plates do not have a common "identity" which can be used to find overlapping structure, such as the center of gravity for mass points and start and end coordinates for beams. Therefore, double plates had to be found and deleted manually. Figure 5.8 shows how double plates typical look like in GeniE. For such a large model, as for the 8600 TEU-vessel (see

Figure 5.5), this was time consuming work. When all overlapping plates at last were found and deleted, the model finally passed the Sestra analysis.
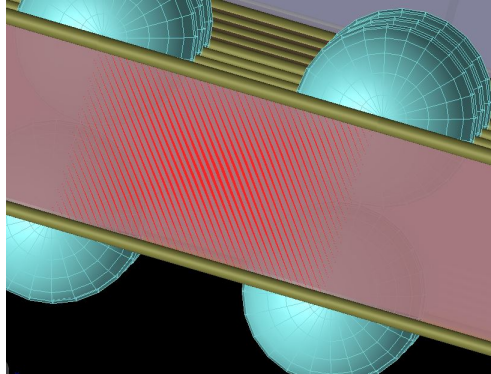
Figure 5.8: Overlapping plates - GeniE

The results obtained for the model, were a simple torsional moment was applied, were analysed in Xtract. It was found that the analysis gave unexpected results. A container carrier exposed to torsional moments is expected to show a typical "s-formed" deformation of transverse deck strips, as described in Figure 2.15 in Chapter 2.5.1. However, visualisation of the results in Xtract did not show any sign of deformation of transverse deck strips. The model was again examined to find out what could have caused the faulty results.

After a while it was found that the hatch cover was modelled with the stiffness of steel (Young's modulus of 206 000 MPa), and with a thickness of 13 cm. This is likely describing the hatch cover of the actual vessel correctly. However, the hatch covers were also attached to the transverse deck strips in the model. This implies that the model represents a ship with an effective deck, closing the ship. The result is that the structure gets a spurious high stiffness, which gives a higher section modulus in deck, bottom and sides.

Another consequence of the modelling fault is that stresses behave different in the FE-analysis than for the actual vessel, i.e. stress concentrations in the sides are too low. In reality, the hatch covers will not contribute to the overall stiffness of the ship. The stiffness of the hatch covers was therefore changed to an artificial low Young's Modulus of 0.01 MPa, such that the stiffness from the hatch covers is neglected. The same was done for the modelled containers, which originally were modelled with a stiffness of 1000 MPa. This, to make sure that the containers did not have any influence on stiffness of the model in the FE-analysis.

Many changes have been made to in order to make the model pass a linear structural analysis in Sestra. Modelling errors made by the person who first made the model were found. It was therefore questionable whether the model represents the real vessel sufficiently. Additionally, it was difficult to verify the geometry in the model, since all stiffeners are modelled with circular cross sections. This might be caused by a lack of information about the geometry, or is a result of the conversion of the model from Patran Nastran, to SESAM. Therefore, additional errors in the model may have been overseen.

5.2.3 Local Model

In addition to the global model, a local model of the transverse deck strip midships was available (see Figure 5.9). A local model represents only a part of the entire model, which is of interest to investigate on a more detailed level than possible in the global model. Local models are often modelled with details that are omitted in the global model. Since the model is smaller, a finer mesh can be used in the analysis, than for a global model. Thus, more accurate results are archived from local models than from global models.

The local model was already a SESAM model. A few modifications were done to the stiffeners, after comparison with drawings of the ship. The local model passed FE-analysis in Sestra right away. The local model has several details that are not included in the global model, such as rounded hatch corners and correct geometry of stiffeners. The local model can be used both by itself, applying boundary conditions and loads directly to the model, or as a part of the global model, using sub modelling as described in Section 5.2.4.
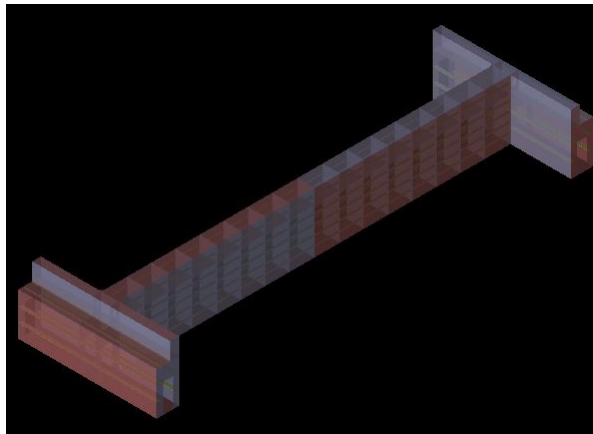
Figure 5.9: Local model of transverse deck strip

5.2.4 Submodeling Technique

Sometimes it may be necessary to increase the model complexity in order to reflect the reality in a proper manner. The simplest way to achieve more accurate results is to decrease the mesh size, and in that way additional evaluation points are created in the model. However, the computational time increases with the number of finite elements, i.e. reduction in mesh size in a large model, increase the computational time of the analysis significantly. The most time consuming analysis that DNV GL performs, may take up to a few weeks. However, most analyses are regarded "too time consuming", and are interrupted if they are not fished within few days. Often, the critical part desired to investigate further, may be local and hence, only a small part of the model needs to be analysed with a fine mesh. In such cases, the submodeling technique can be used (Amdahl; 2010).

In submodeling, a global model is used to apply boundary conditions and to describe the structural behaviour as close to reality as possible. The global analysis is performed with a relatively coarse mesh. Further, a local model of the part desired to investigate with a smaller mesh, is created by copying only this part from the global model into a new workspace. The local model may also be modelled in more detail than the global model, which is the case for the local model of the deck strip, where rounded hatch corners are modelled (see Figure 5.10).

Prescribed boundary conditions are applied to the local model on surfaces that interact with surfaces in the global model. In GeniE this is done by applying support curves to respective surfaces of the structure and set all translations and rotations to prescribed.

The behaviour of the global model is transferred to the local model when the submodel is resolved for the same load case as the global model. Since the local model is considerably smaller than the global model, the mesh size can be reduced significantly compared to the global model. This, without resulting in a too time consuming analysis. Thus, more accurate results are achieved for the local part investigated, than from the global model. Several different submodels can be made for the same global model.
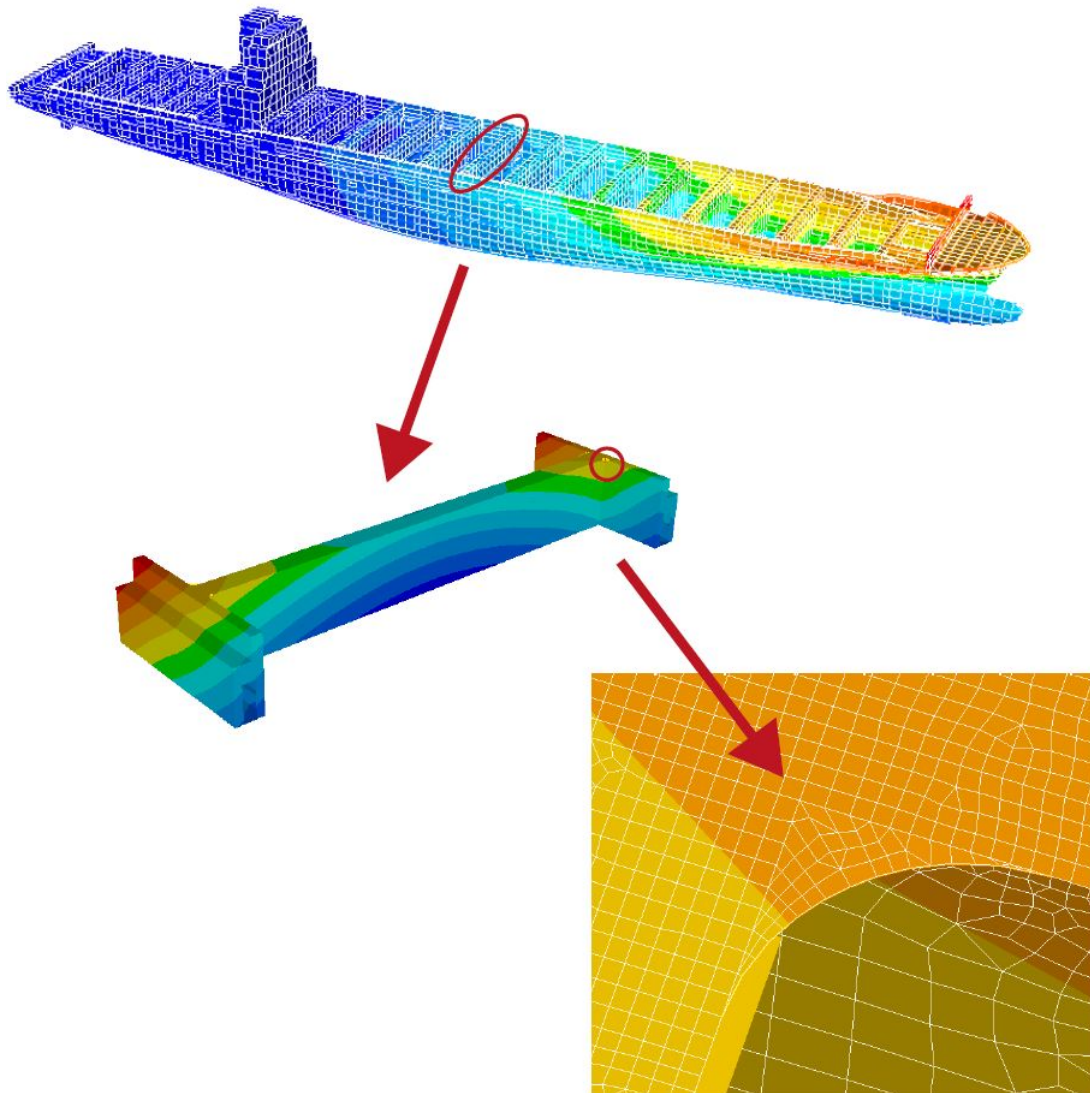
Figure 5.10: Global vs. Local Model

5.2.5   Self-checks

To verify the structure and the reliability of the results, self-checks of the model were performed to investigate how the model represents the overall hull girder stiffness. The hull girder stiffness calculated from the model is compared to values from NAUTICUS Hull, in order to determine whether the model still describes reality in an adequate manner. Self-checks are performed for both vertical and horizontal stiffness, by applying vertical and horizontal bending moment to the model, respectively. Further, the resulting stress in the longitudinal direction

midship was used to calulate the section modulus from Equation 5.1.

$$W = \frac{M}{\sigma} \tag{5.1}$$

NAUTICUS Hull was used to generate a report containing cross sectional data for the vessel. The moment of inertia, I, about the vertical neutral axis, was found from the report and used in Equation 5.2 to calculate the section modulus in the ship side. Section modulus at deck and bottom were found directly from the report.

$$W = \frac{I}{y} \tag{5.2}$$

Where y is equal to half of the breadth of the ship.

The calculated section modulus with both horizontal and vertical bending moments from the model (ship sides, and top and bottom respectively) are presented in Table 5.3 and 5.4. In the same tables the section modulus for the respective positions found from Nauticus Hull are presented.

Table 5.3: Section modulus in ship sides

Global Model		Nauticus Hull	
σ	9.32821 $[N/mm^2]$	I	2328 $[m^4]$
M	10^{12} [N/mm]	y	22.8 $[m]$
W	107.2 $[m^3]$	W	102.1 $[m^3]$

Table 5.4: Section modulus in Deck and bottom

Deck		Bottom	
σ	17.7922 $[N/mm^2]$	σ	16.4815 $[N/mm^2]$
M	10^{12} $[N/mm]$	M	10^{12} $[N/mm]$
W_{Model}	56.2 $[m^3]$	W_{Model}	65.9 $[m^3]$
W_{NH}	55.7 $[m^3]$	W_{NH}	66.1 $[m^3]$

From the self-checks, the model seems to describe the overall hull girder stiffness sufficiently. The largest difference between the section modulus calculated from the model and from NAUTICUS Hull is found in the ship sides, and is about 4.8 %. Despite of all the changes done in the model in order to run a FE-analysis, the model seems to describe the real situation adequately. Hence, the model could be used in torsional analyses in the further work of the project.

5.2.6 Torsional Finite Element Analysis

A torsional analysis with respect to ULS was performed based on DNV GL rule requirements, described in Classification Note 31.7 (DNV; 2013b), which are summarized in Section 3.1.1. Rule stresses are found from FE-analysis in GeniE and Sestra, when rule torsional moments were applied to the model as described in Section 5.2.6.2.

5.2.6.1 Boundary Conditions

Stresses in the transverse deck strip midships due to an applied torsional moment is of main interest to investigate. Therefore, and since no loads from a hydrodynamic analysis are applied to the model, the model was restrained in a simplified manner, compared to the boundary conditions described in Classification Note 31.7 (DNV; 2013b).

According to the classification note, the global model should be supported at two positions at rule Aft Perpendicular, AP (fixed against translation in all three directions at bottom, and fixed against transverse direction at upper deck), and fixed in vertical and transverse direction at rule Forward Perpendicular, FP, bottom. Application of boundary condition from ship rules is illustrated in Figure 5.11 (DNV; 2013b).
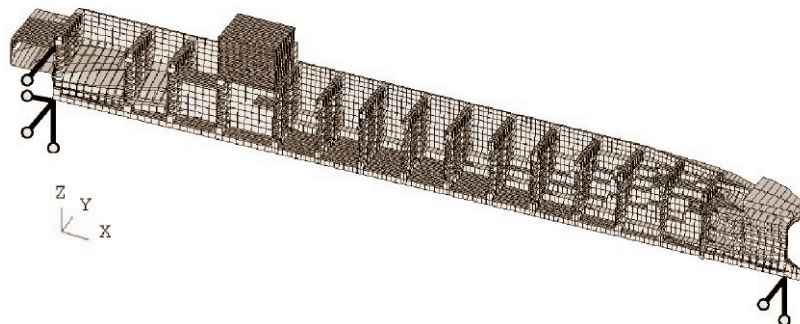
Figure 5.11: Rule boundary conditions - global model (DNV; 2013b)

The simplification of application of boundary conditions was done by fixing the ship against translation in all three directions at the stern of the ship, as shown in Figure 5.12. This leads to an improper behaviour of the after ship compared to reality, but displacements and stresses at the midship section will be described sufficiently.
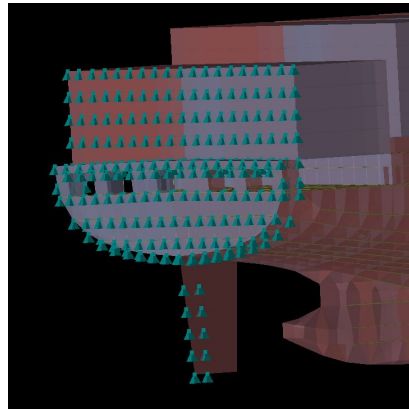
Figure 5.12: Boundary conditions - global model

5.2.6.2   Load Application

MATLAB was used to calculate rule wave torsional and still water moments for both load cases described in Chapter 3.1.1. Input data used in the formulas are listed in Table 4.1, in Chapter 4. MATLAB was further used to calculate the position where forces are to be applied, and the magnitude of the forces.

FE-analyses were performed for both load cases, to find the worst case. Load case 2, turned out to give highest stresses. This load case is therefore further used in the ULS-analysis, as well as in investigation of hatch opening distortions, when determining how much local stress is included in measurements. Figure 5.13 shows the coupled vertical forces applied to the model, which represents the distribution of the torsional moment along the ship length.
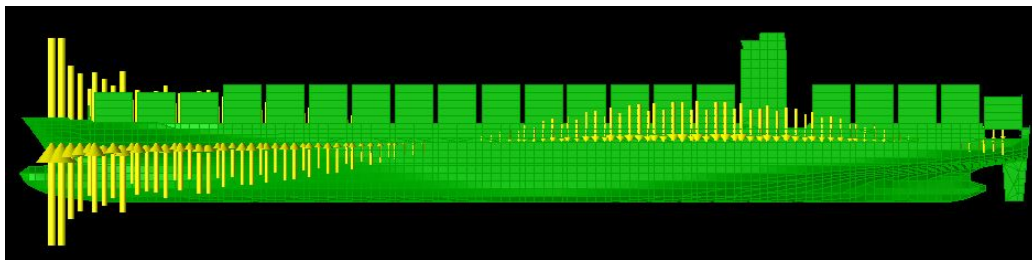
Figure 5.13: Application of forces representing torsional moment

The methods describing FE-modelling in general, and the global and local model of the 8600 TEU vessel in particular, together with input data from ship rules, i.e. boundary conditions and load applications, forms the basis that underlies the FE-analyses carried out in this thesis work. The results from the conducted FE-analyses are presented in the following chapter.

66

6 Presentation and Discussion of Results

A 8600 TEU vessel started to operate on its route from Hamburg to Singapore (Route 1) in 2009, which is a route with relatively calm seas. In 2013 the vessel route was changed, with new destination from Singapore to USA (Route 2). On this route the vessel crosses among others the North Pacific Ocean, which is known for more rough seas. Full scale measurements of the 8600 TEU container vessel have been conducted by DNV GL. These full scale measurements, together with theoretical methods, and a global and a local Finite Element (FE) model, have been used to investigate how torsion contributes to extreme loading and hatch opening distortions. In this chapter, results from the measurement investigations and FE-analyses carried out in the thesis work, are presented.

6.1 Assessment of Routes

Since the 8600 TEU vessel has been operating on two different trades, it was of interest to study how stresses in a transverse deck strip midships were expected to change due to the change in route. Further, it was of interest to investigate how measured stresses actually have changed. In order to compare the two routes, route specific scatter diagrams had to be made. A wave scatter diagram gives the joint probability of wave zero crossing period and significant wave hight. The wave scatter diagrams were made using MATLAB, Excel, and DNV GL software Waqum Explorer. The MATLAB program *HG_GPScoord_WaqumExplorer.m* (see Chapter 5.1 for description), was used to make an input file, which can be read into Waqum Explorer, in order to generate wave statistics for the two routes.

Waqum Explorer uses wave statistics from Global Wave Statistics (GWS), to generate scatter diagrams. Global Wave Statistics provides wave statistics of different oceans, covering the wave climate nearly world wide (BMT; 2011). GWS divides the world oceans into 104 sea regions with different wave climates. The division of the oceans into 104 regions, with corresponding wave climates, is based on 130 years of observations of wave heights, wind speeds and wind directions.
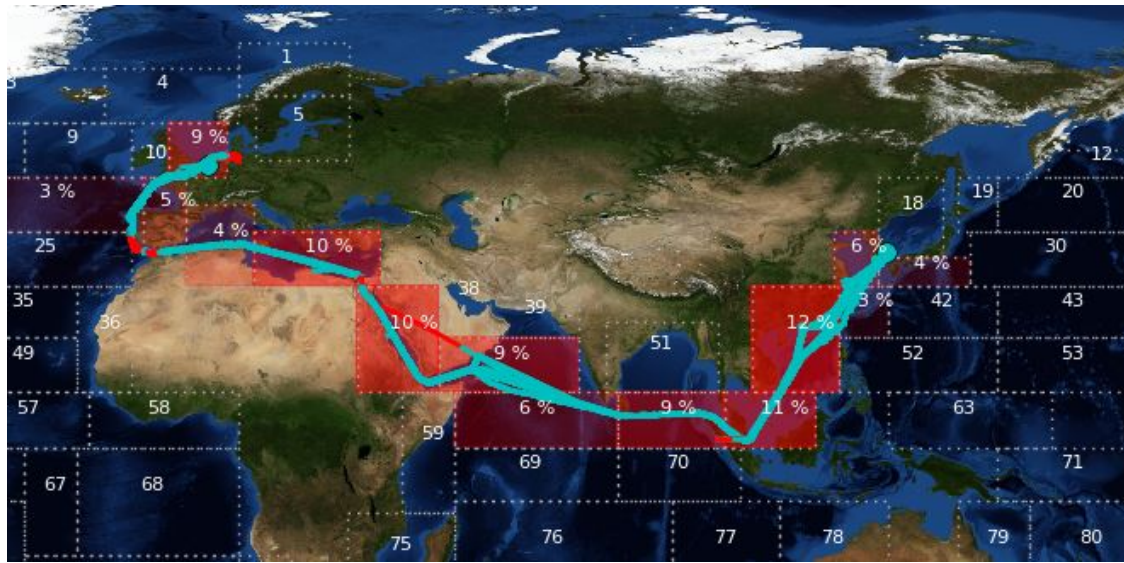
Figure 6.1: Waqum Explorer - Areas for different wave statistics

Figure 6.1 shows the division of the oceans into smaller regions in the area where the vessel operates on its route from Hamburg to Singapore. The figure also shows percent of time the vessel finds itself in the different regions during its time of operation on this route.

Waqum Explorer uses this information to generate a file containing the wave statistics for the specific route. This file can be used in MATLAB, to make the scatter table, which again is plotted in Excel.

		Significant wave height [m]															
		<1.0	1.0-2.0	2.0-3.0	3.0-4.0	4.0-5.0	5.0-6.0	6.0-7.0	7.0-8.0	8.0-9.0	9.0-10.0	10.0-11.0	11.0-12.0	12.0-13.0	13.0-14.0	>14.0	
Mean zero upcrossing period [s]	<1.0	3,60E-06	0,00E+00	0,00E+00	0,00E+00	0,00E+00	0,00E+00	0,00E+00	0,00E+00	0,00E+00	0,00E+00	0,00E+00	0,00E+00	0,00E+00	0,00E+00	0,00E+00	3,60E-06
	1.0-2.0	3,28E-03	2,64E-04	1,72E-05	0,00E+00	0,00E+00	0,00E+00	0,00E+00	0,00E+00	0,00E+00	0,00E+00	0,00E+00	0,00E+00	0,00E+00	0,00E+00	0,00E+00	3,56E-03
	2.0-3.0	4,40E-02	7,47E-03	1,28E-03	1,69E-04	1,59E-05	0,00E+00	0,00E+00	0,00E+00	0,00E+00	0,00E+00	0,00E+00	0,00E+00	0,00E+00	0,00E+00	0,00E+00	5,29E-02
	3.0-4.0	1,12E-01	3,67E-02	1,01E-02	2,25E-03	4,16E-04	6,41E-05	4,68E-06	0,00E+00	0,00E+00	0,00E+00	0,00E+00	0,00E+00	0,00E+00	0,00E+00	0,00E+00	1,62E-01
	4.0-5.0	1,18E-01	7,22E-02	2,93E-02	9,24E-03	2,46E-03	5,80E-04	1,23E-04	2,02E-05	0,00E+00	0,00E+00	0,00E+00	0,00E+00	0,00E+00	0,00E+00	0,00E+00	2,32E-01
	5.0-6.0	7,32E-02	7,57E-02	4,33E-02	1,82E-02	6,38E-03	1,99E-03	5,66E-04	1,49E-04	3,53E-05	2,36E-06	0,00E+00	0,00E+00	0,00E+00	0,00E+00	0,00E+00	2,19E-01
	6.0-7.0	3,22E-02	5,12E-02	3,90E-02	2,08E-02	9,13E-03	3,53E-03	1,25E-03	4,10E-04	1,25E-04	3,39E-05	5,53E-06	0,00E+00	0,00E+00	0,00E+00	0,00E+00	1,58E-01
	7.0-8.0	1,11E-02	2,53E-02	2,47E-02	1,64E-02	8,71E-03	4,05E-03	1,71E-03	6,64E-04	2,40E-04	8,06E-05	2,40E-05	2,26E-06	0,00E+00	0,00E+00	0,00E+00	9,29E-02
	8.0-9.0	3,20E-02	9,77E-03	1,20E-02	9,62E-03	6,14E-03	3,39E-03	1,68E-03	7,62E-04	3,18E-04	1,23E-04	4,35E-05	1,30E-05	2,18E-06	0,00E+00	0,00E+00	4,70E-02
	9.0-10.0	8,53E-04	3,14E-03	4,63E-03	4,41E-03	3,31E-03	2,13E-03	1,22E-03	6,37E-04	3,04E-04	1,34E-04	5,45E-05	1,96E-05	5,66E-06	8,90E-07	0,00E+00	2,08E-02
	10.0-11.0	2,28E-04	8,97E-04	1,50E-03	1,64E-03	1,40E-03	1,03E-03	6,65E-04	3,89E-04	2,09E-04	1,02E-04	4,72E-05	1,73E-05	6,69E-06	1,94E-06	3,30E-07	8,13E-03
	11.0-12.0	6,28E-05	2,45E-04	4,34E-04	5,19E-04	4,91E-04	3,97E-04	2,83E-04	1,81E-04	1,04E-04	5,63E-05	2,56E-05	1,18E-05	4,34E-06	1,22E-06	3,00E-07	2,81E-03
	12.0-13.0	1,73E-05	6,17E-05	9,56E-05	1,08E-04	1,01E-04	8,48E-05	6,19E-05	4,08E-05	2,67E-05	1,60E-05	8,84E-06	4,58E-06	1,86E-06	3,70E-07	0,00E+00	6,30E-04
	13.0-14.0	6,06E-06	1,14E-05	9,70E-06	5,05E-06	3,41E-06	3,70E-07	2,20E-07	1,20E-07	0,00E+00	0,00E+00	0,00E+00	0,00E+00	0,00E+00	0,00E+00	0,00E+00	3,63E-05
	14.0-15.0	1,61E-06	3,33E-06	1,05E-06	0,00E+00	0,00E+00	0,00E+00	0,00E+00	0,00E+00	0,00E+00	0,00E+00	0,00E+00	0,00E+00	0,00E+00	0,00E+00	0,00E+00	5,99E-06
	>15.0	0,00E+00	0,00E+00	0,00E+00	0,00E+00	0,00E+00	0,00E+00	0,00E+00	0,00E+00	0,00E+00	0,00E+00	0,00E+00	0,00E+00	0,00E+00	0,00E+00	0,00E+00	0,00E+00
		3,98E-01	2,83E-01	1,66E-01	8,34E-02	3,86E-02	1,72E-02	7,57E-03	3,25E-03	1,36E-03	5,48E-04	2,09E-04	6,86E-05	2,07E-05	4,42E-06	6,30E-07	1,00E+00

Figure 6.2: Scatter diagram of Route 1 - Europe to Asia trade

Mean zero upcrossing period [s]	Significant wave height [m]															
	<1.0	1.0-2.0	2.0-3.0	3.0-4.0	4.0-5.0	5.0-6.0	6.0-7.0	7.0-8.0	8.0-9.0	9.0-10.0	10.0-11.0	11.0-12.0	12.0-13.0	13.0-14.0	>14.0	
<1.0	1,56E-06	0,00E+00	0,00E+00	0,00E+00	0,00E+00	0,00E+00	0,00E+00	0,00E+00	0,00E+00	0,00E+00	0,00E+00	0,00E+00	0,00E+00	0,00E+00	0,00E+00	1,56E-06
1.0-2.0	1,11E-03	2,80E-05	0,00E+00	0,00E+00	0,00E+00	0,00E+00	0,00E+00	0,00E+00	0,00E+00	0,00E+00	0,00E+00	0,00E+00	0,00E+00	0,00E+00	0,00E+00	1,13E-03
2.0-3.0	1,74E-02	2,06E-03	2,78E-04	3,36E-05	2,81E-06	0,00E+00	0,00E+00	0,00E+00	0,00E+00	0,00E+00	0,00E+00	0,00E+00	0,00E+00	0,00E+00	0,00E+00	1,98E-02
3.0-4.0	5,39E-02	1,39E-02	3,44E-03	7,46E-04	1,44E-04	2,37E-05	2,38E-06	0,00E+00	0,00E+00	0,00E+00	0,00E+00	0,00E+00	0,00E+00	0,00E+00	0,00E+00	7,22E-02
4.0-5.0	7,82E-02	3,75E-02	1,40E-02	4,33E-03	1,18E-03	2,89E-04	6,47E-05	1,14E-05	0,00E+00	0,00E+00	0,00E+00	0,00E+00	0,00E+00	0,00E+00	0,00E+00	1,35E-01
5.0-6.0	7,06E-02	5,89E-02	3,09E-02	1,28E-02	4,52E-03	1,42E-03	4,08E-04	1,05E-04	2,43E-05	0,00E+00	0,00E+00	0,00E+00	0,00E+00	0,00E+00	0,00E+00	1,80E-01
6.0-7.0	4,31E-02	6,15E-02	4,57E-02	2,48E-02	1,11E-02	4,34E-03	1,51E-03	4,79E-04	1,40E-04	3,68E-05	3,27E-06	0,00E+00	0,00E+00	0,00E+00	0,00E+00	1,93E-01
7.0-8.0	1,92E-02	4,16E-02	4,36E-02	3,12E-02	1,78E-02	8,58E-03	3,64E-03	1,39E-03	4,81E-04	1,54E-04	4,53E-05	5,00E-06	0,00E+00	0,00E+00	0,00E+00	1,68E-01
8.0-9.0	7,84E-03	1,94E-02	2,70E-02	2,47E-02	1,74E-02	1,01E-02	5,14E-03	2,32E-03	9,46E-04	3,55E-04	1,22E-04	3,58E-05	9,08E-06	0,00E+00	0,00E+00	1,15E-01
9.0-10.0	3,86E-03	7,31E-03	1,19E-02	1,32E-02	1,10E-02	7,56E-03	4,44E-03	2,30E-03	1,07E-03	4,61E-04	1,82E-04	6,52E-05	1,91E-05	5,06E-06	0,00E+00	6,34E-02
10.0-11.0	2,39E-03	2,83E-03	4,34E-03	5,33E-03	5,08E-03	3,94E-03	2,60E-03	1,50E-03	7,83E-04	3,72E-04	1,64E-04	6,45E-05	2,17E-05	8,20E-06	0,00E+00	2,94E-02
11.0-12.0	1,63E-03	1,39E-03	1,58E-03	1,85E-03	1,87E-03	1,58E-03	1,14E-03	7,19E-04	4,05E-04	2,08E-04	9,71E-05	4,38E-05	1,47E-05	5,04E-06	0,00E+00	1,25E-02
12.0-13.0	1,14E-03	8,25E-04	6,46E-04	5,61E-04	5,04E-04	4,16E-04	3,03E-04	1,92E-04	1,09E-04	5,70E-05	2,76E-05	9,82E-06	3,68E-06	1,03E-06	0,00E+00	4,80E-03
13.0-14.0	8,02E-04	5,37E-04	3,28E-04	1,78E-04	9,01E-05	4,38E-05	2,08E-05	9,78E-06	4,60E-06	1,29E-06	0,00E+00	0,00E+00	0,00E+00	0,00E+00	0,00E+00	2,02E-03
14.0-15.0	5,60E-04	3,61E-04	2,07E-04	1,03E-04	4,74E-05	2,06E-05	8,67E-06	3,60E-06	0,00E+00	0,00E+00	0,00E+00	0,00E+00	0,00E+00	0,00E+00	0,00E+00	1,31E-03
15.0-16.0	3,90E-04	2,40E-04	1,28E-04	5,80E-05	2,37E-05	9,03E-06	3,27E-06	0,00E+00	0,00E+00	0,00E+00	0,00E+00	0,00E+00	0,00E+00	0,00E+00	0,00E+00	8,52E-04
16.0-17.0	2,72E-04	1,59E-04	7,79E-05	3,18E-05	1,14E-05	3,75E-06	0,00E+00	0,00E+00	0,00E+00	0,00E+00	0,00E+00	0,00E+00	0,00E+00	0,00E+00	0,00E+00	5,56E-04
17.0-18.0	1,90E-04	1,05E-04	4,70E-05	1,72E-05	5,37E-06	9,90E-07	0,00E+00	0,00E+00	0,00E+00	0,00E+00	0,00E+00	0,00E+00	0,00E+00	0,00E+00	0,00E+00	3,65E-04
18.0-19.0	1,33E-04	6,89E-05	2,82E-05	9,12E-06	1,65E-06	0,00E+00	0,00E+00	0,00E+00	0,00E+00	0,00E+00	0,00E+00	0,00E+00	0,00E+00	0,00E+00	0,00E+00	2,40E-04
19.0-20.0	9,30E-05	4,53E-05	1,69E-05	4,82E-06	0,00E+00	0,00E+00	0,00E+00	0,00E+00	0,00E+00	0,00E+00	0,00E+00	0,00E+00	0,00E+00	0,00E+00	0,00E+00	1,60E-04
20.0-21.0	6,54E-05	2,98E-05	1,01E-05	1,72E-06	0,00E+00	0,00E+00	0,00E+00	0,00E+00	0,00E+00	0,00E+00	0,00E+00	0,00E+00	0,00E+00	0,00E+00	0,00E+00	1,07E-04
21.0-22.0	4,61E-05	1,96E-05	6,00E-06	9,20E-07	0,00E+00	0,00E+00	0,00E+00	0,00E+00	0,00E+00	0,00E+00	0,00E+00	0,00E+00	0,00E+00	0,00E+00	0,00E+00	7,27E-05
22.0-23.0	3,27E-05	1,30E-05	3,57E-06	0,00E+00	0,00E+00	0,00E+00	0,00E+00	0,00E+00	0,00E+00	0,00E+00	0,00E+00	0,00E+00	0,00E+00	0,00E+00	0,00E+00	4,92E-05
23.0-24.0	2,33E-05	8,59E-06	1,48E-06	0,00E+00	0,00E+00	0,00E+00	0,00E+00	0,00E+00	0,00E+00	0,00E+00	0,00E+00	0,00E+00	0,00E+00	0,00E+00	0,00E+00	3,33E-05
24.0-25.0	1,66E-05	5,71E-06	0,00E+00	0,00E+00	0,00E+00	0,00E+00	0,00E+00	0,00E+00	0,00E+00	0,00E+00	0,00E+00	0,00E+00	0,00E+00	0,00E+00	0,00E+00	2,23E-05
25.0-26.0	1,19E-05	3,82E-06	0,00E+00	0,00E+00	0,00E+00	0,00E+00	0,00E+00	0,00E+00	0,00E+00	0,00E+00	0,00E+00	0,00E+00	0,00E+00	0,00E+00	0,00E+00	1,58E-05
26.0-27.0	8,60E-06	1,73E-06	0,00E+00	0,00E+00	0,00E+00	0,00E+00	0,00E+00	0,00E+00	0,00E+00	0,00E+00	0,00E+00	0,00E+00	0,00E+00	0,00E+00	0,00E+00	1,03E-05
27.0-28.0	6,22E-06	1,18E-06	0,00E+00	0,00E+00	0,00E+00	0,00E+00	0,00E+00	0,00E+00	0,00E+00	0,00E+00	0,00E+00	0,00E+00	0,00E+00	0,00E+00	0,00E+00	7,40E-06
28.0-29.0	4,52E-06	0,00E+00	0,00E+00	0,00E+00	0,00E+00	0,00E+00	0,00E+00	0,00E+00	0,00E+00	0,00E+00	0,00E+00	0,00E+00	0,00E+00	0,00E+00	0,00E+00	4,52E-06
29.0-30.0	3,30E-06	0,00E+00	0,00E+00	0,00E+00	0,00E+00	0,00E+00	0,00E+00	0,00E+00	0,00E+00	0,00E+00	0,00E+00	0,00E+00	0,00E+00	0,00E+00	0,00E+00	3,30E-06
30.0-31.0	1,63E-06	0,00E+00	0,00E+00	0,00E+00	0,00E+00	0,00E+00	0,00E+00	0,00E+00	0,00E+00	0,00E+00	0,00E+00	0,00E+00	0,00E+00	0,00E+00	0,00E+00	1,63E-06
31.0-32.0	1,21E-06	0,00E+00	0,00E+00	0,00E+00	0,00E+00	0,00E+00	0,00E+00	0,00E+00	0,00E+00	0,00E+00	0,00E+00	0,00E+00	0,00E+00	0,00E+00	0,00E+00	1,21E-06
>32	0,00E+00	0,00E+00	0,00E+00	0,00E+00	0,00E+00	0,00E+00	0,00E+00	0,00E+00	0,00E+00	0,00E+00	0,00E+00	0,00E+00	0,00E+00	0,00E+00	0,00E+00	0,00E+00
	3,03E-01	2,49E-01	1,84E-01	1,20E-01	7,08E-02	3,84E-02	1,93E-02	9,02E-03	3,97E-03	1,65E-03	6,41E-04	2,24E-04	6,83E-05	1,93E-05	0,00E+00	1,00E+00

Figure 6.3: Scatter diagram of Route 2 - Asia to North-America trade

In Figures 6.2 and 6.3 the scatter diagram for the two routes are shown. The rows represents different zero upcrossing periods, whereas the columns states the different wave hight classes. To give a more visual understanding of the wave scatter, the cells are color coded. Cells are gradually changing from red to dark green, where red shows incidents with high joint probability of wave height - period combinations, and dark green indicates a joint probability of zero. From the figures one can see that there is a greater spread of the joint probability of upcrossing periods and wave heights for Route 2 than for Route 1, which indicates that Route 2 is more harsh than Route 1.

The file made in Waqum Explorer, containing the scatter diagram, can in combination with results from a hydrodynamic analysis of the vessel, be used to calculate statistics such as hull girder moments. Results from a hydrodynamic analysis done of the 8600 TEU vessel were available. Hence, the long term distribution of stresses in deck, with a probability of exceedance of 10^{-8}, could be computed for the 8600 TEU vessel. This was done to find the maximum expected longitudinal stress in the deck structure for both routes during the life time of the vessel.

Figure 6.4 shows the vertical bending moment calculated with a 10^{-8} probability

of exceedance, in Wacum explorer for Route 1 and Route 2, respectively. Both calculated dynamic vertical bending moment and still water vertical bending moment (NAPA), are shown in the figure. In addition, the rule vertical bending moment for both routes are shown.
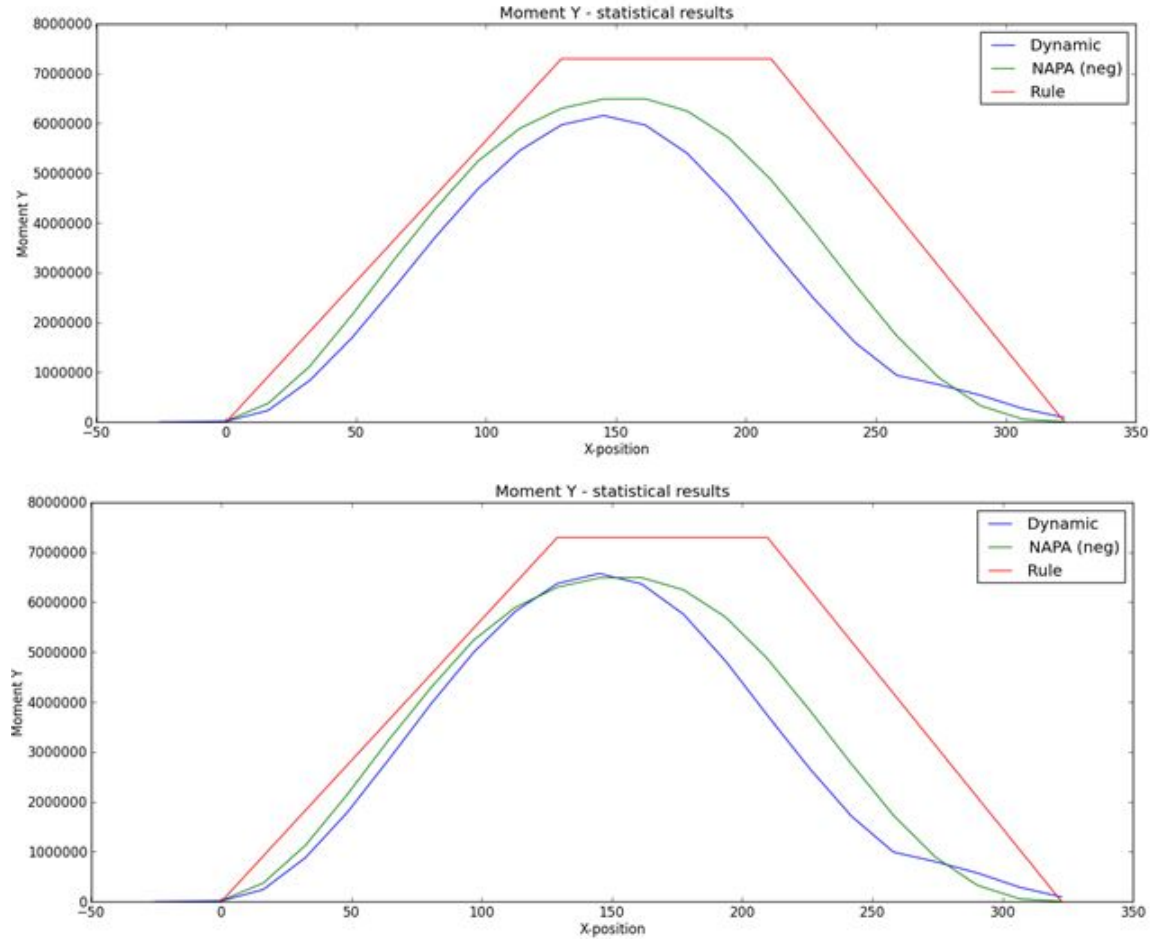
Figure 6.4: Vertical bending moment - Route 1 and Route 2

Still water vertical bending moment and dynamic vertical bending moment midships were found for both routes, and used in Equation 6.1 to calculate the deck stress midships.

$$\sigma_{deck} = \frac{(M_{VB} + M_{SW})}{W_{deck}} \tag{6.1}$$

Maximum expected longitudinal stresses during the vessels lifetime were calculated for both routes, and with a worldwide scatter diagram. The worldwide scatter

diagram assumes uniform heading and a spread of cosine-squared to distribute the energy over heading directions for incoming waves from ahead. Waves from behind (i.e. $[-90°, 90°]$ in Figure 2.17) has zero energy contribution. The results of the calculations are presented in Table 6.1.

Table 6.1: Maximum expected longitudinal stresses in deck

	Route 1	Route 2	Worldwide
M_{VB} [kNm]	$5.96 \cdot 10^6$	$6.37 \cdot 10^6$	$6.36 \cdot 10^6$
M_{ST} [kNm]	$6.49 \cdot 10^6$	$6.49 \cdot 10^6$	$6.49 \cdot 10^6$
W_{Deck} [m^3]	55.7	55.7	55.7
$\sigma_{\textbf{Deck}}$ [MPa]	**223.6**	**230.8**	**230.7**

From the table it can be seen that the still water vertical bending moment for the vessel is independent of where the vessel operates. Only the calculated dynamic vertical bending changes for the different scatter tables. The maximum stress for Route 2 and for the world wide scatter diagram are approximately the same, which means that a worldwide scatter diagram is representative for the second route.

In the deck structure of container carriers, NV-36 steels are commonly used. NV-36 steels yields at 355 MPa, maximum allowed stresses are therefore approximately 250 MPa (calculated with a 10^{-8} probability of exceedance and a world wide scatter diagram) according to ship rules (DNV; 2004). For both routes, expected maximum stresses during the vessels time in operation are within the acceptance criteria. Maximum measured stresses for sensor DMP and DMS, which measures longitudinal stresses midships, are well below the expected values, and hence within the acceptance criteria (see Table 6.2).

As expected, both the scatter tables for each route, and the calculation of predicted maximum longitudinal stress in the deck, verifies that Route 2 is more rough than Route 1, where the vessels follows a relatively sheltered inside passage from Hamburg to Singapore. However, measurement data obtained for both trades, on the other hand, proves different.

Table 6.2: Minimum and maximum stresses (Dynamic and Wave responses)

Sensor		Route 1		Route 2	
		Dynamic [MPa]	Wave [MPa]	Dynamic [MPa]	Wave [MPa]
DT1P	Max	113.5	113.2	104.9	107.0
	Min	-132.6	-128.9	-121.8	-114.3
DT2P	Max	138.5	133.4	119.1	115.3
	Min	-131.0	-129.8	-123.6	-123.0
DT3S	Max	130.7	130.5	121.1	115.3
	Min	-119.3	-119.6	-105.7	-103.1
DT4S	Max	112.3	111.4	107.3	104.6
	Min	-127.4	-119.9	-116.3	-114.1
DMP	Max	112.8	76.0	104.9	57.5
	Min	-136.4	-102.4	-105.2	-59.3
DMS	Max	104.1	65.3	87.2	54.9
	Min	-95.5	-69.4	-78.1	-56.5

Table 6.2 shows extreme values for measured stresses in hog (maximum) and sag (minimum), for both routes. The stresses are measured by 4 sensors, placed on a transverse deck strip (measuring transverse stresses in deck), and two sensors measuring longitudinal stresses in deck, in the midship area, as described in Chapter 4. From the measurements presented in the table, it becomes clear that the stresses measured in deck for Route 1 are higher than the stresses measured in deck for Route 2. This, in spite that the wave environment is more rough on the second route, on which the vessel crosses the North Pacific Ocean on its way from Singapore to USA. From the table, it can also be seen that maximum extreme values in hogging (maximum) and sagging (minimum) are measured in different sensors for the two routes. The reason is most likely that the vessel encounters the waves with different heading angles on the two routes. The same reason may explain why measured stresses are slightly higher for port side sensors. Additionally, if cargo is unevenly distributed over the breadth of the ship, this will also affect measured stresses.

The desire to find out why measured stresses shows a different trend than predicted, resulted in a more thorough investigation of the measurement data. This, to find out whether other factors may have had an influence on the stresses measured on the two different routes. MATLAB was used to make the program, *HG_mapplot.m* (see Chapter 5.1), which reads in the ships GPS coordinates, and generates a map plot of all voyages for both routes. The map plots for Route 1 and Route 2 respectively, are shown in Figure 6.5.

Ship position
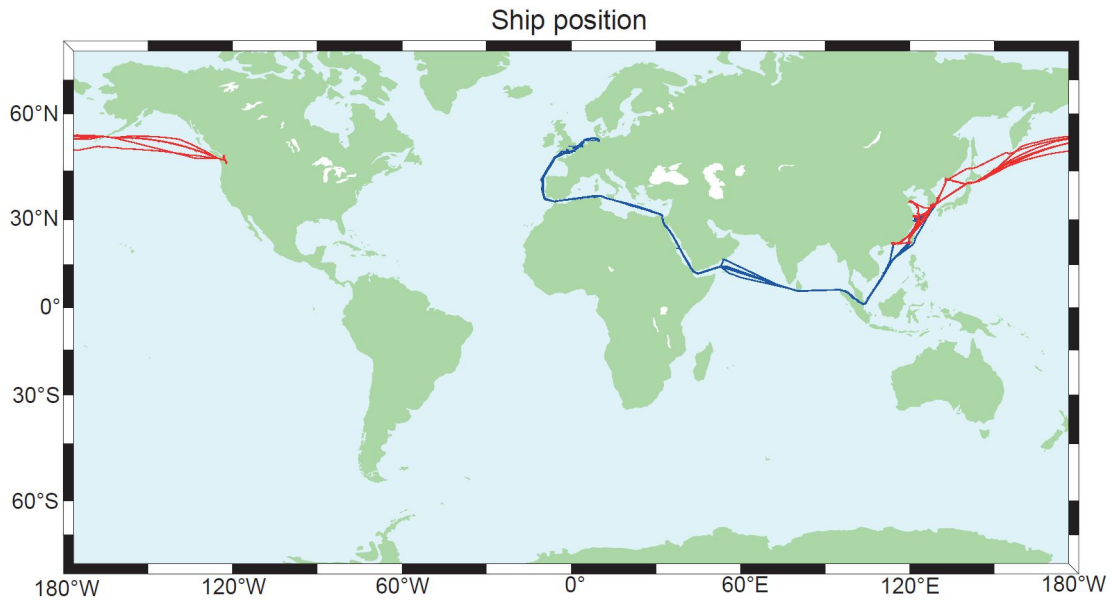
Figure 6.5: Routing - Route 1 (blue), Route 2 (red)

From Figure 6.5, it can be seen that the vessel has been sailing almost exactly the same path on every voyage on its first Route. Hence, no routing to avoid storms etc. has been performed on the first Route. The second Route on the other hand, shows a different trend. In the same figure, it is easy to see that the vessel has been sailing back and forth from Singapore to USA, several times. This implies that the vessel has been routing, and hence, the biggest storms have probably been avoided. Routing is a factor that will influence measured stresses on board a ship. When routing is performed to avoid storms, measured stresses will of course be smaller than if the vessel had not done any routing, just continuing right through the storm and rough seas.

Another point of interest in finding out why measured stress is smaller for Route 2 than Route 1, is the ship speed during voyages. Reducing the ship speed in rough seas, will also reduce the ship resistance and the magnitude of wave induced vibrations, such as slamming, whipping, springing and torsional vibrations, which give high maximum stresses. Therefore, stresses in the ship hull can be significantly smaller, if the vessel speed is reduced when the vessel encounters storms and rough seas. A MATLAB program, $HG\_speed.m$ (see Chapter 5.1), was made, reading in the ship speed over ground for both routes, and plotting graphs with ship speed as percent of time in operation (see Figure 6.6). Speeds in ports are filtered out.

73
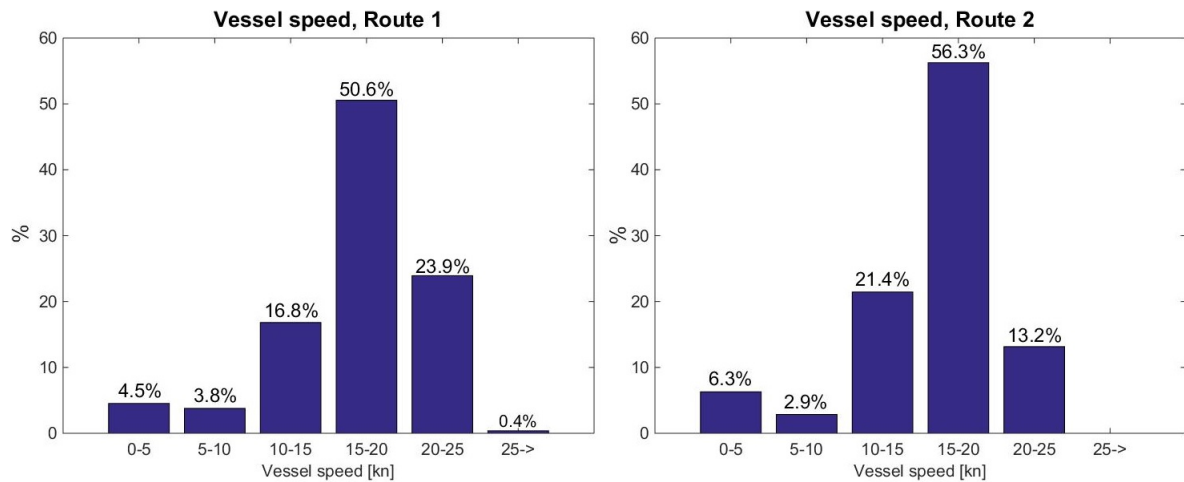
Figure 6.6: Vessel speed, Route 1 and Route 2

From the diagrams in Figure 6.6, it is seen that the vessel operates mainly with a speed over ground between 15 and 20 knots on both routes. However, on Route 1 the ship speed tends to be increased to 20-25 knots (23.9 % of the time) more often than decreased to 10 - 15 knots (16.8 % of the time). Route 2 shows the opposite trend. Here, the speed is increased from 15-20 knots to 20-25 knots only 13.2 % of the time, whereas the speed is reduced to 10 - 15 knots 21.4 % of the time. Thus, by comparing the two diagrams it comes clear that the vessel operates at higher speeds on its route from Hamburg to Singapore (Route 1), than from Singapore to USA (Route 2). The speed reduction on Route 2 compared to Route 1, is another reason why the measured stresses are lower on Route 2, in despite that the wave environment is more rough on this route.

The lowest speeds (0-5 knots) may have been measured when the ship has been anchored. Then, the ship may drift and hence, have a speed relative to the ground although the machinery is turned off. Wind direction and currents may also influence the ships speed relative to the ground. Therefore, the real vessel speed may differ somewhat from the measured "speed over ground". However, the speed above ground gives a sufficient overall picture of the vessels speed under operation.

6.2 Torsional Vibrations

Since torsion is not yet included in the ship rules, it is of particularly interest to investigate whether vibrations due to torsion arises in the hull structure during operation. To include torsion in future ship rules, it is of interest to collect information about torsional vibrations from several container vessels, which again

can be used to get a better understanding of torsional behaviour of open ship structures. Investigation of torsion in several container ships may help to form the basis for implementation of torsion in the ship rules for container carriers, in the future.

Measurement data were read into the MATLAB program, *HG_cleanplot_extreme.m* (see Chapter 5.1), in order to make a plot of the time history of maximum and minimum stresses. Both dynamic stresses and stresses due to waves are plotted. Dynamic stresses are stresses where frequencies below 0.01 Hz are filtered out. This means that stresses from these measurements contains both wave induced stresses and stresses due to for instance vibrations. In the measurement data containing the wave stresses, energy due to vibrations, frequencies above 0.3 Hz are filtered away.

When the measured dynamic stress differs from measured wave stress, vibrations are present in the measurements. No vibrations are present when the ratio between maximum dynamic stress and maximum wave stress is equal to 1 (see Equation 6.2). The same relation as shown in Equation 6.2 applies for minimum dynamic and wave stresses.

$$\frac{max(\sigma_{DYN})}{max(\sigma_{WAV})} = 1 \qquad (6.2)$$

In Figure 6.7 the ratio between minimum dynamic and wave stress is plotted for one of the longitudinal sensors midships, and for the four sensors on the transverse deck strip. From the figure it can be seen that no significant vibrations are measured in the transverse deck strip on the first route. Only torsional vibrations are measured in the deck strip, hence no significant torsional vibrations seems to have occurred for the vessel on its route from Hamburg to Singapore. The sensor measuring the ratio between dynamic stresses and wave stresses in longitudinal direction at the midship section, on the other hand, shows a significant influence of vibrations. These vibrations may be due to for example vertical or horizontal bending moment, or, they may be wave induced, such as whipping, slamming and springing vibrations. The plots for maximum stresses for Route 1, and both minimum and maximum stresses on Route 2, show similar trends as in Figure 6.7.
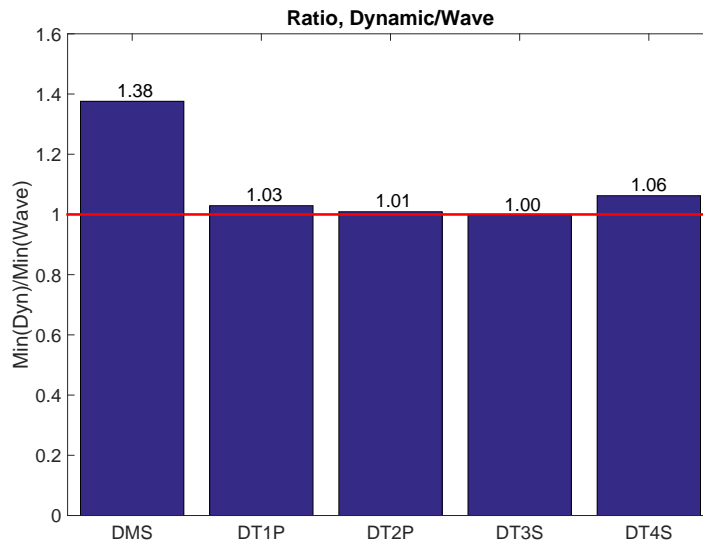
Figure 6.7: Ratio, dynamic stress/ wave stress, Route 1

Although it seems like the vessel has not yet been exposed to any significant torsional vibrations, vibrations do not last for more than a few seconds, and may therefore not be captured by the measured 30 minute statistics, which only stores measurements every 30 minute. Therefore, the MATLAB program uses the time series to find measurements in the 30 minute statistics, were the difference in measured dynamic and wave stress is significant. For the time periods of interest, the MATLAB program inquires whether raw data is available.

For the days with highest measured vibrations, where raw-data was available, frequency spectrums were plotted for both sensors measuring longitudinal stresses, and for the sensors measuring stresses in the transverse deck strip. Comparison of the spectrums, for one sensor measuring longitudinal stresses and one sensor on the transverse deck strip, can tell whether torsional vibrations are present or not. Torsional vibrations are present if the frequency spectrum for the deck strip sensor has a second peak at 2.5 rad/sec, whereas the sensor measuring longitudinal stresses in deck, does not. This is illustrated in Figure 6.8, and seen from Equation 6.3. However, if both spectrum's have a peak at 2.5 rad/sec, it is impossible to say whether they are due to torsional vibrations.
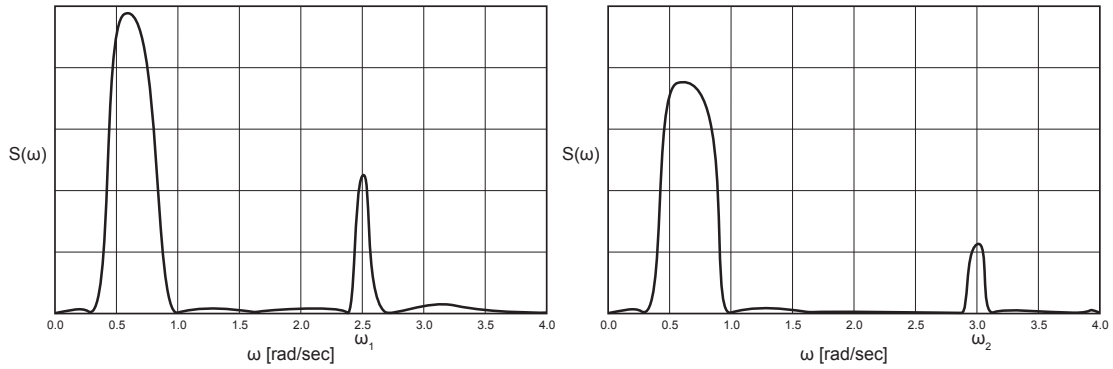
Figure 6.8: Illustration of spectrums where torsion is found

$$\omega_1 \neq \omega_2 \rightarrow Torsion \tag{6.3}$$

Figure 6.9 shows plotted spectrums for Sensors DT3S and DMS. The spectrums are plotted from raw data measurements obtained between 7 and 8 pm the 3rd of November 2011, which is the day and time where most torsional vibrations are found.
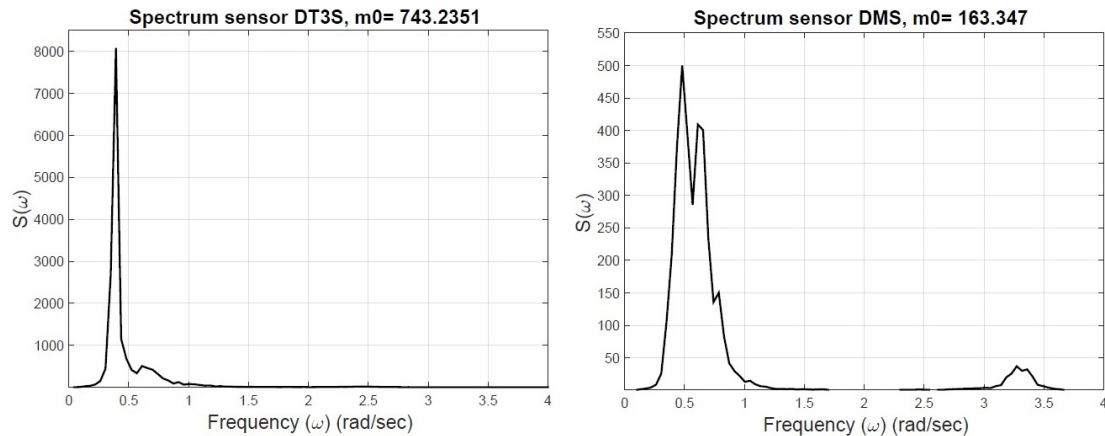

Figure 6.9: Spectrum DT3S and DMS - 03.11.2011, 7 pm

In neither of the spectrums in Figure 6.9, which shows the spectrum plotted for Sensor DT3S and DMS respectively, a second peak at 2.5 rad/sec is present. However, when plotting the spectrums with log scale, the trend described in Figure 6.8 can barley be seen, see Figure 6.10.
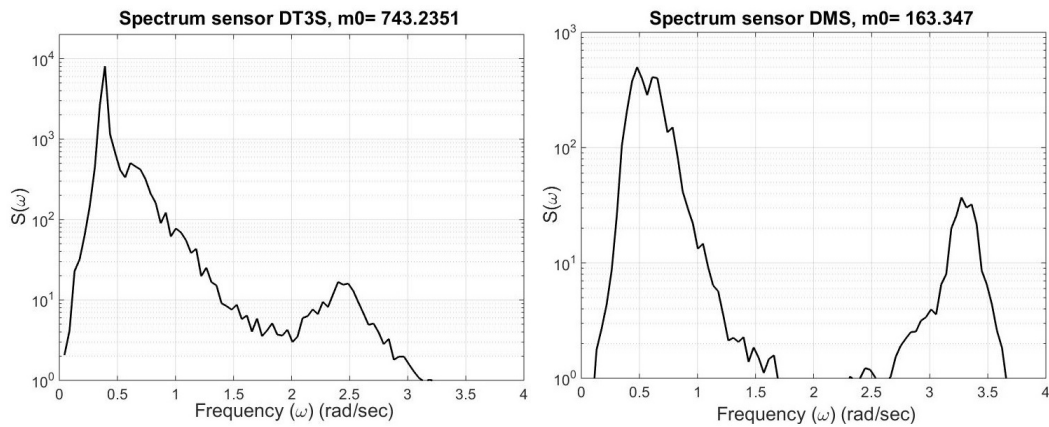
Figure 6.10: Spectrum DT3S and DMS - 03.11.2011, 7 pm, log scale

Only a minor sign of torsion is seen by comparing the spectrums for sensor DMS and DT3S, although they are plotted with log-scale (Figure 6.10). In Figure 6.11 measured vibrations are plotted for all sensors on the transverse deck strip the 3rd of November 2011. It can be seen that approximately the same amount of torsional vibrations are measured for all deck strip sensors that day. No significant torsional vibrations are found neither from the 30 minute statistics, nor from raw data. It should be noted that raw data was not available for the most interesting days in the time series. Thus, the ship may have experienced more significant torsional vibrations than found from the available measurement data. However, it is unlikely that the ship has experienced any significant torsional vibrations, since only minor signs of torsional vibrations are found from available measurement data.
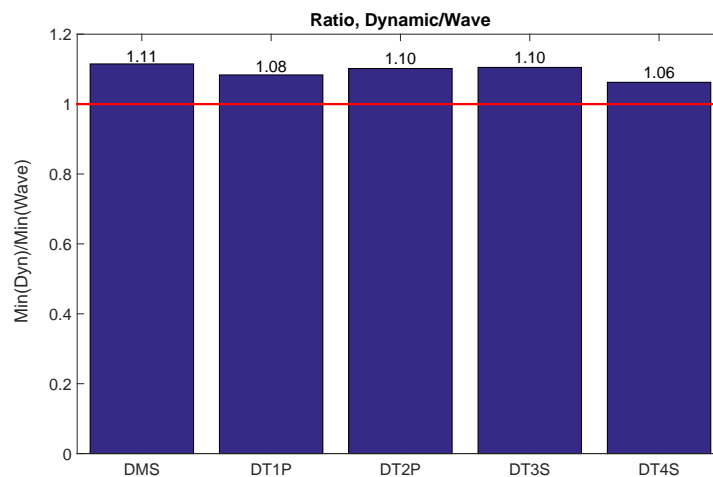

Figure 6.11: Ratio, dynamic stress/ wave stress, Route 1

78

6.3 Ultimate Limit State - *ULS*

A global FE-analysis of the container vessel has been performed, with respect to Ultimate Limit State (ULS) due to torsion. A coarse mesh was used to obtain nominal stresses. Rule stresses with respect to ULS were found by applying torsional moments, calculated from ship rules. Figure 6.12 shows the container vessel, deformed due to torsion.
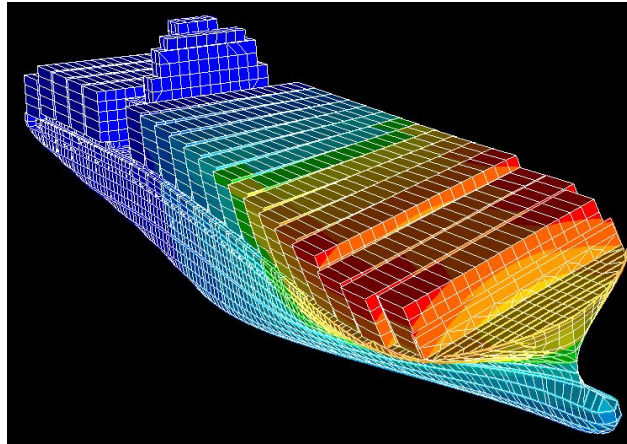
Figure 6.12: Global Model - torsional deformation

The aim with the global FE-analysis was to compare measured stresses on the transverse deck strip midships, with values for ULS rule stresses, with respect to yielding, obtained from the analysis. Maximum measured stress for all sensors located on the deck strip are presented in Table 6.1. Since a coarse mesh is used in the analysis to obtain nominal stresses in the deck strip, the stresses found from the model are averaged over a relatively large mesh element. Thus, stress linearity was used to find the stresses at the measurement positions from the model. Figure 6.13 shows how the stress varies over the length and the breadth of the deck strip.
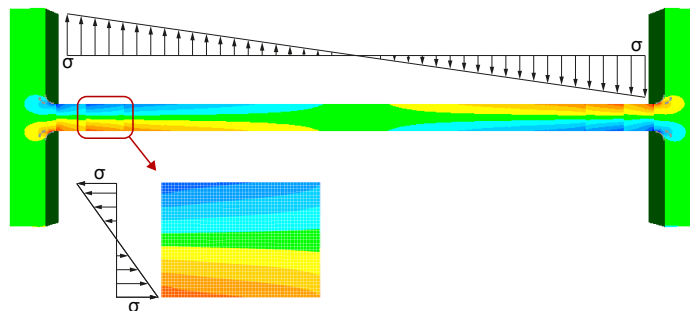
Figure 6.13: Linear variation of stresses

79

Acceptable stresses with respect to ULS, on the measurement points for all 4 sensors on the transverse deck strip, are shown in Figure 6.14. The figure is a cut out of the global FE-model, showing three deck strips in the midship area.
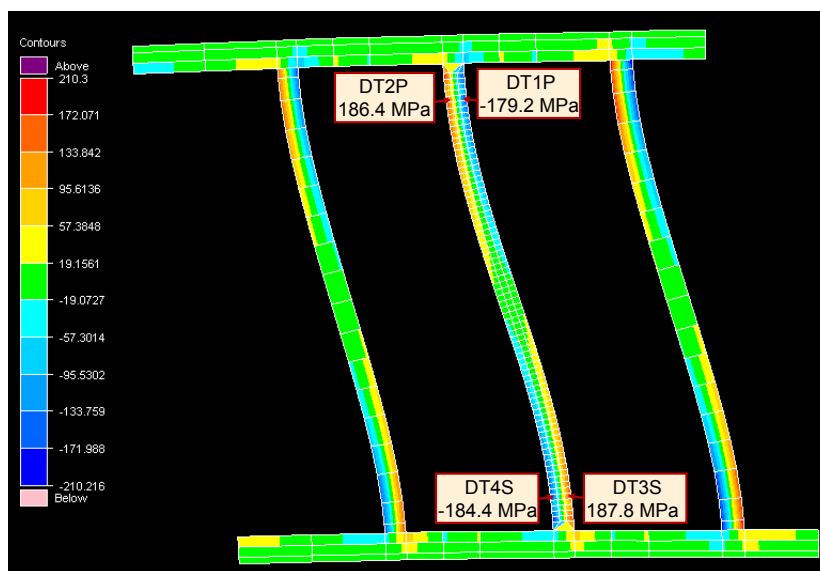
Figure 6.14: ULS rule stresses at measurement points

Values for both measured stresses and ULS stresses obtain from the FE-analyses are presented in Table 6.3.

Table 6.3: Measured Stress vs. ULS Stress

	DT1P	DT2P	DT3S	DT4S
ULS Rule Stress [MPa]	179.2	186.4	187.9	184.4
Measured Stress Route 1 [MPa]	132.6	138.5	130.7	127.4
Measured Stress Route 2 [MPa]	121.8	123.6	121.1	116.3
Route 1 [measured/rule]	0.74	0.74	0.70	0.69
Route 2 [measured/rule]	0.68	0.66	0.64	0.63

From the table it can be seen that measured stresses are approximately 0.69 - 0.74 of ULS rule stresses on Route 1 and 0.63 - 0.68 % on Route 2. Hence, maximum measured stresses for both routes are within the acceptance criteria for ULS, with respect to yield.

6.4   Local Stresses

Since local stresses may be included in the measurements, the same analysis of the transverse deck strip was performed with fine mesh. This was done using the submodelling technique, which is described in Chapter 5.2.4. A mesh of approximately 50 x 50 mm was used to get a sufficient representation of local stresses. Stress linearity was used to find stresses at the sensors locations (see Figure 6.13). Values obtained from the FE-analysis are shown in Figure 6.15.
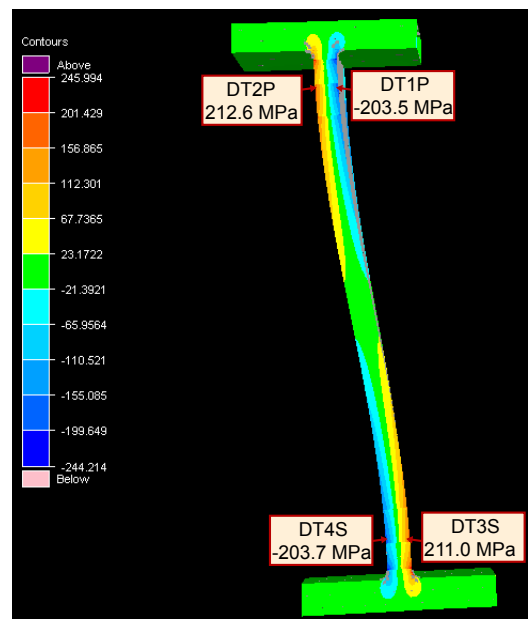
Figure 6.15: Local stresses at measurement points

In Table 6.4, both global (nominal) stresses and local stresses, obtained from the global model and from the local model respectively, are presented.

Table 6.4: Global vs. Local stresses

	DT1P	DT2P	DT3S	DT4S
Global (nominal) Stresses [MPa]	-179.2	186.4	187.9	-184.4
Local Stresses [MPa]	-203.5	212.6	211.0	-203.7
% Local Stress	13.6	14.1	12.3	10.5

From the table, it is seen that local stresses obtained from the submodel, with fine mesh, are about 10-15 % higher than nominal stresses obtained from the global model with coarse mesh. This means that 10-15 % of the measured stresses

81

are expected to represent local stresses. The local stresses in the measurements are most likely due to the fact that the sensors are located close to hatch corners and close to a weld between two deck plates. Hatch corners and welds are sources to stress concentrations, i.e. hot spot stresses, which will influence the measured stresses if the sensors are located close to such areas.

By considering the stress distribution in the transverse deck strip (see Figure 6.15), it can be seen that the sensors are not placed where local stresses are at its highest. When it comes to examine yielding, as well as fatigue, it is desired that the measurements includes maximum local stresses, i.e. stress concentrations at hatch corners. For hatch opening distortions on the other hand, it is preferred that the sensors measure nominal stresses in the deck strip. As the placement of the sensors includes 10-15 % local stresses, measured stresses are not optimal neither for determination of ULS or FLS, nor the hatch opening distortion. Although the results are not optimal, they give good indications for both the limit states and hatch opening distortions.

6.5 Hatch Opening Distortion

Container vessels, exposed to torsional loads will show a typical "s-formed" deformation of the transverse deck strips as a result of the large openings in the deck structure. It was of particular interest to use measured stresses to estimate the magnitude of the hatch opening distortion, at the transverse deck strip midships. Extreme values for measured stresses, which are listed in Table 6.1, are used in the calculations. This, because the greatest measured stress, results in the largest deformation, which means worst case.

The calculations were done simplified, with use of both hand calculations, DNV GL Software; NAUTICUS 3D-Beam, and by applying a forced displacement to a Finite Element model of the deck strip. In addition, the hatch opening distortion was calculated directly from the global model. The simplified calculations were done to find out whether or not simplified and less time consuming methods can be used in later studies of hatch opening distortions, or if a global model must be used for this purpose.

6.5.1 Hand Calculations

To start with, the deck strips behaviour when the vessel is exposed to torsional loads, was simplified to a beam. The deck strip is assumed to be fixed at the ship sides. Thus, the beam is fixed against translation and rotation in all directions at

82

one end, and only free to deform in z-direction at the other end, as illustrated in Figure 6.16. The calculation of moment and shear force at the supports for this specific case, is found from Equations 6.4 and 6.5, respectively (Mathisen; 2013).
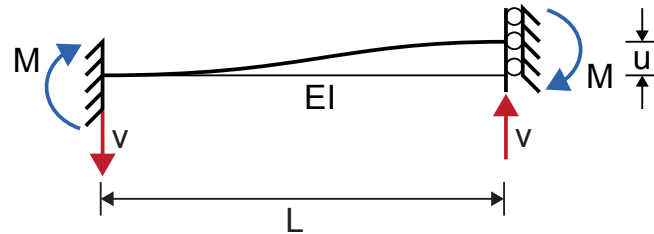
Figure 6.16: Beam deflection

$$M = \frac{6EI}{L^2}u \tag{6.4}$$

$$v = \frac{12EI}{L^3}u \tag{6.5}$$

To calculate the moment at the end of the beam, the beam was given a prescribed unit displacement, $u = 1mm$. The deck strip was assumed to have a constant cross section, as illustrated in Figure 6.17. The belonging cross section properties are listed in Table 6.5.
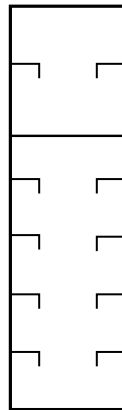

Figure 6.17: Cross section of transverse deck strip midships

Table 6.5: Cross section properties

Cross section property	Symbol	Value	Unit
Area	A	240 144	mm^2
Length of deck strip	L	39 100	mm
Moment of Inertia	I	$1.5433 * 10^{11}$	mm^4
Young's modulus	E	206 000	MPa
Section modulus	W	$1.7148 \cdot 10^8$	mm^3
Prescribed displacement	u	1	mm

The moment calculated from Equation 6.4, using the cross section properties listed in Table 6.5 gave a moment of:

$M = 124.77 \ kNm$

Further, Equation 6.6 was used to estimate the stress in the deck strip.

$$\sigma = \frac{M}{W} \tag{6.6}$$

With hand calculations the estimated stress in the deck strip, became:

$\sigma_{hand} = 0.728 \ MPa$

The calculated stress due to a forced displacement of 1 mm, was converted to real hatch opening distortion using the following relation:

$$\frac{\sigma_{model}}{u_{model}} = \frac{\sigma_{measured}}{u_{real}} \rightarrow u_{real} = \frac{\sigma_{measured}}{\sigma_{model}} u_{model} \tag{6.7}$$

Values obtained for hatch opening distortions for maximum and minimum measured stresses are presented in Table 6.6.

Table 6.6: Hatch opening distortion - Hand calculations

Hand Calculations					
	Route 1		Route 2		
	$\sigma_{Measured}$ [MPa]	Distortion [mm]	$\sigma_{Measured}$ [MPa]	Distortion [mm]	
DT1P	Max 113.5	156.0	Max 104.9	144.2	
	Min -132.6	-182.2	Min -121.8	-167.4	
DT2P	Max 138.5	190.3	Max 119.1	163.7	
	Min -131.0	-180.0	Min -123.6	-169.9	
DT3S	Max 130.7	179.6	Max 121.1	166.4	
	Min -119.3	-164.0	Min -105.7	-145.3	
DT4S	Max 112.3	154.3	Max 107.3	147.5	
	Min -127.4	-175.1	Min -116.3	-159.8	

From the table it is seen that the hatch opening distortion varies between 154.3 mm and 190.3, mm depending on the sensor used in the calculations, for Route 1. Hatch opening distortions are lower for Route 2, since measured stresses on this route are lower.

6.5.2 NAUTICUS 3D-Beam

In DNV GL Software, NAUTICUS 3D-beam, the deck strips behaviour when the vessel is exposed to torsional loads, was again simplified to a beam, which is assumed to be fixed at both ship sides. The 3D-beam model of the deck strip was fixed against translation and rotation in all directions at one and, and free to deform in z-direction and fixed in all other directions at the other end. The beam was applied a forced displacement of, $u = 1mm$. The deck strip was modelled with the cross section, illustrated in Figure 6.17. Belonging cross section properties were calculated in 3D-Beam. The analysis in 3D-beam gave an estimated deck strip stress of:

$$\sigma_{3D-Beam} = 0.704 \ MPa$$

The calculated stress due to a forced displacement of 1 mm, was converted to real hatch opening distortion using the same relationship as for hand calculations (Equation 6.7). Values obtained for hatch opening distortions for maximum and minimum measured stresses are presented in Table 6.7.

Table 6.7: Hatch opening distortion - 3D-Beam

3D-Beam					
	Route 1			Route 2	
	$\sigma_{Measured}$ [MPa]	Distortion [mm]		$\sigma_{Measured}$ [MPa]	Distortion [mm]
DT1P	Max 113.5	161.1	Max 104.9		148.9
	Min -132.6	-188.3	Min -121.8		-172.9
DT2P	Max 138.5	196.6	Max 119.1		169.1
	Min -131.0	-186.0	Min -123.6		-175.5
DT3S	Max 130.7	185.6	Max 121.1		171.9
	Min -119.3	-169.4	Min -105.7		-150.1
DT4S	Max 112.3	159.4	Max 107.3		152.3
	Min -127.4	-180.9	Min -116.3		-165.1

From the table it is seen that the hatch opening distortion varies between 159.4 mm and 196.6 mm for Route 1, depending on the sensor used in the calculations. These values are slightly higher than for hand calculations. 3D-Beam uses the same formulas to calculate stresses as for hand calculations. Since the difference in the results from 3D-Beam and hand calculations are small, this verifies that the hand calculations are carried out correctly, and vice versa. The minor difference in the results comes from the different methods for calculating cross section properties.

6.5.3   Local Model

Hatch opening distortion was also calculated simplified using the local FE-model of the deck strip. Boundary conditions and loads were applied directly to the model, i.e. submodelling is not used in these calculations. Just as the det model used in hand calculations and in 3D-Beam, the model was fixed at one end, and free to deform in z-direction and fixed in all other directions at the other end. The model was given a prescribed displacement of $u = 1mm$. Figure 6.18 shows the deformed model (scaled), due to the applied forced displacement. In the same figure the undeformed model is shown in blue. The approximate location of the different sensors are marked on the undeformed model.
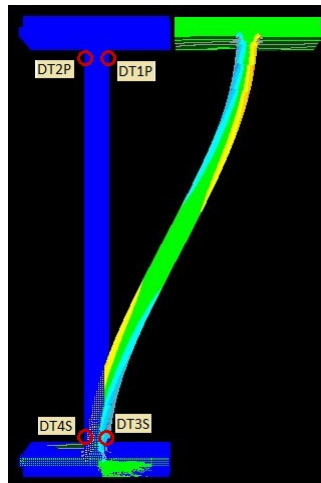
Figure 6.18: Local model - undeformed and deformed

Stresses obtained at the different measuring positions are listed in Table 6.8. Stress linearity was used to estimate the magnitude of stresses at the position where the sensors are located.

Table 6.8: Local model - Stresses

	DT1P	DT2P	DT3S	DT4S
Stresses [MPa]	0.605	0.624	0.623	0.604

The resulting Hatch opening distortion from measured stresses are presented in Table 6.9. Equation 6.7 was used to calculate the hatch opening distortions.

Table 6.9: Hatch opening distortion - Local Model

Local Model				
	Route 1		Route 2	
	$\sigma_{Measured}$ [MPa]	Distortion [mm]	$\sigma_{Measured}$ [MPa]	Distortion [mm]
DT1P	Max 113.5	186.1	Max 104.9	172.0
	Min -132.6	-217.4	Min -121.8	-199.7
DT2P	Max 138.5	220.2	Max 119.1	189.4
	Min -131.0	-208.3	Min -123.6	-196.5
DT3S	Max 130.7	208.6	Max 121.1	193.2
	Min -119.3	-190.4	Min -105.7	-168.7
DT4S	Max 112.3	184.6	Max 107.3	176.4
	Min -127.4	-209.4	Min -116.3	-191.2

Hatch opening distortions calculated from the local FE-model are greater than calculated from 3D-Beam and with hand calculations. Hatch opening distortions obtained using a local model, are between 184.6 mm and 220.2 mm for Route 1. The local model is more accurate than hand calculations and 3D-Beam, where a constant cross section is assumed. In reality the cross section of the transverse deck strip varies over the breadth of the ship, and hence the use of the other simplified methods give less accurate results. In addition, the solution method for calculating stresses, is more complex when the finite element method is used.

6.5.4 Global Model

Hatch opening distortions were also calculated using the global model of the container vessel. When a container vessel is exposed to a torsional moment, the ship sides are free to deform and rotate. Because of this, and the fact that the deck strip is not completely fixed at the ship sides, it will not only deform in the longitudinal direction of the ship, as assumed in the previous calculations of hatch opening distortions. Therefore, the relative deformation in longitudinal direction due to the applied torsional moment had to be calculated for the global model. Relative deformations are complex, and therefore difficult to calculate. The definition of the relative deformation of the deck strip, when it deforms as a part of the global model i.e. the real deformation of the deck strip, is illustrated in Figure 6.19.
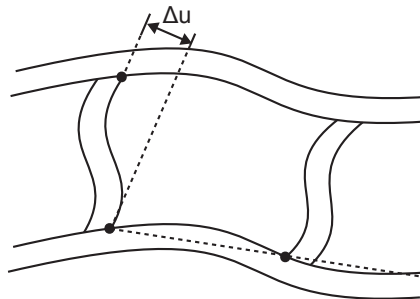

Figure 6.19: Relative deformation of deck strip

Since relative displacements of ship structures are complex, and difficult to calculate, this is done simplified by only considering deformations in x- and y-direction (longitudinal and transverse). The relative deformation in x-direction due to deformation in z-direction is neglected, since it is assumed to be much smaller than the contribution from x- and y-direction. Equation 6.8 is used to calculate the relative deformation of the deck strip, and has been used in earlier studies on torsional responses of container ships, performed by DNV GL (DNV; 2013a). The

positions on the FE-model where the deflections in Equation 6.8 are obtained from, are shown in Figure 6.20.

$$\Delta u = dx_1 - dx_2 + [\frac{(dy_3 - dy_4)}{2} - \frac{(dy_1 - dy_2)}{2}]\frac{B_{Hatch}}{L_{Hatch}} \quad (6.8)$$

Where L_{Hatch} is the length of the hatch in the ships longitudinal direction. B_{Hatch} is the hatch width and the deformation of the hatch corner is given by dx_n and dy_n, where n defines the hatch corner.

1. Aft Port

2. Aft Starboard

3. Forward Port

4. Forward Starboard
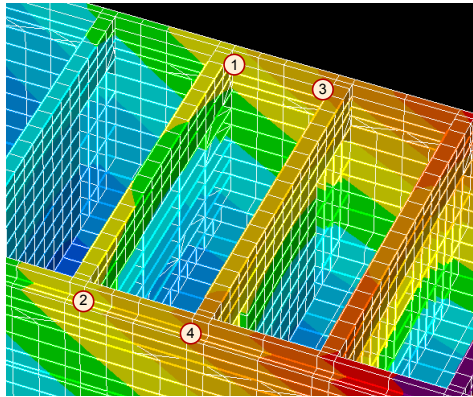
Figure 6.20: Read out positions, relative deflection

The relative deformation of hatch openings were calculated for all hatches along the ship, using ULS rule torsional moments as described in Chapter 3.1.1. This, to find the maximum hatch opening distortion the ship is allowed to experience during its lifetime. In Figure 6.21, calculated maximum hatch opening distortion for all cargo holds, due to the ULS rule stresses with respect to yield, are shown. It should be noticed that the results are representative for real hatch opening distortions midships and forward, but not after ships, due to fixed boundary conditions at the stern. From the figure it can be seen that hatch opening distortions are close to zero at the deck house (DH) and forecastle (Upper FWD), since these structures represents torsional constraints.
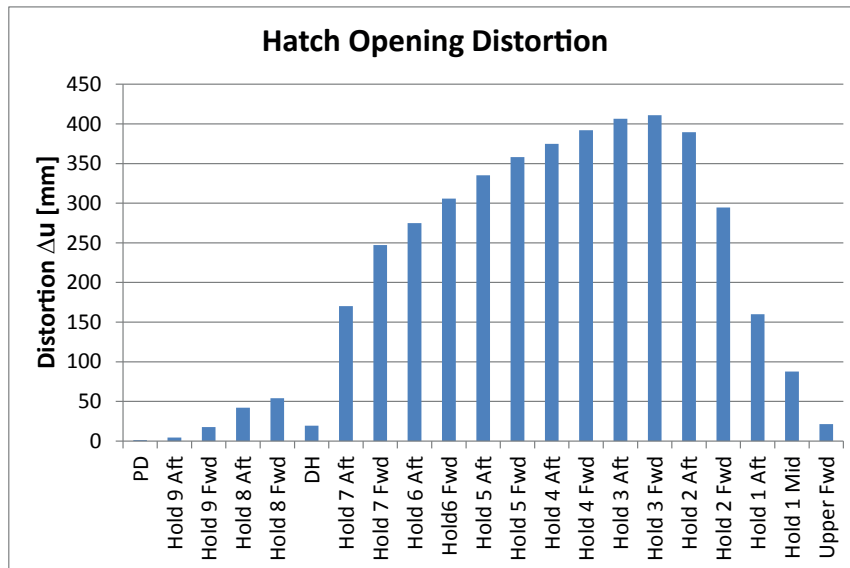
Figure 6.21: Relative hatch opening distortions

The four sensors considered in this project work, are located on the deck strip at Hold 5 Aft in Figure 6.21. From the figure it can be seen that hatch opening distortions can become as high as 335 mm for the vessel at this location, before yielding of the structure occurs. However, collapse due to e.g. buckling may take place, and ULS with respect to buckling should therefore also be assessed. Hatch opening distortions are at its highest at Hold 3 Fwd, where the deformations reaches 411 mm. A hatch opening distortion of 335-411 mm is significant. It is important that containers are placed such that they are not being crushed by the movement of transverse structure due to the hatch opening distortion (DNV; 2013b).

To calculate the hatch opening distortion due to measured stresses, stresses obtained from the submodel (see Table 6.4), were used. This was done, since local stresses are included in the measurements, and must therefore be taken into consideration. The respective hatch opening distortion, is presented in Table 6.10.

Table 6.10: Hatch opening distortion - Global model

		Global (Sub) Model		
	Route 1		Route 2	
	$\sigma_{Measured}$ [MPa]	Distortion [mm]	$\sigma_{Measured}$ [MPa]	Distortion [mm]
DT1P	Max 113.5	203.7	Max 104.9	188.3
	Min -132.6	-238.0	Min -121.8	-218.6
DT2P	Max 138.5	237.9	Max 119.1	204.6
	Min -131.0	-225.0	Min -123.6	-212.3
DT3S	Max 130.7	226.3	Max 121.1	209.7
	Min -119.3	-206.6	Min -105.7	-183.0
DT4S	Max 112.3	201.3	Max 107.3	192.4
	Min -127.4	-228.4	Min -116.3	-208.5

For Route 1, hatch opening distortions obtained from the global FE-model, are between 201.3 mm and 230.8 mm. Hatch opening distortion calculated from the global model is higher than for simplified calculations. This because of the fact that the deck strip deforms and rotates in all directions when it is analysed as a part of the ship. Additionally, the deck strip is not completely fixed to the ship sides, as assumed in the simplified calculations. An analysis with the global model gives the best approximation to the real deformations of the entire ship, and hence the deck strip. Therefore, the hatch opening distortions calculated from the global model are more accurate than calculated from simplified methods.

In Table 6.11 hatch opening distortions due to stresses measured with Sensor DT3S are summarized for all calculation methods. Distortions due to measured sagging (minimum) and hogging (maximum) stresses are listed in the first and second row for each calculation method, respectively. Hatch opening distortions are summarized for Sensor DT3S, since this sensor is assumed to be the most reliable sensor after analysing the measurement data (see Chapter 5.1). Hatch opening distortions due to measured stresses for Sensor DT3S, calculated with the global FE-model, varies between +226.6 and -206.3 mm. This implies that the deck strip has experienced a total variation of 432.9 mm in hatch opening distortion, since the vessel deforms in opposite directions in sag and hog.

Table 6.11: Hatch opening distortion, Sensor DT3S

	Distortion [mm]	
	Route 1	Route 2
Hand Calculations	179.6 -164.0	166.4 -145.3
3D-Beam	185.6 -169.4	171.9 -150.1
Local Model	208.6 -190.4	193.2 -168.7
Global Model	226.3 -206.6	209.7 -183.0

Values for hatch opening distortion for the simplified calculation methods are between 7-21% lower than calculated from the global model. Hence, the same calculations must be performed for other container vessels to see if similar results are obtained, before it can be concluded whether simplified methods can be used. If further studies of container ships give the same relation between the simplified methods and the global model, simplified methods might be used by introducing a scaling factor.

7 Conclusion

A 8600 TEU vessel has been operating on two different trades. On Route 1, the vessel follows a relatively sheltered passage from Hamburg to Singapore, whereas the vessel crosses the North Pacific Ocean from Singapore to USA on Route 2. Long term distribution of deck stresses verifies that Route 2, which is known for more rough seas, gives the worst prediction of stresses. However, measured stresses proves different.

No significant routing has been observed on the first route. On the second route on the other hand, the vessel has been routing, i.e. the roughest seas have been avoided. This will again influence and lower measured stresses. Investigations of the ship speed during operation, prove that the vessel operates at higher speeds on Route 1, than on Route 2. With speed reduction, the ship resistance, and the risk for occurrence of high stresses due to wave induced vibrations, such as whipping, springing and torsional vibrations, are lowered. Routing and speed reduction are therefore important reasons why measured stresses are higher for Route 1, in despite that the wave environment is more rough on Route 2.

No significant torsional vibrations are found neither from the 30 minute statistics, nor from raw data. Although torsional vibrations are found to be of minor importance for this specific vessel, torsional vibrations may be of higher importance for container ships in general. Therefore, investigation of torsion in other container ships must be conducted to find whether it needs to be implemented in the ship rules for container carriers in the future.

Global FE-analyses were conducted in order to compare measured stresses on a transverse deck strip midships, with values for ULS rule stresses for yield. The results show that maximum measured stresses are approximately 0.69 - 0.74 of ULS rule stresses for Route 1 and 0.63 - 0.68 on Route 2, i.e. measured stresses on both routes are within the acceptance criteria for ULS.

A FE-analysis with respect to rule ULS stresses was also performed with fine mesh, to estimate the presence of local stresses in the measurements. It was found that local stresses are about 10-15 % higher than nominal stresses obtained from the global model, i.e. 10-15 % of the measured stresses are local stresses. The local stresses in the measurements are most likely due to the fact that the sensors are located close to hatch corners and close to a weld between two deck plates, which are sources to stress concentrations, i.e. hot spot stresses.

Relative deformation of hatch openings was calculated for all hatches along the ship, using ULS rule torsional moments. It was found that hatch opening

distortions can reach 335 mm at the deck strip where the sensors are located, before yielding of the structure occurs. However, collapse due to e.g. buckling may take place, and ULS with respect to buckling should therefore also be assessed. The largest hatch opening distortion obtained is located further forward, at cargo hold 3, where the deformation reaches 411 mm.

Calculations of the hatch opening distortions due to measured stresses were done with a global FE-model, and simplified, in terms of hand calculations, 3D-Beam and a local FE-model. This, in order to find out whether or not simplified and less time consuming methods can be used in later studies of hatch opening distortions.

The local FE-model gave higher accuracy than results from hand calculations and 3D-Beam, as it reflects cross section properties more precise. However, the global model gives the best approximation to real deformations, due to the fact that the deck strip deforms and rotates in all directions when it is analysed as a part of the ship. Additionally, the deck strip is not completely fixed in the ship sides, as assumed in the simplified methods.

Values for hatch opening distortion for the simplified methods are between 7-21% lower than calculated from the global model. Hence, the same calculations must be performed for other container vessels to see if similar results are obtained, before it can be concluded whether simplified methods can be used, introducing a scaling factor.

When investigating measured stresses with respect to yielding and fatigue, it is desired that maximum local stresses, i.e. stress concentrations at hatch corners, are included in the measurements. For hatch opening distortions on the other hand, it is preferred that the sensors measure nominal stresses in the deck strip. As the placement of the sensors includes 10-15 % local stresses, measured stresses are not optimal neither for determination of ULS or FLS, nor the hatch opening distortion. Although the results are not optimal, they give good indications for both the limit states and hatch opening distortions.

Measured stresses for Route 1, were high, and were expected to be even higher for Route 2. Therefore, the change of trade to the Asia to USA trade could have lead to extremely high stresses, which again could have fatal consequences. However, from the comparison between the measurements from the two different routes, it seems that routing and speed reduction on the Asia to USA trade has kept stresses, torsional vibrations and hatch opening distortions at a lower level than predicted.

8 Recommendations for Further Work

Torsion becomes of increased importance as container ships are built constantly larger, especially when transverse structure is considered. Therefore, it is of further interest and importance to investigate how and if torsion affects the fatigue damage accumulation. This can be done by examining how measured stresses in the transverse deck strip are compared to rule values, with respect to fatigue. It is also of interest to estimate the magnitude of fatigue at hatch corners for the 8600 TEU vessel, since they are sources to hotspot stresses. This, to ensure that the fatigue rates at hatch corners are within the acceptance criteria.

Torsional stresses increase when a vessel is heading through oblique waves. It could therefore be of interest to find out how wind and wave conditions affects the magnitude of torsional stresses acting on the ship hull. In addition, analyses have shown that the ship speed has a significant impact on fatigue damage accumulation. From these analyses, the torsional effect on fatigue damage accumulation seems to be of minor significance since torsional moments are of greater magnitude in oblique seas. However, this assumption needs to be further examined before drawing any conclusions.

Because of the huge hatch openings which characterizes a container ship, they are exposed to large diagonal deformations of hatch openings. They are also exposed to hot spot stresses close to hatch corners and warping stresses due to complex torsional moments in waves, compared to other seagoing vessels. In analyses with respect to Ultimate Limit State in this thesis work, measured stresses are compared to rule ULS stresses with respect to the yielding criteria for transverse structure. It is of further interest to conduct a similar analysis, emphasizing transverse structure with respect to the buckling criteria for ULS.

When analyses are done with respect to fatigue and buckling, these results, together with the results from the analyses of yielding and hatch opening distortions, can be used to propose a setup for further placement of sensors. Since the hull monitoring system, and especially the sensors are expensive, it is desirable to achieve reliable results with respect to yielding, buckling, hatch opening distortions and fatigue, using as few sensors as possible. It is of interest to compose a standard setup, for all container carriers to increase the efficiency of installation, maintenance and post processing of measurements. This will again ensure a more cost-effective and reliable hull monitoring system, as well as higher expertise within hull monitoring of container vessels.

Torsional vibrations were not considered important for the 8600 TEU vessel. However, torsional vibrations may be of higher importance for other container

vessels. Therefore, a more thorough investigation of torsion in several container ships must be conducted to document the importance of torsional vibrations. This will again form the basis for making the decision on whether torsion needs to be implemented in the ship rules for container carriers in the future.

Hatch opening distortions for the 8600 TEU vessel were estimated with different calculation methods. This, in order to find out whether or not simplified and less time consuming methods can be used in later studies of hatch opening distortions, or if a global model must be used for this purpose. Since simplified methods gave lower results than the global model, the same calculations must be conducted for other container vessels to see if similar results are obtained, before it can be concluded whether simplified methods can be used. If future investigation of hatch opening distortions verifies that other container vessels have the same degree of accuracy, these methods may be used, introducing a scaling factor.

Bibliography

Amdahl, J. (2010). Marin Teknikk 2, Compendium TMR4167, Faculty of Engineering Science and Technology, NTNU.

BMT (2011). Global Wave Statistics. Visited on 18.05.2015.
  URL: *http://www.globalwavestatisticsonline.com/*

DNV (2004). Hull Structural Design - Ships with Length 100 metres and Above, *Part* **3**.

DNV (2013a). 18K TEU Container Vesel, Global and Local ULS Analyses.

DNV (2013b). Classification Note No. 31.7, CSA - Strength Analysis of Hull Structures in Container carriers.

DNV (2013c). Classification Note No. 34.1, CSA - Direct Analysis of Ship Structures.

DNV (2014a). Classification Note No. 30.7, Fatigue Assessment of Ship Structures.

DNV (2014b). DNV-OS-C101, *Design of Offshore Steel Structures, General (LFRD Method)* .

DNV (2014c). DNV-OS-C102, *Structural Design of Offshore Ships* .

DNV GL (2013). Full Scale Measurements – Whipping, Springing and Warping Stresses. Visited on 24.02.2015.
  URL: *http://www.dnv.in/industry/maritime/servicessolutions/consulting/ technical-consulting/str/fullscale.asp*

Faltinsen, O. (1993). *Sea Loads on Ships and Offshore Structures*, Vol. 1, Cambridge University Press.

Haslum, K., Nordenstrom, N., Pedersen, B. and Tonnessen, A. (1973). Torsional Response of a Ship in the Seaway with Particular Reference to an LNG Tanker, *Norwegian Maritime Research* **1**(3).

Haslum, K. and Tonnessen, A. (1973). An Analysis of Torsion in Ship Hulls: European Shipbuilding, Vol 21, Nos 5–6 (1972), pp 67–90, *Computer-Aided Design* **5**(3): 196.

IMO (2014). Virtual publications, SOLAS. Visited on 14.09.2014.
  URL: *http://vp.imo.org/Customer/Subscriptions/IMOVEGA/MemberPages/ IMODocumentPrintFriendly.aspx?resultIndex=22*

Kahl, A., Fricke, W., Paetzold, H., von Selle, H. et al. (2014). Whipping Investigations Based on Large-Scale Measurements and Experimental Fatigue Testing, *The Twenty-fourth International Ocean and Polar Engineering Conference*, International Society of Offshore and Polar Engineers.

Li, Z. and Ringsberg, J. W. (2012). Fatigue Routing of Container Ships - Assessment of Contributions to Fatigue Damage from Wave-induced Torsion and Horizontal and Vertical bending, *Ships and Offshore Structures* **7**(2): 119–131.

Light Structures (2009). *Functional Description - SENSFIB*.

Mathisen, K. M. (2013). Lecture Notes: TMR 4190 - Finite Element Methods in Structureal Analysis, Lecture 1: Introduction and Fundamental Concepts.

Moan, T. (2003). Finite Element - Modelling and Analysis of Marine Structures, Compendium TMR4190, Faculty of Engineering Science and Technology, NTNU.

Paik, J. K., Thayamballi, A. K., Pedersen, P. T. and Park, Y. I. (2001). Ultimate Strength of Ship Hulls under Torsion, *Ocean Engineering* **28**(8): 1097–1133.

Shama, M. (2010). *Torsion and Shear Stresses in Ships*, Springer.

Storhaug, G. (2012). The Effect of Heading on Springing and Whipping Induced Fatigue Damage Measured on Container Vessels, *Proceedings of the sixth International Conference on Hydroelasticity in Marine Technology*.

Storhaug, G. (2013a). Can your Containership Sustain Whipping? Visited on 28.09.2014.
URL: *http://vp.imo.org/Customer/Subscriptions/IMOVEGA/MemberPages/ IMODocumentPrintFriendly.aspx?resultIndex=22*

Storhaug, G. (2013b). Safeguarding Container Ship Hulls Against Collapse. Visited on 24.02.2015.
URL: *http://www.dnv.com/industry/maritime/publications/archive/maritime _ update/2013/02_ 2013/Safeguarding_ container_ ship_ hulls_ against_ collapse.asp*

Tang-Jensen, P. and Shi, B. (2007). It's not just a matter of size.

Tozer, D. and Penfold, A. (2001). Ultra-Large Container Ships (ULCS): Designing to the Limit of Current and Projected Terminal Infrastructure Capabilities, *Lloyd's Register Technical Association Paper* (5): 2001–2002.

Tozer, D. and Penfold, A. (2007). Large Container Ships and the NPX.

Van Dokkum, K. (2008). *Ship Knowledge: Ship Design, Construction and Operation*, Dokmar.

Appendices

A   Analogy Between Torsion and Bending

To get a better understanding and explanation of the effect of a moment and an axial force acting on an open cross section, and hence the bimoment, the analogy between torsion and the more well known bending theory has been consulted. The analogy between torsion and bending is retrieved from Haslum et al. (1973).

| **Torsion** | **Bending** |
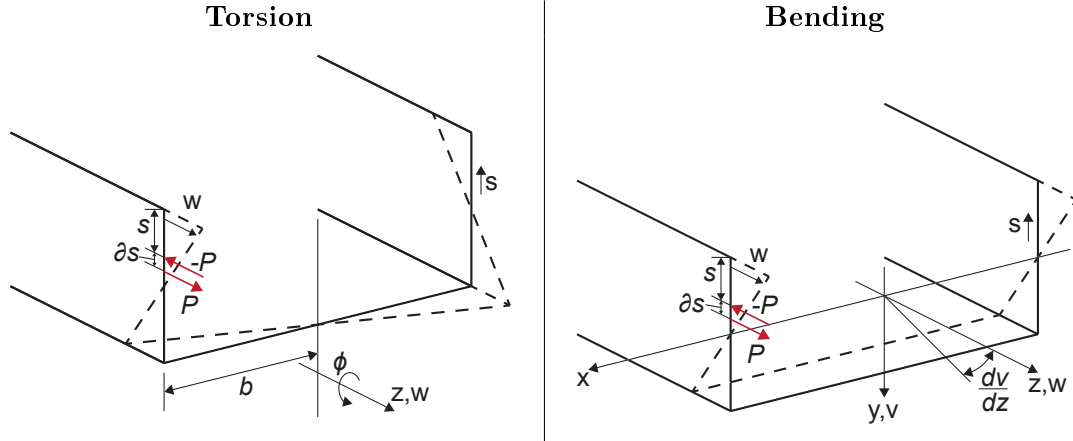
Axial displacements

$$w = -\frac{d\phi}{dz}\Omega$$

$$w = -\frac{dv}{dz}y$$

Twist ϕ':

$$\phi' = \frac{T}{GI_t}$$

Shear angle γ:

$$\gamma = \frac{S}{GA_s}$$

Bimoment M_Ω:

$$M_\Omega = -EI_{\Omega\Omega}\frac{d^2\phi}{dz^2}$$

Bending moment M:

$$M = -EI\frac{d^2v}{dz^2}$$

Warping torque T_Ω:

$$T_\Omega = \frac{dM_\Omega}{dz} = -EI_{\Omega\Omega}\frac{d^3\phi}{dz^3}$$

Shear force S:

$$S = \frac{dM}{dz} = -EI\frac{d^3v}{dz^3}$$

An Axial force P in positive direction causes:

Bimoment:

$$M_\Omega = P\Omega$$

Bending moment:

$$M_x = Py$$

A couple of forces P cause:

$$M_\Omega = P\delta s \frac{\Omega(s + \delta s) - \Omega(s)}{\delta s}$$

$$M_x = P\delta s \frac{y(s + \delta s) - y(s)}{\delta s}$$

which gives

$$M_\Omega = M\frac{d\Omega}{ds}$$

where $M = P\delta s$ and $P(s + \delta s)$ is positive

which gives

$$M_x = M\frac{dy}{ds}$$

where $M = P\delta s$ and $P(s + \delta s)$ is positive

For the couple shown above

$$\frac{d\Omega}{ds} = b$$

$$\frac{dy}{ds} = 1$$

which gives

$$M_\Omega = Mb$$

which gives

$$M_x = M$$

III

B   Sensor List

1	DT1P_WL_STAT1800s	100	DAP_VIB_STAT1800s	200	SWSFatigueRate_STAT1800s
2	DT1PT_WL_STAT1800s	101	IAS_VIB_STAT1800s	201	SWPFatigueRate_STAT1800s
3	DT2PT_WL_STAT1800s	102	IAP_VIB_STAT1800s	202	SFSFatigueRate_STAT1800s
4	DMPT_WL_STAT1800s	103	DFP_VIB_STAT1800s	203	SFPFatigueRate_STAT1800s
5	DT2P_WL_STAT1800s	104	DFS_VIB_STAT1800s	204	DASFatigueRate_STAT1800s
6	DMP_WL_STAT1800s	105	DT1P_VIB_STAT1800s	205	DAPFatigueRate_STAT1800s
7	ISP_WL_STAT1800s	106	DT2P_VIB_STAT1800s	206	IASFatigueRate_STAT1800s
8	ISPT_WL_STAT1800s	107	DT3S_VIB_STAT1800s	207	IAPFatigueRate_STAT1800s
9	SWPT_WL_STAT1800s	108	DT4S_VIB_STAT1800s	208	DFPFatigueRate_STAT1800s
10	SFPT_WL_STAT1800s	109	SF_VIB_STAT1800s	209	DFSFatigueRate_STAT1800s
11	SWP_WL_STAT1800s	110	SA_VIB_STAT1800s	210	DT1PFatigueRate_STAT1800s
12	SFP_WL_STAT1800s	111	AFV_VIB_STAT1800s	211	DT2PFatigueRate_STAT1800s
13	DT3S_WL_STAT1800s	112	DMPmod_VIB_STAT1800s	212	DT3SFatigueRate_STAT1800s
14	DT3ST_WL_STAT1800s	113	DMSmod_VIB_STAT1800s	213	DT4SFatigueRate_STAT1800s
15	DT4ST_WL_STAT1800s	114	HSP_VIB_STAT1800s	214	SFFatigueRate_STAT1800s
16	DMST_WL_STAT1800s	115	HSS_VIB_STAT1800s	215	SAFatigueRate_STAT1800s
17	DT4S_WL_STAT1800s	116	DMP_DLC_STAT1800s	216	AFVFatigueRate_STAT1800s
18	DMS_WL_STAT1800s	117	DMS_DLC_STAT1800s	217	DMPmodFatigueRate_STAT1800s
19	ISS_WL_STAT1800s	118	ISS_DLC_STAT1800s	218	DMSmodFatigueRate_STAT1800s
20	ISST_WL_STAT1800s	119	ISP_DLC_STAT1800s	219	HSPFatigueRate_STAT1800s
21	SWST_WL_STAT1800s	120	SWS_DLC_STAT1800s	220	HSSFatigueRate_STAT1800s
22	SFST_WL_STAT1800s	121	SWP_DLC_STAT1800s	221	DMPFatigueRateWAV_STAT1800s
23	SWS_WL_STAT1800s	122	SFS_DLC_STAT1800s	222	DMSFatigueRateWAV_STAT1800s
24	SFS_WL_STAT1800s	123	SFP_DLC_STAT1800s	223	ISSFatigueRateWAV_STAT1800s
25	IAP_WL_STAT1800s	124	DAS_DLC_STAT1800s	224	ISPFatigueRateWAV_STAT1800s
26	IAPT_WL_STAT1800s	125	DAP_DLC_STAT1800s	225	SWSFatigueRateWAV_STAT1800s
27	IAST_WL_STAT1800s	126	IAS_DLC_STAT1800s	226	SWPFatigueRateWAV_STAT1800s
28	DAPT_WL_STAT1800s	127	IAP_DLC_STAT1800s	227	SFSFatigueRateWAV_STAT1800s
29	IAS_WL_STAT1800s	128	DFP_DLC_STAT1800s	228	SFPFatigueRateWAV_STAT1800s
30	DAP_WL_STAT1800s	129	DFS_DLC_STAT1800s	229	DASFatigueRateWAV_STAT1800s
31	DAS_WL_STAT1800s	130	DMP_WAV_STAT1800s	230	DAPFatigueRateWAV_STAT1800s
32	DAST_WL_STAT1800s	131	DMS_WAV_STAT1800s	231	IASFatigueRateWAV_STAT1800s
33	DFST_WL_STAT1800s	132	ISS_WAV_STAT1800s	232	IAPFatigueRateWAV_STAT1800s
34	DFPT_WL_STAT1800s	133	ISP_WAV_STAT1800s	233	DFPFatigueRateWAV_STAT1800s
35	DFS_WL_STAT1800s	134	SWS_WAV_STAT1800s	234	DFSFatigueRateWAV_STAT1800s
36	DFP_WL_STAT1800s	135	SWP_WAV_STAT1800s	235	DT1PFatigueRateWAV_STAT1800s
37	ACC2_WL_STAT1800s	136	SFS_WAV_STAT1800s	236	DT2PFatigueRateWAV_STAT1800s
38	ACC1_WL_STAT1800s	137	SFP_WAV_STAT1800s	237	DT3SFatigueRateWAV_STAT1800s
39	SFT_WL_STAT1800s	138	DAS_WAV_STAT1800s	238	DT4SFatigueRateWAV_STAT1800s
40	SF_WL_STAT1800s	139	DAP_WAV_STAT1800s	239	SFFatigueRateWAV_STAT1800s
41	SA_WL_STAT1800s	140	IAS_WAV_STAT1800s	240	SAFatigueRateWAV_STAT1800s
42	SAT_WL_STAT1800s	141	IAP_WAV_STAT1800s	241	AFVFatigueRateWAV_STAT1800s
43	Ref2_WL_STAT1800s	142	DFP_WAV_STAT1800s	242	AFV_VIB_SlamCount0_STAT1800s
44	RefT_WL_STAT1800s	143	DFS_WAV_STAT1800s	243	SA_VIB_SlamCount0_STAT1800s
45	Ref1_WL_STAT1800s	144	DT1P_WAV_STAT1800s	244	SF_VIB_SlamCount0_STAT1800s
46	DT1P_RAW_STAT1800s	145	DT2P_WAV_STAT1800s	245	NavTime_STAT1800s

47	DT1PT_RAW_STAT1800s	146	DT3S_WAV_STAT1800s	246	Latitude_STAT1800s
48	DT2PT_RAW_STAT1800s	147	DT4S_WAV_STAT1800s	247	Longitude_STAT1800s
49	DMPT_RAW_STAT1800s	148	SF_WAV_STAT1800s	248	SOG_STAT1800s
50	DT2P_RAW_STAT1800s	149	SA_WAV_STAT1800s	249	COG_STAT1800s
51	DMP_RAW_STAT1800s	150	AFV_WAV_STAT1800s	250	HDT_STAT1800s
52	ISP_RAW_STAT1800s	151	DMPmod_WAV_STAT1800s	251	ROTRATE_STAT1800s
53	ISPT_RAW_STAT1800s	152	DMSmod_WAV_STAT1800s	252	WindDirection_STAT1800s
54	SWPT_RAW_STAT1800s	153	HSP_WAV_STAT1800s	253	WindSpeed_STAT1800s
55	SFPT_RAW_STAT1800s	154	HSS_WAV_STAT1800s	254	RudderAngle_STAT1800s
56	SWP_RAW_STAT1800s	155	DMP_DYN_STAT1800s	255	DepthBelowSurface_STAT1800s
57	SFP_RAW_STAT1800s	156	DMS_DYN_STAT1800s	256	DepthBelowTransducer_STAT1800s
58	DT3S_RAW_STAT1800s	157	ISS_DYN_STAT1800s	257	STW_STAT1800s
59	DT3ST_RAW_STAT1800s	158	ISP_DYN_STAT1800s	258	STWtransverse_STAT1800s
60	DT4ST_RAW_STAT1800s	159	SWS_DYN_STAT1800s	259	SOGlon_STAT1800s
61	DMST_RAW_STAT1800s	160	SWP_DYN_STAT1800s	260	SOGtransverse_STAT1800s
62	DT4S_RAW_STAT1800s	161	SFS_DYN_STAT1800s	261	DistanceTravelledTotalNM_STAT1800s
63	DMS_RAW_STAT1800s	162	SFP_DYN_STAT1800s	262	RPMVOLTS_STAT1800s
64	ISS_RAW_STAT1800s	163	DAS_DYN_STAT1800s	263	RPMORDER_STAT1800s
65	ISST_RAW_STAT1800s	164	DAP_DYN_STAT1800s	264	RaxisLinearAcceleration_STAT1800s
66	SWST_RAW_STAT1800s	165	IAS_DYN_STAT1800s	265	PaxisLinearAcceleration_STAT1800s
67	SFST_RAW_STAT1800s	166	IAP_DYN_STAT1800s	266	YaxisLinearAcceleration_STAT1800s
68	SWS_RAW_STAT1800s	167	DFP_DYN_STAT1800s	267	FaxisLinarDisplacement_STAT1800s
69	SFS_RAW_STAT1800s	168	DFS_DYN_STAT1800s	268	SaxisLinearDisplacement_STAT1800s
70	IAP_RAW_STAT1800s	169	DT1P_DYN_STAT1800s	269	DaxisLinearDisplacement_STAT1800s
71	IAPT_RAW_STAT1800s	170	DT2P_DYN_STAT1800s	270	Roll_STAT1800s
72	IAST_RAW_STAT1800s	171	DT3S_DYN_STAT1800s	271	Pitch_STAT1800s
73	DAPT_RAW_STAT1800s	172	DT4S_DYN_STAT1800s	272	Yaw_STAT1800s
74	IAS_RAW_STAT1800s	173	SF_DYN_STAT1800s	273	FaxisLinearAcceleration_STAT1800s
75	DAP_RAW_STAT1800s	174	SA_DYN_STAT1800s	274	SaxisLinearAcceleration_STAT1800s
76	DAS_RAW_STAT1800s	175	AFV_DYN_STAT1800s	275	DaxisLinearAcceleration_STAT1800s
77	DAST_RAW_STAT1800s	176	DMPmod_DYN_STAT1800s	276	RollAA_STAT1800s
78	DFST_RAW_STAT1800s	177	DMSmod_DYN_STAT1800s	277	PitchAA_STAT1800s
79	DFPT_RAW_STAT1800s	178	HSP_DYN_STAT1800s	278	YawAA_STAT1800s
80	DFS_RAW_STAT1800s	179	HSS_DYN_STAT1800s	279	RollAV_STAT1800s
81	DFP_RAW_STAT1800s	180	VerticalBendingMid_STAT1800s	280	BendMomentAft_STAT1800s
82	AFV_RAW_STAT1800s	181	HorizontalBendingMid_STAT1800s	281	BendMomentMid_STAT1800s
83	SFT_RAW_STAT1800s	182	WarpingStressMid_STAT1800s	282	BendMomentFwd_STAT1800s
84	SF_RAW_STAT1800s	183	AxialForceMid_STAT1800s	283	RudderOrder_STAT1800s
85	SA_RAW_STAT1800s	184	AltVerticalBendingMid_STAT1800s	284	SPARE1_STAT1800s
86	SAT_RAW_STAT1800s	185	AltHorizontalBendingMid_STAT1800s	285	SPARE2_STAT1800s
87	DMPmod_RAW_STAT1800s	186	AltWarpingStressMid_STAT1800s	286	SPARE3_STAT1800s
88	DMSmod_RAW_STAT1800s	187	AltAxialForceMid_STAT1800s	287	SPARE4_STAT1800s
89	HSP_RAW_STAT1800s	188	VerticalBendingAft_STAT1800s	288	SPARE5_STAT1800s
90	HSS_RAW_STAT1800s	189	HorizontalBendingAft_STAT1800s	289	SPARE6_STAT1800s
91	DMP_VIB_STAT1800s	190	WarpingStressAft_STAT1800s	290	SPARE7_STAT1800s
92	DMS_VIB_STAT1800s	191	AxialForceAft_STAT1800s	291	SPARE8_STAT1800s

C MATLAB files

The following MATLAB programs are included in Appendix B:

- **B1:** *HG_mapplot.m*
- **B2:** *HG_speed.m*
- **B3:** *HG_GPScoord_WaqumExplorer.m*
- **B4:** *HG_cleanplot_extreme.m*
- **B5:** *HG_Raw_spectrum.m*
- **B6:** *HG_ULS.m*

These are also included in the attached zip-folder

C.1 HG_mapplot.m

```matlab
1   %%
2   % HG_mapplot.m − Plots map with route of loaded voyage
3   % Nanna Martine Jacobsen
4   % Spring 2015
5   % Master thesis project
6   % −−−−−−−−−−−−−−−−−−−−−−−−−−−−−−−−−−−−−−−−−−−−−−−−−−−−−−−−−−−−−−−−−−−−−−−−−−− //
7   %% Explanations:
8   % Date strings with format 'yyyymmdd' are used
9   % Input:  − path_i       : Path containing input files
10  %         − start_d      : First date to be included
11  %         − end_d        : Last date to be included
12  %         − chn          : Channel numbers to be included (chn = [246 247] )
13  %         − par          : Statistical parameter
14  %         − keytype      : Type of file
15  %         − fid          : Part of file name ( 'IAS_extract' )
16  %         − tm           : 0       : No output except output string
17  %                          1       : Print list to screen
18  %                          File name : print to file (default directory)
19  % Output: − path_o       : path for output
20  %         − f_f          : First file in file list
21  %         − f_e          : Last file in file list
22  %         − f_n          : Number of input files
23  % −−−−−−−−−−−−−−−−−−−−−−−−−−−−−−−−−−−−−−−−−−−−−−−−−−−−−−−−−−−−−−−−−−−−−−−−−−− //
24  % Functions used:        readDateInterval.m
25  % −−−−−−−−−−−−−−−−−−−−−−−−−−−−−−−−−−−−−−−−−−−−−−−−−−−−−−−−−−−−−−−−−−−−−−−−−−− //
26  close all
27  clear all
28  % −−−−−−−−−−−−−−−−−−−−−−−−−−−−−−−−−−−−−−−−−−−−−−−−−−−−−−−−−−−−−−−−−−−−−−−−−−− //
29
30  %% Input and output data
31  folder = 'C:\Data\HG\Stat30\';
32  keytype = 'Stat30_*';
33  dateInterval = [20090515 20090703]; %From Hamburg to Singapore
34  %dateInterval = [20140513 20140529]; %From Singapore to USA
35  %dateInterval = [20131008 20140712]; %Route2
36  %dateInterval = [20090605 20131008]; %Route1
37
38  % Sensors
39  lat_sens = 246; % GPSLatitude_STAT1800s
40  long_sens = 247; % GPSLongitude_STAT1800s
41  stat_param = 2; % Statistical parameter (2: Average, 3: Standard Deviation)
42  save = false;
43
44  [time,data,sensors] = readDateInterval(folder,keytype,dateInterval);
45
46  % Find start and stop index of the voyage
47  first_time_start = 0;
48  first_time_stop = 0;
49  for i = 1:size(time,1),
50      [year, month, day, hour, minute, second] = unixsecs2date(time(i,1));
51      time_i = year*10000 + month * 100 + day;
52      if first_time_start == 0 && time_i >= dateInterval(1),
53          first_time_start = 1;
54          index_start = i;
```

```matlab
55          end
56          if first_time_stop == 0 && time_i >= dateInterval(2),
57               first_time_stop = 1;
58               index_stop = i;
59          end
60     end
61
62    % Create latitude, longitude and time vectors for the voyage
63    LAT = data(index_start:index_stop,lat_sens,stat_param);
64    LONG = data(index_start:index_stop,long_sens,stat_param);
65    time_voy = time(index_start:index_stop,1);
66
67    % Get date vector for days on world map
68    count_days = 0;
69    for i = 1:size(time_voy,1),
70          if i == 1,
71               count_days = count_days +1;
72               days(count_days,1) = time_voy(i,1);
73               LONG_d(count_days,1) = LONG(i,1);
74               LAT_d(count_days,1) = LAT(i,1);
75          end
76          if i >1
77               [year_ref, month_ref, day_ref, hour_ref, minute_ref, second_ref]...
78                    = unixsecs2date(time_voy(i-1,1));
79               [year, month, day, hour, minute, second] = unixsecs2date(time_voy(i,1));
80               if year ~= year_ref || month ~= month_ref || day ~= day_ref
81                    count_days = count_days +1;
82                    days(count_days, 1) = time_voy(i,1);
83                    LONG_d(count_days,1) = LONG(i,1);
84                    LAT_d(count_days,1) = LAT(i,1);
85               end
86          end
87     end
88
89     [~,dates] = unixsecs2date_strings(days);
90
91    LONG = LONG(any(LONG,2) ,:);
92    LAT = LAT(any(LAT,2) ,:);
93    %%
94    cd('C:\Data\HG\Matlab_routines_Nanna\m_map');
95
96    %%
97    cd('C:\Data\HG\Matlab_routines_Nanna\m_map');
98    figure('Name','HG_IMO','NumberTitle','off','Color',[1 1 1], 'OuterPosition',[0,0,1920,1200])
99        m_proj('miller','lat',[-75 75]);
100        m_coast('patch',[.7 1 .7],'edgecolor','none');
101        m_grid('box','fancy','linestyle','none','backcolor',[.9 .99 1]);
102        m_line(LONG,LAT,'marker','square','markersize',1,'color','r','linewi',3);
103    title('Ship position','fontsize',14,'fontweight','bold');
104    for i = 1:size(days,1)
105        date_string = strcat(dates{i,1}(5:6),'/',dates{i,1}(7:8));
106    end
107
108    cd('C:\Data\HG\Matlab_routines_Nanna\');
109
110    %% Read input-data for plotting all voyages for both routes in the same map plot:
111     Route2 = load('C:\Data\HG\Matlab_routines_Nanna\Route2.txt')
112     Route1 = load('C:\Data\HG\Matlab_routines_Nanna\Route1.txt');
113
114     %Route2 = transpose(sortrows(Route2'.',1).')
115     POS = [Route2(Route2(:,1)>0,1) Route2(Route2(:,1)>0,2)]
116     NEG = [Route2(Route2(:,1)<0,1) Route2(Route2(:,1)<0,2)]
117
118    %% Plot both routes:
119    cd('C:\Data\HG\Matlab_routines_Nanna\m_map');
120    figure('Name','HG_IMO','NumberTitle','off','Color',[1 1 1], 'OuterPosition',[0,0,1920,1200])
121        m_proj('miller','lat',[-75 75]);
122        m_coast('patch',[.7 1 .7],'edgecolor','none');
123        m_grid('box','fancy','linestyle','none','backcolor',[.9 .99 1]);
124        m_line(Route1(:,1), Route1(:,2),'marker','square','markersize',1,'color','b','linewi',1);
125        m_line(POS(:,1),POS(:,2),'marker','square','markersize',1,'color','r','linewi',1);
126        m_line(NEG(:,1),NEG(:,2),'marker','square','markersize',1,'color','r','linewi',1);
127     %m_line(Route2(:,1), Route2(:,2),'marker','square','markersize',1,'color','r','linewi',3);
128    title('Ship position','fontsize',14,'fontweight','bold');
129    for i = 1:size(days,1)
130        date_string = strcat(dates{i,1}(5:6),'/',dates{i,1}(7:8));
131    end
132
133    cd('C:\Data\HG\Matlab_routines_Nanna\');
134
135    % End of Program HG_mapplot.m
136    % ------------------------------------------------------------------------------ //
```

C.2   HG_speed.m

```matlab
1   %%
2   % HG_speed.m − Plots speed over ground
3   % Nanna Martine Jacobsen
4   % Spring 2015
5   % Master thesis project
6   % −−−−−−−−−−−−−−−−−−−−−−−−−−−−−−−−−−−−−−−−−−−−−−−−−−−−−−−−−−−−−−−−−−−− //
7   %% Explanations:
8   % Date strings with format 'yyyymmdd' are used
9   % Input:  − path_i      : Path containing input files
10  %         − start_d     : First date to be included
11  %         − end_d       : Last date to be included
12  %         − chn         : Channel numbers to be included (chn = [248 180 192] )
13  %         − par         : Statistical parameter
14  %         − fid         : Part of file name ( 'IAS_extract' )
15  %         − tm          : 0       : No output except output string
16  %                         1       : Print list to screen
17  %                         File name : print to file (default directory)
18  % Output: − path_o      : path for output
19  %         − f_f         : First file in file list
20  %         − f_e         : Last file in file list
21  %         − f_n         : Number of input files
22  % −−−−−−−−−−−−−−−−−−−−−−−−−−−−−−−−−−−−−−−−−−−−−−−−−−−−−−−−−−−−−−−−−−−− //
23  % Functions used:        IMO_read_time.m
24  %                        IMO_extract_stat_range.m
25  % −−−−−−−−−−−−−−−−−−−−−−−−−−−−−−−−−−−−−−−−−−−−−−−−−−−−−−−−−−−−−−−−−−−− //
26  close all
27  clear all
28  % −−−−−−−−−−−−−−−−−−−−−−−−−−−−−−−−−−−−−−−−−−−−−−−−−−−−−−−−−−−−−−−−−−−− //
29  %% Input and output data
30  path_i='C:\Data\HG\Stat30\';
31  path_o='C:\Data\HG\Matlab_output\';
32
33  start_days=[20090605; 20131008]; % Route1 Route 2
34  end_days=[20131008; 20140712]; %  Route1 Route 2
35  % start_days=[20090515; 20140513]; % Hamburg Singapore(OBS!)
36  % end_days=[20090703; 20140529]; % Singapore USA
37
38  max_VBM = zeros(1,2);
39
40  for j=1:2
41      start_d = num2str(start_days(j));
42      end_d = num2str(end_days(j));
43
44  chn= [248 180 192];   %SOG − Speed over ground, Vertical bending, VBM
45  par=2;                %par=6 %2=mean, 6=minimum, 7=maximum, 8=peak to peak
46  fid='test';
47  tm=0;
48  [f_f,f_e,f_n] = IMO_extract_stat_range(path_i,start_d,end_d,chn,par,path_o,fid,tm)
49  % Read in data
50  filename=['C:\Data\HG\Matlab_output\' fid '_' start_d '_' end_d '.bin'];
51
52  testmode=1;
53  [time,data,sensors] = IMO_read_time( filename, testmode );
54  no=length(data(:,1))
55  vessel_speed = data(:,1)*1.944;          % Convert m/s −> kn
56  intervals = zeros(1,6);
57  count0 = 0;
58
59  %% Generate Vessel speed intervals
60  for i=1:length(vessel_speed)
61      if vessel_speed(i)< 0.1
62          count0 = count0 + 1;
63      elseif vessel_speed(i)<5 && vessel_speed(i)>0.1
64          intervals = intervals + [1, 0, 0, 0, 0, 0];
65      elseif vessel_speed(i)>=5 && vessel_speed(i)<10
66          intervals = intervals + [0, 1, 0, 0, 0, 0];
67      elseif vessel_speed(i)>=10 && vessel_speed(i)<15
68          intervals = intervals + [0, 0, 1, 0, 0, 0];
69      elseif vessel_speed(i)>=15 && vessel_speed(i)<20
70          intervals = intervals + [0, 0, 0, 1, 0, 0];
71      elseif vessel_speed(i)>=20 && vessel_speed(i)<25
72          intervals = intervals + [0, 0, 0, 0, 1, 0];
73      elseif vessel_speed(i)>=25
74          intervals = intervals + [0, 0, 0, 0, 0, 1];
75      end
76  end
77  speed_not0 = length(vessel_speed)−count0;  % Transit speed (Filtering out time in port)
78
79  %% Vertical Bending:
```

```matlab
80   Vertical_Bending = data(:,2);
81   VBM = data(:,3);
82
83   %%% Plot figures:
84   figure(j)
85   x = 1:6;
86   y = intervals/speed_not0*100;
87   bar(x,y)
88   title(['Vessel speed, Route ', num2str(j)])
89   set(gca, 'XTickLabel', {'0-5', '5-10', '10-15', '15-20', '20-25', '25->'})
90   ylabel('%')
91   xlabel('Vessel speed [kn]')
92   ylim([0, 60])
93   % add the values
94     for i=1:6,
95       TH(i) = text(x(i),y(i),[num2str(y(i),'%0.1f'), '%']);
96     end
97    % Use the handles TH to modify some properties
98     set(TH,'Horizontalalignment','center',...
99    'verticalalignment','bottom') ;
100
101   figure(j+2)
102   plot((time-time(1))/3600/24, VBM,'k')
103   xlabel('time(days)')
104   ylabel('VBM')
105
106   %%% Max values VBM
107   max_VBM(j) = max(abs(VBM));
108   end
109
110   % End of Program HG_speed.m
111   % ───────────────────────────────────────────────────────────────────── //
```

C.3   HG_ GPScoord_WaqumExplorer.m

```matlab
1    %%%
2    % HG_GPScoord_WaqumExplorer.m — Script to print GPS data input for Route Generator
3    %                                     in Waqum Explored
4    % ORFRE 15.11.2013,
5    % Modified by Nanna Martine Jacobsen
6    % Spring 2015
7    % Master thesis project
8    % ───────────────────────────────────────────────────────────────────── //
9    %%% Explanations:
10   % Date strings with format 'yyyymmdd' are used
11   % Input:  - path_i       : Path containing input files
12   %         - dateinterval : [First date to be included,  Last date to be included]
13   %         - chn          : Channel numbers to be included (chn = [248 180 192] )
14   %         - par          : Statistical parameter
15   %         - key          : Input type
16   %         - fid          : Part of file name ( 'IAS_extract' )
17   %         - tm           : 0          : No output except output string
18   %                          1          : Print list to screen
19   %                          File name : print to file (default directory)
20   % Output: - path_o       : path for output
21   %         - f_f          : First file in file list
22   %         - f_e          : Last file in file list
23   %         - f_n          : Number of input files
24   % ───────────────────────────────────────────────────────────────────── //
25   % Functions used:        readDateInterval.m
26   % ───────────────────────────────────────────────────────────────────── //
27   % Output file:           GPS_coordinates_Bonny_Ferrol.jnl
28   % ───────────────────────────────────────────────────────────────────── //
29   close all
30   clear all
31   % ───────────────────────────────────────────────────────────────────── //
32
33   %%% Input and output data
34   path_in='C:\Data\HG\Stat30\';
35   path_out='C:\Data\HG\Matlab_output\';
36   name = 'GPS_coordinates'; % _Route1 _Route2
37   key = 'Stat*';
38   %dateInterval = [20131008 20140711]; %route2
39   dateInterval = [20090605 20131008]; %route1
40   dep = 'Bonny';
41   arr = 'Ferrol';
42   filename = strcat(name, '_', dep, '_', arr, '.jnl');
43   stat_param = 2; % statistical parameter 2 = mean
44   lat_sens = 246;
```

```matlab
45    long_sens = 247;
46
47    [~,data,~] = readDateInterval(path_in, key, dateInterval);
48
49    fid = fopen(strcat(path_out, filename), 'w');
50
51
52    %% Writes dummy info
53    fprintf(fid, '%% Scatter diagram exported by orfre\n');
54    fprintf(fid, '%%  from waves.Environment.write_jnl()\n');
55    fprintf(fid, '%% Contains a total of 2856 sea states\n');
56    fprintf(fid, '%% WaqumExplorer Comment <Percentage in zone>\n');
57    fprintf(fid, '%% WaqumExplorer Comment <Zone IDs>\n');
58
59    %% Writes longitudes
60    fprintf(fid, '%% WaqumExplorer Comment <Way point LONS> ');
61    for i = 1:size(data,1)-1;
62        long = data(i,long_sens,stat_param);
63        fprintf(fid, '%.2f,\t', long);
64    end
65    long = data(end,long_sens,stat_param);
66    fprintf(fid, '%.2f\n', long);
67
68    %% Writes latitudes
69    fprintf(fid,'%% WaqumExplorer Comment <Way point LATS> ');
70    for i = 1:size(data,1)-1;
71        lat = data(i,lat_sens,stat_param);
72        fprintf(fid, '%.2f,\t', lat);
73    end
74    lat = data(end,lat_sens,stat_param);
75    fprintf(fid, '%.2f\n', lat);
76
77    %% Writes more dummy info
78    fprintf(fid, '%% Create spreading functions\n');
79    fprintf(fid, 'CREATE WAVE-SPREADING-FUNCTION COS2 ''Cosine power 2 spreading'' COSINE-POWER 2\n\n');
80
81    fprintf(fid, '%% Create the scatter diagrams:\n\n');
82
83    fprintf(fid, 'CREATE WAVE-STATISTICS WS ''Exported scatter diagram WS'' SCATTER-DIAGRAM PROBABILITY\n');
84    fprintf(fid, '( ONLY \n');
85    fprintf(fid, '%%   Hs [m]     Tz [s]          prob       (spectrum and parameters)\n');
86    fprintf(fid, '   0.500000    2.000000  0.00001310     %% PM     2     {}\n');
87    fprintf(fid, '   )\n');
88    fprintf(fid, 'ASSIGN WAVE-SPREADING-FUNCTION WS COS2 ALL\n\n\n');
89
90
91    fprintf(fid, '%% Link headings and heading probabilities\n');
92    fprintf(fid, 'ASSIGN WAVE-DIRECTION-PROBABILITY      0.0   0.08333333\n');
93    fprintf(fid, 'ASSIGN WAVE-DIRECTION-PROBABILITY     30.0   0.08333333\n');
94    fprintf(fid, 'ASSIGN WAVE-DIRECTION-PROBABILITY     60.0   0.08333333\n');
95    fprintf(fid, 'ASSIGN WAVE-DIRECTION-PROBABILITY     90.0   0.08333333\n');
96    fprintf(fid, 'ASSIGN WAVE-DIRECTION-PROBABILITY    120.0   0.08333333\n');
97    fprintf(fid, 'ASSIGN WAVE-DIRECTION-PROBABILITY    150.0   0.08333333\n');
98    fprintf(fid, 'ASSIGN WAVE-DIRECTION-PROBABILITY    180.0   0.08333333\n');
99    fprintf(fid, 'ASSIGN WAVE-DIRECTION-PROBABILITY    210.0   0.08333333\n');
100   fprintf(fid, 'ASSIGN WAVE-DIRECTION-PROBABILITY    240.0   0.08333333\n');
101   fprintf(fid, 'ASSIGN WAVE-DIRECTION-PROBABILITY    270.0   0.08333333\n');
102   fprintf(fid, 'ASSIGN WAVE-DIRECTION-PROBABILITY    300.0   0.08333333\n');
103   fprintf(fid, 'ASSIGN WAVE-DIRECTION-PROBABILITY    330.0   0.08333333\n\n');
104
105   fprintf(fid, '%% Link headings and scatter diagrams\n');
106   fprintf(fid, 'ASSIGN WAVE-STATISTICS        0.0    WS\n');
107   fprintf(fid, 'ASSIGN WAVE-STATISTICS       30.0    WS\n');
108   fprintf(fid, 'ASSIGN WAVE-STATISTICS       60.0    WS\n');
109   fprintf(fid, 'ASSIGN WAVE-STATISTICS       90.0    WS\n');
110   fprintf(fid, 'ASSIGN WAVE-STATISTICS      120.0    WS\n');
111   fprintf(fid, 'ASSIGN WAVE-STATISTICS      150.0    WS\n');
112   fprintf(fid, 'ASSIGN WAVE-STATISTICS      180.0    WS\n');
113   fprintf(fid, 'ASSIGN WAVE-STATISTICS      210.0    WS\n');
114   fprintf(fid, 'ASSIGN WAVE-STATISTICS      240.0    WS\n');
115   fprintf(fid, 'ASSIGN WAVE-STATISTICS      270.0    WS\n');
116   fprintf(fid, 'ASSIGN WAVE-STATISTICS      300.0    WS\n');
117   fprintf(fid, 'ASSIGN WAVE-STATISTICS      330.0    WS\n\n');
118
119   fprintf(fid, '%% DONE! Created 1 scatter diagrams');
120
121   fclose(fid);
122   fprintf(['\n*** File ', filename, ' sucessfully written! ***\n\n']);
123
124   % End of Program HG_GPScoord_WaqumExplorer.m
125   % -------------------------------------------------------------------------- //
```

C.4 HG_cleanplot_extreme.m

```matlab
1  %%
2  % HG_cleanplot_extreme.m - Program plotting timeseries, and finding extremevalues
3  %                          for measured stresses, identifying days were torsional
4  %                          vibrations may be present.
5  % Nanna Martine Jacobsen
6  % Spring 2015
7  % Master thesis project
8  % ----------------------------------------------------------------------------- //
9  %% Explanations:
10 % Date strings with format 'yyyymmdd' are used
11 % Input:   - path_i        : path containing input files
12 %          - start_d       : first date to be included
13 %          - end_d         : last date to be included
14 %          - chn           : channel numbers to be included ( chn = [1:200] )
15 %          - par           : statistical parameter
16 %          - fid           : part of file name ( 'IAS_extract' )
17 %          - tm            : 0         : no output except output string
18 %                            1         : print list to screen
19 %                            file name : print to file (default directory)
20 % Output:  - path_o        : path for output
21 %          - f_f           : first file in file list
22 %          - f_e           : last file in file list
23 %          - f_n           : number of input files
24 % ----------------------------------------------------------------------------- //
25 % Functions used:         IMO_read_time.m
26 %                         IMO_extract_stat_range.m
27 % ----------------------------------------------------------------------------- //
28 % Input files:            HHI1940_Sensor_Bands.dat   % used to filter out
29 %                                                    nontrustworthy measurements
30 %                         Raw_data_days_filtered.txt % Available Raw data days
31 % ----------------------------------------------------------------------------- //
32 close all
33 clear all
34 % ----------------------------------------------------------------------------- //
35 %% Input and output data:
36 path_i='C:\Data\HG\Stat30\'
37 path_o='C:\Data\HG\Matlab_output\'
38
39 %% Dates:
40 % Route 1:
41 %start_d='20090605';
42 %end_d='20131008';
43
44 % Route 2
45 %start_d='20131008';
46 %end_d='20140712';
47
48 % Worst day
49 start_d='20111103';
50 end_d='20111103';
51
52 %% Read in and make file containing all measurements in the chosen time intervall
53 chn=[1:1:200]; % Read in all channels
54
55 % ---------------------------------------------------------------------------------
56 par=6    %2=mean, 6=minimum, 7=maximum, 8=peak to peak
57 fid='Stat30';
58 tm=0;
59 [f_f,f_e,f_n] = IMO_extract_stat_range(path_i,start_d,end_d,chn,par,path_o,fid,tm);
60
61 % Read in data
62 filename=['C:\Data\HG\Matlab_output\' fid '_' start_d '_' end_d '.bin'];
63 testmode=1;
64 [time,dataMin,sensors] = IMO_read_time( filename, testmode ); % hogging = positive
65
66 % ---------------------------------------------------------------------------------
67 par=7 %no=1, mean=2, stdev=3, skewness=4, kurtosis=5, min=6, max=7,
68 fid='Stat30'
69 tm=0
70 [f_f,f_e,f_n] = IMO_extract_stat_range(path_i,start_d,end_d,chn,par,path_o,fid,tm);
71
72 % Read in data
73 filename=['C:\Data\HG\Matlab_output\' fid '_' start_d '_' end_d '.bin'];
74 testmode=1
75 [time,dataMax,sensors] = IMO_read_time( filename, testmode ); %sagging=negative
76
77 % ---------------------------------------------------------------------------------
78 par=2 %2=mean, 6=minimum, 7=maximum, 8=peak to peak
79 fid='Stat30';
```

```matlab
80  tm=0;
81  [f_f,f_e,f_n] = IMO_extract_stat_range(path_i,start_d,end_d,chn,par,path_o,fid,tm);
82
83  % Read in data
84  filename=['C:\Data\HG\Matlab_output\' fid '_' start_d '_' end_d '.bin'];
85  testmode=0;
86  [time,data,sensors] = IMO_read_time( filename, testmode );
87
88  % ----------------------------------------------------------------------------------------
89
90  %% Filtering out untrusworthy measurements
91
92  WL_LUT = load('C:\Data\HG\HHI1940_Sensor_Bands.dat');
93      [r c] = size(WL_LUT);
94      [NOBS d1] = size(dataMin);
95      WL_OK = (ones(NOBS,r) == 0);
96
97      for i=1:r,
98        WL_OK(:,i)=((dataMin(:,i) > WL_LUT(i,2)) & (dataMax(:,i) < WL_LUT(i,3)) &...
99                    (dataMax(:,i)-dataMin(:,i) < WL_LUT(i,4)) );
100     end
101
102 save data_Stat5_20111010 dataMin dataMax data time sensors WL_OK chn
103
104 %% Channels
105 REF = [45 44 43];                      % REF1_WL, REFT_WL, REF2_WL
106 WL_Statistics = [18 16;...             % Channel for DMS_WL    [6 4]DMP
107                  1  2;...              % Channel for DT1P_WL
108                  5  3;...              % Channel for DT2P_WL
109                  13 14;...             % Channel for DT3S_WL
110                  17 15];              % Channel for DT4S_WL
111 % ----------------------------------------------------------------------------------------
112 RAW = [63 61;...          % Raw data wav and total; DMS    [51 49] DMP
113        46 47;...          % Raw data wav and total; DT1P
114        50 48;...          % Raw data wav and total; DT2P
115        58 59;...          % Raw data wav and total; DT3S
116        62 60];            % Raw data wav and total; DT4S
117 % ----------------------------------------------------------------------------------------
118 WavDyn = [131 156;...         % Channel for DMS WAV and DMS DYN    [130 155] DMP
119           144 169;...         % Channel for DT1P WAV and DT1P DYN
120           145 170;...         % Channel for DT2P WAV and DT2P DYN
121           146 171;...         % Channel for DT3S WAV and DT3S DYN
122           147 172];           % Channel for DT4S WAV and DT4S DYN
123
124 ind = [REF, WL_Statistics(1,:); REF, WL_Statistics(2,:); REF, WL_Statistics(3,:);...
125        REF, WL_Statistics(4,:); REF, WL_Statistics(5,:)];
126
127
128 %% Runs through all the sensors
129 for i = 1:5;
130
131 %logical AND test for each period, True if WL_OK is %T for all sensor indices
132 % in iDMP and so on..
133 v=and(WL_OK(:,ind(i,:)),'c');
134 v1 = find(sum(v,2)==size(ind,1));
135 no=length(dataMin(:,1));
136 NO=length(v1);
137
138 % Difference between Wave and Dyn
139 Min = dataMin(v1,WavDyn(i,2))-dataMin(v1,WavDyn(i,1));
140 Max = dataMax(v1,WavDyn(i,2))-dataMax(v1,WavDyn(i,1));
141
142 % PLOTS:
143 figure(i)
144 plot((time(v1)-time(1))/48/1800,dataMin(v1,WavDyn(i,2)),'b',...
145      (time(v1)-time(1))/48/1800,dataMin(v1,WavDyn(i,1)),'r',...
146      (time(v1)-time(1))/48/1800,dataMax(v1,WavDyn(i,2)),'b',...
147      (time(v1)-time(1))/48/1800,dataMax(v1,WavDyn(i,1)),'r');
148 legend('Dyn','Wav',2)
149 xlabel('Days')
150 ylabel('Extreme values (Hogging is positive) [MPa]')
151
152 % figure(14+i)
153 % plot((time(v1)-time(1))/48/1800, Min,'r',...
154 %      (time(v1)-time(1))/48/1800, Max,'b');
155 % legend('Min values','Max values',2)
156 % xlabel('Days')
157 % ylabel('Dyn-Wav values (Hogging is positive) [MPa]')
158
159 if i == 1
160     title('Extremals, Sensor DMS')
161     MaxDMSDyn=max(dataMax(v1,WavDyn(i,2)));
162     MaxDMSWave=max(dataMax(v1,WavDyn(i,1)));
```

```matlab
163        MinDMSDyn=min(dataMin(v1,WavDyn(i,2)));
164        MinDMSWave=min(dataMin(v1,WavDyn(i,1)));
165
166    elseif i==2
167        title('Extremals, Sensor DT1P')
168        MaxDT1PDyn=max(dataMax(v1,WavDyn(i,2)));
169        MaxDT1PWave=max(dataMax(v1,WavDyn(i,1)));
170        MinDT1PDyn=min(dataMin(v1,WavDyn(i,2)));
171        MinDT1PWave=min(dataMin(v1,WavDyn(i,1)));
172
173    elseif i==3
174        title('Extremals, Sensor DT2P')
175        MaxDT2PDyn=max(dataMax(v1,WavDyn(i,2)));
176        MaxDT2PWave=max(dataMax(v1,WavDyn(i,1)));
177        MinDT2PDyn=min(dataMin(v1,WavDyn(i,2)));
178        MinDT2PWave=min(dataMin(v1,WavDyn(i,1)));
179
180    elseif i==4
181        title('Extremals, Sensor DT3S')
182        MaxDT3SDyn=max(dataMax(v1,WavDyn(i,2)));
183        MaxDT3SWave=max(dataMax(v1,WavDyn(i,1)));
184        MinDT3SDyn=min(dataMin(v1,WavDyn(i,2)));
185        MinDT3SWave=min(dataMin(v1,WavDyn(i,1)));
186        Min3 = Min;
187        Max3 = Max;
188        v3=v1;
189
190    elseif i==5
191        title('Extremals, Sensor DT4S')
192        MaxDT4SDyn=max(dataMax(v1,WavDyn(i,2)));
193        MaxDT4SWave=max(dataMax(v1,WavDyn(i,1)));
194        MinDT4SDyn=min(dataMin(v1,WavDyn(i,2)));
195        MinDT4SWave=min(dataMin(v1,WavDyn(i,1)));
196
197    end
198    end
199
200    %% Input data on Raw data days
201    Rawdata_days = load('Raw_data_days_filtered.txt');
202    x1 = str2num(start_d);
203    x2 = str2num(end_d);
204    t1 = datetime(x1,'ConvertFrom','yyyymmdd');
205    t2 = datetime(x2,'ConvertFrom','yyyymmdd');
206    all_dates = (t1:t2)';
207    dates_str=num2str(yyyymmdd(all_dates));
208    dates=str2num(dates_str);
209
210    %% Finding max difference:
211    Max_difference = zeros(1,2);
212    b=0;
213    for i = 1:length(Min3)
214        datooo = (time(v3(i)) - time(1))/48/1800;
215        round_down_datooo = floor(datooo)+1;
216
217        day_found = ismember(dates(round_down_datooo), Rawdata_days);
218
219    if abs(dataMin(v3(i),WavDyn(4,2)))>=100 || dataMax(v3(i),WavDyn(4,2))>=100
220
221    if abs(Min3(i))>Max3(i) && abs(Min3(i))>abs(Max_difference(1,1)) && day_found==1
222        Mmin = Min3(i);
223        Max_difference([1 2 3]) = [-Mmin, round_down_datooo, i];
224    elseif abs(Min3(i))<=Max3(i) && Max3(i)>Max_difference(1,1) && day_found ==1
225        Mmax = Max3(i);
226        Max_difference([1 2 3]) = [Mmax, round_down_datooo, i];
227    end
228    end
229
230    end
231    %%
232    Max_difference_RAW = Max_difference(1)
233    Raw_date = [dates(Max_difference(2)), Max_difference(3)]
234    after_days = [(time(v3(Max_difference(3))) - time(1))/48/1800, Max_difference(2)]
235    %

236
237    %% Sensor Ratios
238    ratio_DMS_max = MaxDMSDyn/MaxDMSWave;
239    ratio_DT1P_max = MaxDT1PDyn/MaxDT1PWave;
240    ratio_DT2P_max = MaxDT2PDyn/MaxDT2PWave;
241    ratio_DT3S_max = MaxDT3SDyn/MaxDT3SWave;
242    ratio_DT4S_max = MaxDT4SDyn/MaxDT4SWave ;
243    ratio_DMS_min = MinDMSDyn/MinDMSWave;
244    ratio_DT1P_min= MinDT1PDyn/MinDT1PWave;
245    ratio_DT2P_min= MinDT2PDyn/MinDT2PWave;
```

XIV

```matlab
246  ratio_DT3S_min= MinDT3SDyn/MinDT3SWave;
247  ratio_DT4S_min= MinDT4SDyn/MinDT4SWave;
248
249  x=1:5;
250  y = [ratio_DMS_max ratio_DT1P_max ratio_DT2P_max ratio_DT3S_max ratio_DT4S_max];
251  figure(6)
252  bar(1:5,[ratio_DMS_max ratio_DT1P_max ratio_DT2P_max ratio_DT3S_max ratio_DT4S_max])
253  hold on
254  plot(xlim,[1 1], 'r')
255  title('Ratio , Dynamic/Wave')
256  set(gca, 'XTickLabel', {'DMS', 'DT1P', 'DT2P', 'DT3S', 'DT4S'})
257  ylabel('Max(Dyn)/Max(Wave)')
258  ylim([0, 1.6])
259  % add the values
260    for i=1:5,
261      TH(i) = text(x(i),y(i),[num2str(y(i),'%0.2f')]);
262    end
263   % Use the handles TH to modify some properties
264    set(TH,'Horizontalalignment','center',...
265    'verticalalignment','bottom')
266
267  y = [ratio_DMS_min ratio_DT1P_min ratio_DT2P_min ratio_DT3S_min ratio_DT4S_min];
268  figure(7)
269  bar(1:5,[ratio_DMS_min ratio_DT1P_min ratio_DT2P_min ratio_DT3S_min ratio_DT4S_min])
270  hold on
271  plot(xlim,[1 1], 'r')
272  title('Ratio , Dynamic/Wave')
273  set(gca, 'XTickLabel', {'DMS', 'DT1P', 'DT2P', 'DT3S', 'DT4S'})
274  ylabel('Min(Dyn)/Min(Wave)')
275  ylim([0, 1.6])
276  % add the values
277    for i=1:5,
278      TH(i) = text(x(i),y(i),[num2str(y(i),'%0.2f')]);
279    end
280   % Use the handles TH to modify some properties
281    set(TH,'Horizontalalignment','center', 'verticalalignment','bottom');
282
283  % Plot Max / Min values
284  figure(20)
285  plot((time(v3)-time(1))/48/1800, Min3,'r',...
286      (time(v3)-time(1))/48/1800, Max3,'b');
287  hold on
288  plot(xlim,[Max_difference_RAW Max_difference_RAW], 'g')
289  plot(xlim,[-Max_difference_RAW -Max_difference_RAW], 'g')
290  legend('Min values','Max values',2)
291  xlabel('Days')
292  ylabel('Dyn-Wav values (Hogging is positive) [MPa]')
293
294  % End of Program HG_cleanplot_extreme.m
295  % ———————————————————————————————————————————————————————————— //
```

C.5   HG_Raw_spectrum.m

```matlab
 1  %%
 2  % HG_Raw_spectrum.m - Fourier transforms timeseries, plotting frequency spectrums
 3  % Nanna Martine Jacobsen
 4  % Spring 2015
 5  % Master thesis project
 6  % ———————————————————————————————————————————————————————————— //
 7  %% Explanations:
 8  % Date strings with format 'yyyymmdd' are used
 9  % Input:  - path_i        : Path containing input files
10  %         - start_d       : First date to be included
11  %         - end_d         : Last date to be included
12  %         - chn           : Channel numbers to be included (chn = [1 2 15 16 17 18] )
13  %         - par           : Statistical parameter
14  %         - keytype       : Type of file
15  %         - fid           : Part of file name ('IAS_extract')
16  %         - tm            : 0        : No output except output string
17  %                           1        : Print list to screen
18  %                           File name : print to file (default directory)
19  % Output: - path_o        : path for output
20  %         - f_f           : First file in file list
21  %         - f_e           : Last file in file list
22  %         - f_n           : Number of input files
23  % ———————————————————————————————————————————————————————————— //
24  % Functions used:        readDateInterval.m
25  %                        IMO_write_time.m
26  %                        IMO_read_time.m
```

```matlab
27  %                              spegen_t.m
28  %                              filter_ts.m
29  %                              bpfilt.m
30  % ------------------------------------------------------------------------ //
31  close all
32  clear all
33  % ------------------------------------------------------------------------ //
34
35  %% Input and output data:
36  path_i='C:\Data\HG\Raw42Hz\20111102_20111103\';
37  path_o='C:\Data\HG\Matlab_output\';
38  par=3;
39  fid='Raw';
40  start_d='20111102'
41  end_d='20111103'
42
43  % Checking that the sensor list is the same over the time interval
44  folder = path_i;
45  keytype = 'Raw42Hz_*';
46  dateInterval = [str2num(start_d) str2num(end_d)];
47
48  [time,data,sensors] = readDateInterval(folder,keytype,dateInterval);
49
50  %%
51  % Read in data
52  filename=['C:\Data\HG\Matlab_output\' fid '_' start_d '_' end_d '.bin'];
53  testmode=1;
54  [cnt,mess] = IMO_write_time( filename,time,data,sensors,testmode );
55
56  %filename='C:\Data\HG\Raw42Hz\20111102_20111103\Raw42Hz_20111103_070000.bin';
57  %filename='C:\Data\HG\Raw42Hz\20120207_20120208\Raw42Hz_20120207_210000.bin';
58
59  [time,data,sensors] = IMO_read_time( filename, testmode );
60
61  %% Plots:
62  % Plot time history for sensors
63  % Sensor: (1 = DMS, 2 = DMP, 15 = DT1P, 16 = DT2P, 17 = DT3S, 18 = DT4S)
64  figure(1)
65  plot((time-time(1))/60,data(:,17)-mean(data(:,17)),'.b')
66  hold on
67  plot((time-time(1))/60,data(:,1)-mean(data(:,1)),'.r')
68  hold off
69  xlabel('Minutes')
70  ylabel('STD Stresses [MPa]')
71  s = ['Time history, sensor DT3S'];
72  title(s);
73
74  % DT1P, DT2P, DT3S, DT4S, relations
75  figure(2)
76  plot((time-time(1)),data(:,15)-mean(data(:,15)),'-k',(time-time(1)),data(:,16) ...
77      -mean(data(:,16)),'.r',(time-time(1)),data(:,17)-mean(data(:,17)),'.b',...
78      (time-time(1)),data(:,18)-mean(data(:,18)),'.g')
79  legend('DT1P','DT2P','DT3S','DT4S')
80  xlabel('Time [sec]')
81  ylabel('Stress [MPa]')
82   xlim([800 880])
83
84  % Plot spectrum for desired sensor
85  i=3;
86  sen = 17;            % Sensor: (15 = DT1P, 16 = DT2P, 17 = DT3S, 18 = DT4S)
87  xt = data(:,sen)-mean(data(:,sen));
88  NB = 25;
89  dt = time(2)-time(1);
90
91  [Sf,ff]=spegen_t(xt,NB,dt,i);
92
93  fc1 = 0.02;
94  fc2 = 1.5;
95  [xtbp]=bpfilt(xt,dt,fc1,fc2);
96  [Sf,ff]=spegen_t(xtbp,NB,dt,i);
97
98  x = xt;
99  t = time;
100 j=7;
101
102 % Plot spectrum for sensor DMS
103 i=5;
104 xt = data(:,1)-mean(data(:,1));
105 [Sf,ff]=spegen_t(xt,NB,dt,i);
106 [xtbp]=bpfilt(xt,dt,fc1,fc2);
107 [Sf,ff]=spegen_t(xtbp,NB,dt,i);
108
109 x = xt;
```

```
110  t = time;
111  j=8;
112  [XL,XH] = filter_ts(x,t,j);
113
114  % Low vs High frequency signals
115  figure(11)
116  plot((time-time(1)),XL,'b', (time-time(1)),XH,'g')
117  xlabel('Days')
118  ylabel('Dynamic Stress [MPa]')
119  legend('High Frequency Signal','Low Frequency Signal')
120  xlim([2360 2480])
121
122  % End of Program HG_Raw_spectrum.m
123  % ———————————————————————————————————————————————————————— //
```

C.6 HG_ULS.m

```
1
2    %%
3    % HG_ULS.m − Calculating ULS torsional moments from ship rules
4    %
5    % Nanna Martine Jacobsen
6    % Spring 2015
7    % Master thesis project
8    % ———————————————————————————————————————————————————————— //
9    clear all
10   close all
11   % ———————————————————————————————————————————————————————— //
12   %% Explanations:
13   % Input file:          Uses the input file spacings.txt to read in
14   %                      information about frame spcacings along the lengt
15   %                      of the ship.
16   %
17   % Output file:         Writes the output files Genie−Input−LC1T.txt
18   %                      and Genie−Input−LC2T.txt, which can be used in
19   %                      GeniE, to apply torsional loads.
20   % ———————————————————————————————————————————————————————— //
21   % Symbols:             L = Rule Length
22   %                      Lpp = Length between perpendiculars
23   %                      B = Breadth
24   %                      T = Scantling draft
25   %                      Awp = Water plane area
26   %                      Sc = Location of shear center from baseline
27   %                      ze = Distance between shear center and 0.7T
28   %                      Cswp = Water plane area coeficcient
29   %                      CB = Block coefficient
30   % ———————————————————————————————————————————————————————— //
31   %%
32   % Ship input:
33   L = 318.4;            % Rule Length [m]
34   Lpp = 324.82;         % Length between perpendiculars[m]
35   B = 45.6;             % Breadth [m]
36   T = 14.5;             % Scantling draft [m]
37   Awp = 888.44;         % Water plane area [m2]
38   Sc = −13.635;         % Location of shear center from baseline [m]
39   CB = 0.621;           % Block coefficient [−]
40
41   %
42   ze = 0.7*T−Sc;        % Distance between shear center and 0.7T [m]
43   Cswp = 0.825;         % Water plane area coeficcient [−] (Awp/(L*B));
44
45   % Symbolic variable
46   syms x
47
48   KT1 = 1.40*sin(2*pi*x/L);
49   KT2 = 0.13*(1−cos(2*pi*x/L));
50   M1 = KT1*L^(5/4)*(T+0.3*B)*CB*ze;    %[kNm]
51   M2 = KT2*L^(4/3)*B^2*Cswp;           %[kNm]
52
53   MWT1 = M1 + M2;                      %[kNm]
54   MWT2 = M1 − M2;                      %[kNm]
55
56   %x_values:
57   x_values = 0:1:L;
58
59   %Max and min values of MWTs:
60   MWT1_max = max(subs(MWT1,x, x_values));
61   MWT2_min = min(subs(MWT2,x, x_values));
62   MST_max = 0.3*L*B^2;                 %[kNm]
```

```
63
64  %
65  MST1 = MST_max*MWT1/MWT1_max;            %[kNm]
66  MST2 = -MST_max*MWT2/MWT2_min;           %[kNm]
67
68  %% 6.6.1 ULS
69  MWH = 0.22*L^(9/4)*(T+0.3*B)*CB*(1-cos(2*pi*x/L));   %[kNm]
70
71  LC_HT1 = MWH + MST1 + MWT1;              %[kNm]
72  LC_HT2 = MWH + MST2 + MWT2;              %[kNm]
73
74  %% 6.7.3
75  spacings = load('spacings.txt');                 % Reads inputdata containing webframe spacings
76  forward_spacings = spacings(:,1:2);          % [m]
77  x_interval = spacings(:, 3);                  % [m]
78  b = spacings(:,4);
79
80
81  sfwd = [forward_spacings(2:end, 2); Lpp-spacings(end,3)];   % Forward spacing [m]
82  saft = [spacings(1,3); forward_spacings(1:(end-1),2)];      % Aft spacing [m]
83
84  % Integration Limits:
85  x1 = x - saft/2;
86  x2 = x + sfwd/2;
87
88  %% FWH
89  diff_MWH = diff(MWH,x);
90  %FWH = 0;
91  FWH =0.5*(subs(diff_MWH, x, x2) - subs(diff_MWH, x, x1));
92
93  %6.7.3.2 Torsional Moments
94  ze_FWH = 4.592-Sc;
95  MT_FWH = ze_FWH*diff_MWH;
96
97  DeltaM1 = M1 - MT_FWH;
98  FM1_b = -(subs(DeltaM1, x, x2) - subs(DeltaM1, x, x1));
99  FM2_b = -(subs(M2, x, x2) - subs(M2, x, x1));
100 FMST1_b = -(subs(MST1, x, x2) - subs(MST1, x, x1));
101 FMST2_b = -(subs(MST2, x, x2) - subs(MST2, x, x1));
102
103 %%
104 FM1 = FM1_b./b;
105 FM2 =  FM2_b./b;
106 FMST1 =  FMST1_b./b;
107 FMST2 = FMST2_b./b;
108
109 %% From symbolic to Numerical values:
110 for i =1:length(x_interval)
111 FWH(i) = vpa(subs(FWH(i), x, x_interval(i)),5);
112 FM1(i) = vpa(subs(FM1(i), x, x_interval(i)),5);
113 FM2(i) = vpa(subs(FM2(i), x, x_interval(i)),5);
114 FMST1(i) = vpa(subs(FMST1(i), x, x_interval(i)),5);
115 FMST2(i) = vpa(subs(FMST2(i), x, x_interval(i)),5);
116 end
117
118 disp([FWH, FM1, FM2, FMST1]);
119 F_total_LC1 = vpa((FM1 + FM2 + FMST1),5);
120 F_total_LC2 = vpa((FM1 - FM2 + FMST2),5);
121
122
123 %% PLOTS:
124 % Rule torsional moments:
125 figure(1)
126 plot(x_values/L, subs(MST1, x, x_values) ,'r',...
127      x_values/L, subs(MST2, x, x_values) ,'b',...
128      x_values/L, subs(MWT1, x, x_values) ,'g',...
129      x_values/L, subs(MWT2, x, x_values) ,'c',...
130      x_values/L, subs(MWT1+MST1, x, x_values));
131 grid on
132 xlim([0 1]);
133
134 % LC1:
135 figure(2)
136 plot(x_interval/L, F_total_LC1, 'r', x_interval/L, FM1, 'b', x_interval/L, FM2, 'g',...
137      x_interval/L, FMST1, 'c')
138 grid on
139 xlim([0 1]);
140
141 % LC2:
142 figure(3)
143 plot(x_interval/L, F_total_LC2, 'r', x_interval/L, FM1, 'b', x_interval/L, -FM2, 'g',...
144      x_interval/L, FMST2, 'c')
145 grid on
```

XVIII

```
146  xlim([0  1]);
147
148  % Applied Forces
149  figure(4)
150  plot(x_interval/L, FMST1, 'c', x_interval/L, FMST2, 'r')
151  grid on
152  xlim([0  1]);
153
154  %% Print to GeniE, Loadcase 1:
155  fid   = fopen('Genie-Input-LC1.txt', 'w');
156  F_Genie = double(vpa(F_total_LC1*1000,5));
157  x_Genie = double(vpa(x_interval*1000,5));
158  % Port side:
159  for i=1:length(F_total_LC1);
160      textid = 'PLoad%d = PointLoad(LC1, FootprintPoint(Point(%f mm, %f mm,20144 mm)),
161       PointForceMoment(Vector3d(0 N, 0 N, %f N), Vector3d(0 N*mm, 0 N*mm, 0 N*mm)));\r\n';
162      fprintf(fid, textid, i, x_Genie(i), -b(i)*1000/2, F_Genie(i));
163  end
164  % Starboard:
165  for i=1:length(F_total_LC1);
166      textid = 'PLoad%d = PointLoad(LC1, FootprintPoint(Point(%f mm, %f mm,20144 mm)),
167       PointForceMoment(Vector3d(0 N, 0 N, %f N), Vector3d(0 N*mm, 0 N*mm, 0 N*mm)));\r\n';
168      fprintf(fid, textid, i+length(F_total_LC1), x_Genie(i), b(i)*1000/2, -F_Genie(i));
169  end
170  fclose(fid);
171
172  %% Print to GeniE, Loadcase 2:
173  fid   = fopen('Genie-Input-LC2.txt', 'w');
174  F_GenieLC2 = double(vpa(F_total_LC2*1000,5));
175  x_GenieLC2 = double(vpa(x_interval*1000,5));
176  % Port side:
177  for i=1:length(F_total_LC2);
178      textid = 'PLoad%d = PointLoad(LC1, FootprintPoint(Point(%f mm, %f mm,20144 mm)),
179       PointForceMoment(Vector3d(0 N, 0 N, %f N), Vector3d(0 N*mm, 0 N*mm, 0 N*mm)));\r\n';
180      fprintf(fid, textid, i, x_GenieLC2(i), -b(i)*1000/2, F_GenieLC2(i));
181  end
182  % Starboard:
183  for i=1:length(F_total_LC2);
184      textid = 'PLoad%d = PointLoad(LC1, FootprintPoint(Point(%f mm, %f mm,20144 mm)),
185       PointForceMoment(Vector3d(0 N, 0 N, %f N), Vector3d(0 N*mm, 0 N*mm, 0 N*mm)));\r\n';
186      fprintf(fid, textid, i+length(F_total_LC2), x_GenieLC2(i), b(i)*1000/2, -F_GenieLC2(i));
187  end
188  fclose(fid);
189
190  % End of Program HG_ULS.m
191  % ------------------------------------------------------------------------------------ //
```